

# UC San Diego

## UC San Diego Electronic Theses and Dissertations

### Title

Regulation of the Blood-Brain Barrier by Neural Activity

### Permalink

<https://escholarship.org/uc/item/7w59j6vh>

### Author

Pulido, Robert

### Publication Date

2019

Peer reviewed|Thesis/dissertation

UNIVERSITY OF CALIFORNIA SAN DIEGO

Regulation of the Blood-Brain Barrier by Neural Activity

A dissertation submitted in partial satisfaction of the requirements for the degree  
Doctor of Philosophy

in

Biology

by

Robert S. Pulido

Committee in Charge:

Professor Richard Daneman, Chair  
Professor Shelley Halpain, Co-Chair  
Professor Brenda Bloodgood  
Professor Sreekanth Chalasani  
Professor Mark Ginsberg

2019

©

Robert S. Pulido, 2019

All rights reserved

The Dissertation of Robert S. Pulido is approved, and it is acceptable in quality and form for publication on microfilm and electronically:

---

---

---

---

---

---

Co-Chair

Chair

University of California San Diego

2019

## TABLE OF CONTENTS

Signature Page.....	iii
Table of Contents.....	iv
List of Figures.....	vii
List of Tables.....	ix
Acknowledgements.....	x
Vita.....	xi
Abstract of the Dissertation.....	xii
<b>Chapter One:</b> Introduction to the Blood-Brain Barrier.....	1
The importance of the blood-brain barrier in health and disease.....	2
Molecular properties of the blood-brain barrier.....	4
Cellular components of the neurovascular unit and regulation of the blood-brain barrier....	6
<b>Chapter Two:</b> Neural Activity Regulates Molecular Properties of the Brain Vasculature.....	8
Introduction.....	9
Results.....	10
DREADDs as a tool to manipulate glutamatergic activity <i>in vivo</i> .....	10
DREADDs-mediated, neural activity-regulated brain endothelial transcriptome..	10
Neural activity regulates ABC efflux transporter expression and function.....	14
Discussion.....	15
Figures.....	19
Materials and Methods.....	32
Acknowledgements.....	38
<b>Chapter Three:</b> The Role of Endothelial Circadian Clock Genes in Mediating Neural Activity- Dependent Regulation of Blood-Brain Barrier Efflux and Brain Function.....	39
Introduction.....	40
Results.....	42

Neural activity regulates endothelial PAR bZip transcription factors.....	42
PAR bZip transcription factors are required for diurnal rhythmic expression of BBB efflux .....	42
Generation and characterization of endothelial-specific, tamoxifen-inducible <i>Bmal1</i> conditional knockout.....	43
Endothelial circadian clock genes are required for diurnal rhythmic function of BBB efflux.....	44
Neural activity regulates BBB efflux <i>through</i> endothelial circadian clock genes...44	
The endothelial circadian clock regulates affect-related behavior.....	45
Discussion.....	47
Figures.....	49
Materials and Methods.....	57
Acknowledgements.....	64
<b>Chapter Four: Behaviorally Motivated Changes in Neural Activity Regulate Molecular Properties of the Brain Vasculature.....</b>	<b>65</b>
Introduction.....	66
Results.....	67
A paradigm that manipulates neural activity through volitional behavior.....	67
The brain endothelial transcriptome in response to behaviorally motivated changes in neural activity.....	67
Comparison of brain endothelial response to behaviorally motivated changes vs. DREADDs-mediated changes in neural activity.....	67
Discussion.....	71
Figures.....	73
Materials and Methods.....	83
Acknowledgements.....	87
<b>Chapter Five: Discussion of Implications in Brain Waste Clearance and Alzheimer’s disease...88</b>	
Figures.....	91

<b>Appendix A: Signaling Mechanisms of Neural Activity-Dependent Regulation of the Brain Vasculature.....</b>	<b>93</b>
Introduction.....	94
Results.....	96
Discussion.....	98
Figures.....	101
Materials and Methods.....	106
 <b>Appendix B: The Role of the Mechanosensitive Ion Channel <i>Piezo1</i> in Barrier Development...109</b>	
Introduction.....	110
Results.....	112
Discussion.....	113
Figures.....	115
Materials and Methods.....	117
 References.....	 118

## LIST OF FIGURES

Figure 2.1: DREADDs as a Tool to Manipulate Glutamatergic Activity <i>in vivo</i> .....	19
Figure 2.2: DREADDs-Mediated, Neural Activity-Regulated Brain Endothelial Transcriptome..	20
Figure 2.3: Neural Activity-Regulated BBB Transcriptome.....	22
Figure 2.4: Neural Activity Regulates ABC Transporter Expression and Function.....	23
Figure 2S.1: Further Validation of DREADDs.....	24
Figure 2S.2: DREADDs-Mediated, Neural Activity-Regulated Brain Endothelial Transcriptome Cell Purity.....	25
Figure 3.1: Neural Activity-Regulated Endothelial PAR bZip Transcription Factors are required for Diurnal Rhythmic Expression of Pgp.....	49
Figure 3.2: Endothelial Circadian Clock Genes are required for Diurnal Rhythmic Function of BBB Efflux.....	50
Figure 3.3: Neural Activity Regulates BBB Efflux <i>through</i> Endothelial Circadian Clock Genes...51	
Figure 3.4: EC-Bmal1 cKOs display Depressive-like Behavior.....	52
Figure 3S.1: DREADDs-Mediated, Neural Activity-Regulated Endothelial Circadian Clock Genes.....	53
Figure 3S.2: Generation and Characterization of EC-Bmal cKO Mice.....	54
Figure 3S.3: EC-Bmal cKO Mice do not display Learning and Memory Deficits nor Anxiety-like Behavior.....	56
Figure 4.1: Behaviorally motivated, Neural Activity-Regulated Brain Endothelial Transcriptome.....	73
Figure 4.2: Comparison of brain endothelial response to behaviorally motivated changes vs. DREADDs-mediated changes in neural activity.....	74
Figure 4S.1: Behaviorally Motivated, Neural Activity-Regulated Brain Endothelial Transcriptome Cell Purity.....	76
Figure 4S.2: Behaviorally Motivated, Neural Activity-Regulated Endothelial Circadian Clock Genes.....	77
Figure 4S.3: Behaviorally Motivated, Neural Activity-Regulated BBB Transcriptome.....	78

Figure 4S.4. Neural Activity-Regulated Slc Transporter Transcriptome.....	79
Figure 5.1: Model of neural activity-dependent expression of endothelial circadian clock-regulated PAR bZip transcription factors which regulate BBB efflux transport and maintain neurochemical balance.....	92
Figure A.1: Astrocyte Gq-DREADDs.....	101
Figure A.2: Astrocyte Gq-DREADDs RNA sequencing.....	102
Figure AS.1: Astrocytic Calcium-Regulated Brain Endothelial Transcriptome Cell Purity.....	105
Figure B.1: CNS endothelial Piezo1 is required for BRB development, but not BRB maintenance.....	115

## LIST OF TABLES

Table 2S.1: DAVID Pathway Analysis for 748 genes <i>downregulated</i> by glutamatergic activation.....	26
Table 2S.2: DAVID Pathway Analysis for 625 genes <i>upregulated</i> by glutamatergic activation....	27
Table 2S.3: DAVID Pathway Analysis for 603 genes <i>downregulated</i> by glutamatergic silencing.....	28
Table 2S.4: DAVID Pathway Analysis for 718 genes <i>upregulated</i> by glutamatergic silencing.....	29
Table 2S.5: DAVID Pathway Analysis for 138 genes <i>upregulated</i> after glutamatergic silencing AND <i>downregulated</i> after glutamatergic activation.....	30
Table 2S.6: DAVID Pathway Analysis for 105 genes <i>upregulated</i> after glutamatergic activation AND <i>downregulated</i> after glutamatergic silencing.....	31
Table 4S.1: DAVID Pathway Analysis for 508 genes <i>downregulated</i> by whisker stimulation.....	81
Table 4S.2: DAVID Pathway Analysis for 727 genes <i>upregulated</i> by whisker stimulation.....	82
Table A.1: DAVID Pathway Analysis for 572 genes <i>upregulated</i> by astrocytic calcium signaling.....	103
Table A.2: DAVID Pathway Analysis for 157 genes <i>downregulated</i> by astrocytic calcium signaling.....	104

## ACKNOWLEDGEMENTS

I would first like to thank my advisor Richard Daneman for all the time and effort he dedicated to helping me become a better scientist. He is an amazing mentor that fosters a uniquely positive and open minded environment. His guidance and unconditional support throughout my graduate career was invaluable to the growth and confidence in my skills. I think he saw something in me that I did not know was there. I will always be grateful for the opportunity he gave me to work together.

I am extremely grateful to the members of the Daneman Lab, past and present. I would especially like to thank Roeben Munji who has helped technically with my experiments for several years. Without him, this work would've taken much longer or simply not been achieved. I would also like to thank Tamara Chan who is a naturally talented scientist whose master's work under my mentorship brought my thesis work to another level that wouldn't have been possible without her.

Chapters 2, 3 and 4 are all part of a manuscript under revision for publication of the material as it may appear in Neuron, 2019, Pulido RS, Munji RN, Chan TC, Quirk CR, Weiner GA, Weger BD, Elmsaouri S, Malfavon M, Gachon F, Leutgeb S, Daneman R. The dissertation author is the primary investigator and first author of this material.

## VITA

- 2014 Bachelor of Arts in Neuroscience and Biology, Boston University
- 2019 Doctor of Philosophy in Biology, University of California San Diego

## PUBLICATIONS

**Pulido RS**, Munji RN, Chan TC, Quirk CR, Weiner GA, Weger BD, Elmsaouri S, Malfavon M, Gachon F, Leutgeb S, Daneman R. Neural Activity Regulates Blood-Brain Barrier Efflux Transport through Endothelial Circadian Genes. *Neuron* (In Revision).

Weiner GA\*, Shah S\*, Angelopoulos CM, Bartakova A, **Pulido RS**, Murphy A, Nudleman E, Daneman R\*, Goldberg JL\*. Cholinergic neural activity directs layer-specific angiogenesis and blood-retinal barrier formation in the developing retina. *Nature Communications* (2019).

## **ABSTRACT OF THE DISSERTATION**

Regulation of the Blood-Brain Barrier by Neural Activity

by

Robert S. Pulido

Doctor of Philosophy in Biology

University of California San Diego 2019

Professor Richard Daneman, Chair

Professor Shelley Halpain, Co-Chair

The blood vessels in the central nervous system (CNS) have a series of unique properties, termed the blood-brain barrier (BBB), which stringently regulate the entry of molecules into the

brain, thus maintaining proper brain homeostasis. Despite the dynamic nature of the brain, the BBB has largely been studied in a static context. We sought to understand if the BBB exhibited plasticity and whether neural activity could regulate BBB properties. Using both chemogenetics and a volitional behavior paradigm, we identified a core set of brain endothelial genes whose expression is regulated by neural activity. In particular, neuronal activity regulates BBB efflux transporter expression and function, which is critical for excluding many small lipophilic molecules from the brain parenchyma. Furthermore, we found that neural activity regulates the expression of circadian clock genes within brain endothelial cells, which in turn mediate the activity-dependent control of BBB efflux transport. These results have important clinical implications for efficiency of CNS drug delivery in the day vs. night, the BBB's role in clearance of CNS waste products including A $\beta$  in health and Alzheimer's Disease, and understanding how neural activity can control these and other diurnal processes.

## **CHAPTER ONE:**

### Introduction to the Blood-Brain Barrier

## **The importance of the blood-brain barrier in health and disease**

Blood vessels provide a physical framework for the transport of oxygen and essential nutrients throughout the body. Although the blood vessels that make up the circulatory system are highly interconnected, they are heterogeneous in both physical and functional properties, often based on the tissue they vascularize(1). The central nervous system (CNS) is a very unique structure that importantly integrates information from the external and internal environment to coordinate and influence all parts of the body. The blood vessels that vascularize the CNS have coevolved with this unique environment to exhibit a series of distinct properties compared to peripheral blood vessels. While blood vessels in most tissue are relatively permeable, CNS blood vessels stringently regulate the movement of ions, molecules and cells between the blood and the CNS. These unique properties which include tight junctions which limit paracellular diffusion, low rates of transcytosis and lack of fenestrae limiting transcellular diffusion, low expression of leukocyte adhesion molecules limiting immune surveillance from circulating peripheral immune cells, efflux transporters limiting passive diffusion of small lipophilic molecules and solute carrier transporters which important vital nutrients(2–6). Together they are referred to as the blood-brain barrier (BBB).

The BBB serves two major evolutionary purposes: 1) to tightly regulate the chemical and ionic microenvironment of the CNS for proper neuronal function and 2) to limit the entry of toxins, pathogens and the body's peripheral immune system to protect the CNS which lacks regenerative capacity. Proper development and maintenance of the BBB is critical for brain homeostasis and neural protection. This need to insulate and protect the CNS is an evolutionarily conserved mechanism in both invertebrates and vertebrates(7).

The BBB however, is susceptible to malfunction in which breakdown permits the entry of foreign molecules and cells that contribute to neural dysfunction and eventually neuronal death and degeneration. BBB breakdown is a critical component of several neurological diseases such as stroke, traumatic brain injury, epilepsy, multiple sclerosis, Alzheimer's Disease (AD) and several other neurodegenerative diseases(5,8–10). Although the triggers of these diseases are vastly different, their effect on the BBB are quite similar suggesting that there is a common pathway for BBB dysfunction and the brain vasculature as a potentially drug target in these diseases.

The BBB also poses a major obstacle for drug delivery to the CNS in the aforementioned diseases as well as all neurological diseases(11). There have been several innovative strategies to bypass the BBB for drug delivery which each have advantages and disadvantages. The most direct method is by injecting the drug into the cerebrospinal fluid of the spinal cord or cerebral ventricles(12). However, this is quite invasive, requires experts who can deliver the drug and cannot be repeated frequently if the drug needs to be administered often. Intranasal administration has also shown to be effective at getting all types of drugs into the CNS due to the unique connections that the olfactory receptor neurons and the trigeminal nerve innervate between the brain and the external environment(13). However, this can be damaging to the nasal epithelium over long-term repeated administration. Co-administration of efflux transporter inhibitors limit these transporters from restricting entry of many small molecule drugs, but in doing so also allow many endogenous molecules to enter the brain that otherwise wouldn't and therefore these inhibitors can have major side effects(14). Also, biphasic antibodies with one arm binding to the transferrin receptor which is part of a transcytotic pathway in the brain vasculature and the other arm binding to its target antigen in the brain permits a "Trojan horse" delivery(15–17). Lastly,

focused ultrasound allows transient opening of the BBB in precise regions with minimal invasiveness and high temporal specificity(18,19). Understanding the basic molecular and cellular mechanisms of how the BBB functions and malfunctions in health and disease will allow expansion of current strategies and development of novel strategies to treat neurological diseases.

### **Molecular properties of the blood-brain barrier**

The properties of the BBB are predominantly possessed by the brain endothelial cells which form the vessel walls. However, the BBB is not a single entity, but a series of properties that together allow CNS endothelial cells to stringently regulate the movement of molecules and cells between the blood and neural tissue.

First, CNS endothelial cells are held together by tight junctions (TJs) which create a high electrical resistance paracellular diffusion barrier and polarize the cells into distinct luminal and abluminal compartments(20). The claudins are the major TJ protein family with Claudin-5 being the most abundant at the BBB and essential for BBB function(21,22). Occludin, junctional adhesion molecules (JAMs), zona occludens (ZOs) and lipolysis-stimulated lipoprotein receptor are other BBB-enriched TJ proteins that form complexes to tightly hold brain endothelial cells together(23–28).

CNS endothelial cells are also unique in the properties that they do not possess that are normally expressed in peripheral endothelial cells. They lack fenestra and exhibit low rates of transcytosis in comparison to peripheral endothelial cells, thus limiting transcellular movement of molecules(29). CNS endothelial cells also have low expression of leukocyte adhesion molecules (LAMs), which are robustly expressed on peripheral endothelial cells, thus limiting CNS immune surveillance from peripheral immune cells(30). Interestingly, upregulation of transcytosis and

LAMs are a common result of BBB breakdown in injury and disease, suggesting that brain endothelial cells have the genetic capacity to express them and that their expression is constitutively inhibited in health(31).

CNS endothelial cells are also unique in their enriched expression of a wide array of two categories of specialized transporters. The first of these are specialized solute carrier (Slc) transporters which have narrow substrate specificities and collectively import a wide range of essential nutrients for the brain(32). Although the CNS vasculature evolved numerous strategies to maintain a sealed environment, it also evolved a clever strategy by using these Slc transporters to precisely regulate the essential ions, nutrients and proteins that the high energy-expending CNS vitally requires. CNS endothelial cells express a large breadth of Slc transporters and are most notably enriched for GLUT1 (Slc2a1), MCT1 (Slc16a1) and LAT1 (Slc7a5) which import the vital nutrients glucose, lactate and large amino acids respectively(33–35). Slc transporters are generally found on both the luminal and abluminal surface of brain endothelial cells.

The second major category of transporters expressed by CNS endothelial cells are adenosine triphosphate (ATP)-binding cassette (ABC) efflux transporters which are primarily embedded in the luminal side of CNS endothelial cells and restrict the passage of many molecules into the neural tissue by utilizing ATP to actively efflux small lipophilic molecules that would otherwise passively diffuse across the endothelial cell membrane(14). ABC transporters have broad substrate specificities including many small molecule drugs and xenobiotics thus presenting a major obstacle for drug delivery to the CNS(11). Therefore, inhibitors of these efflux transporters, including Pgp/Abcb1 and BCRP/Abcg2, are highly sought after to aid in drug delivery to the CNS. Although the ABC efflux transporters have predominantly been studied in the context of preventing entry of exogenous molecules into the CNS, they also have a role in the

efflux of endogenous molecules, including steroids which are critical regulators of mood and behavior(7), and neural waste products such as amyloid beta ( $A\beta$ )(36) and dysfunction of efflux transport has been hypothesized as a mechanism of  $A\beta$  accumulation in Alzheimer's disease (AD)(10).

### **Cellular components of the neurovascular unit and regulation of the blood-brain barrier**

Although BBB properties are predominantly possessed by brain endothelial cells, they are induced and maintained by cues from the CNS microenvironment to properly function(37). The neurovascular unit (NVU) refers to the myriad of cell types that exist at the interface between the blood and the brain. The NVU is composed by endothelial cells which form the walls of the blood vessels, mural cells which latch onto the endothelial cells, neurons which are the main component of the brains electrochemical network, astrocytes which are found in between neuronal synapses and blood vessels, and extracellular matrix proteins secreted by multiple cell types(38). These components dynamically interact with each other to regulate blood flow and BBB properties to maintain brain homeostasis during development and adulthood.

Astrocytes, a glial cell type which have processes called endfeet that ensheath blood vessels, have been shown to be critical regulators of barrier properties in brain endothelial cells. Transplantation studies and *in vitro* studies have shown that extrinsic cues from astrocytes are sufficient to induce barrier properties in endothelial cells(39–43). Several *in vivo* studies have also identified astrocyte-derived cues that are critical for BBB integrity(44–46). However, evidence for astrocytic regulation of the BBB likely reflects more of a maintenance role rather than one of development because BBB formation precedes astrocyte formation during development(47,48).

Pericytes, which are a type of mural cell that tightly latch onto capillary endothelial cells in a discontinuous layer, have been shown to have more of an essential role in BBB formation during development(31,49). Pericyte formation and migration into the brain does precede BBB formation during development. Mice that lack functional pericytes in development do not form a functional BBB leading to premature lethality. Interestingly, pericytes seem to be critical for inhibiting expression of transcytosis and LAMs as their expression is upregulated in the absence of functional pericytes. Although pericytes are likely inhibiting transcytosis through induction of endothelial expression of Mfsd2a(50,51), no pericyte-derived signaling cues have definitively been identified as essential for BBB formation.

Neural progenitor cells (NPCs) have also been shown to be critical regulators of BBB properties. It was first shown that co-culturing NPCs with brain endothelial cells was sufficient to increase BBB properties *in vitro*(52). It was later shown *in vivo* that NPC-derived Wnt/beta-catenin signaling was essential for proper CNS angiogenesis, enrichment of several Slc transporters in CNS endothelial cells and maintenance of the BBB(53,54).

Although extrinsic cues from cells in the NVU has been extensively studied, the BBB has largely been studied in a static context. Once the BBB is formed and properly maintained, it assumed to be permanently fixed in health. However, the brain is a very dynamic organ with constant changes in neural activity. Therefore, it is possible that the BBB exhibits plasticity in response to neural activity to meet the dynamic demands of the neural circuitry without overt leakiness.

## **CHAPTER TWO:**

Neural Activity Regulates Molecular Properties of the Brain Vasculature

## INTRODUCTION

The BBB has largely been studied as a static structure: a wall protecting the CNS from potential toxins. The brain, however, is highly dynamic with constant fluctuations in neural activity and energy demand. Therefore, it would be plausible that the vasculature could dynamically respond to meet the changing demands of the neural circuitry. The majority of neurovascular communication has been studied in the context of blood flow whereby increased neural activity leads to an increase in localized blood flow through the process of neurovascular coupling (NVC)(55,56). It is also established that neurovascular signaling is critical for postnatal angiogenesis in the brain(57,58). However, much less is known about whether the properties of the BBB are plastic and how these properties respond to changes in neuronal activity. Interestingly, a study utilizing single cell sequencing to analyze the gene expression in different cells of the visual cortex in different light paradigms identified that there were changes to vascular cells in addition to neurons and glia, suggesting that experience may indeed alter brain endothelial gene expression(59). Because the BBB is essential for regulating the CNS microenvironment, changes in transport, signaling, metabolism or other BBB properties without overt ‘leakiness’ of the BBB to non-specific molecules, could significantly alter the extracellular environment and thus neural circuit function and behavior. Therefore we sought to understand how plastic the BBB is, and whether neural activity can regulate specific barrier properties. Interestingly, increased neural activity has been shown to highly correlate with A $\beta$  accumulation in both mouse models of AD and humans suggesting that it may be an upstream driver of AD(60–66). However, the role of the cerebral vasculature in this context has not been explored.

## RESULTS

### **DREADDs as a tool to manipulate glutamatergic activity *in vivo***

In order to determine how glutamatergic neural activity regulates the cerebral vasculature, we first generated two chemogenetic mouse models to express Designer Receptors Exclusively Activated by Designer Drugs (DREADDs) in glutamatergic neurons including *CamKII $\alpha$ -tTA;TRE-hM3Dq* (“hM3Dq-Activating”) mice to activate glutamatergic neurons and *CamKII $\alpha$ -tTA; TRE-hM4Di* (“hM4Di-Silencing”) to silence glutamatergic neurons (Figure 2.1 A) in response to administration of clozapine-N-oxide (CNO)(67). In these models, the DREADDs were densely expressed in the cortex and hippocampus (Figure 2.1 B, 2S.1 A), so we carried out all experiments involving chemogenetics in these brain regions. To determine the temporal dynamics of neural activity modulation we used *in vivo* multi-electrode recordings to examine the neural activity in the cortex/hippocampus of these mice following injection of CNO. Intraperitoneal injection of 0.5 mg/kg CNO was sufficient to cause a robust increase in gamma local field potential (LFP) power in the hM3Dq-Activating mice, without eliciting seizures (Figure 2.1 C), and a significant increase in locomotor activity (Figure 2S.1 B). The increase in neural activity was initially observed at 15 minutes post-CNO injection, peaked at 1 hour post-injection and lasted until 3 hours post-injection. No increase in gamma local field potential or locomotor activity was observed in the littermate controls (Figure 2.1 E, 2S.1 B). Intraperitoneal injection of 1.0 mg/kg CNO in the hM4Di-Silencing mice robustly attenuated gamma LFP power and locomotor activity which was not observed in littermate controls (Figure 2.1 D, 2.1 F, 2S.1 C). The neuronal silencing

was initially observed 15 minutes post-CNO, maximum silencing was observed around 1 hour and it lasted the full 3 hours of recording.

### **DREADDs-mediated, neural activity-regulated brain endothelial transcriptome**

We next aimed to determine how neural activity regulates brain endothelial gene expression. Three hours following CNO injection into hM3Dq-Activating and paired littermate controls (0.5mg/kg CNO) or hM4Di-Silencing and paired littermate controls (1.0mg/kg CNO), we isolated brain endothelial cells via fluorescence-activated cell sorting (FACS, Figure 2.2 A, Figure 2S.2 A, 2S.2 B) and then examined their gene expression by RNA sequencing.

There were 625 genes significantly upregulated and 748 genes significantly downregulated by glutamatergic activation (Figure 2.2 B). Pathway analysis revealed that a large number of downregulated genes were involved in amino acid and lipid metabolic pathways suggesting that neural activity downregulates brain endothelial metabolism (Table 2S.1). There was a very robust enrichment of upregulated genes in pathways involving adherens junctions and cytoskeletal remodeling (Table 2S.2). These changes are likely due to increased NVC-mediated blood flow in these brain regions as shear stress-dependent regulation of the adherens junctions and consequently the cytoskeleton in the endothelium is a well-established phenomenon in the vasculature(68–70). There was also an enrichment for upregulated pathways involving protein synthesis and transport suggesting that there is a global demand for more proteins in the vasculature in response to increased neural activity (Table 2S.2). When we looked at known BBB-enriched genes (Figure 2.3), TJ gene expression, including claudin5 (*Cldn5*), occludin (*Ocln*), zo-1 (*Tjp1*), zo-2 (*Tjp2*), Lipolysis stimulated receptor (*LSR*) and Tricellulin (*Marveld2*), they were largely unaffected by increased neural activity. BBB-enriched Slc transporters were also largely unaffected with the exception of a significant downregulation of *Slc39a10*, a putative zinc transporter. Surprisingly,

glut1 (*Slc2a1*), which is critical for transporting glucose into the brain, was unaffected by glutamatergic activation which is important for importing glucose into the brain. Perhaps for this time frame, the active neurons are able to utilize other mechanisms for energy. There were largely no changes to LAMs, including *Icam1*, *Vcam1*, *Alcam*, E-selectin (*Sele*) and P-selectin (*Selp*) with the exception of a robust and significant upregulation of *Mcam*. Although upregulation of LAMs can be an inflammatory response to injury and disease, this change could represent their role in cell structure in response to shear stress. Transcytotic genes such as *Tfrc*, *Cav1* and *Plvap* were unaffected by glutamatergic activation. Most strikingly, there were 4 major ABC efflux transporters that were significantly downregulated by glutamatergic activation (*Pgp/Abcb1a*, *Mrp4/Abcc4*, *Abca3*, *Abcd4*) suggesting that efflux transport is regulated by neural activity.

We further identified 718 genes significantly upregulated and 603 genes significantly downregulated by glutamatergic silencing (Figure 2.2 C). Notably, there was downregulation of pathways enriched in adherens junctions likely indicating a response to decreased local blood flow when neural activity is low (Table 2S.3). Interestingly, metabolism-related genes were also downregulated after glutamatergic silencing (Table 2S.3). Specifically, steroid metabolism was uniquely downregulated after glutamatergic silencing. However, genes involving lipid metabolism were also downregulated similar to after glutamatergic activation. Many of the downregulated lipid metabolism genes were different between the activating and silencing experiments suggesting that the overall lipid metabolic program is modulated by neural activity. When we looked at known BBB-enriched genes (Figure 2.3), surprisingly *Cldn5* and *Tjp1* were significantly downregulated and upregulated respectively. There were 4 BBB-enriched Slc transporters involved in glucose (*glut1/Slc2a1*; upregulated), amino acid (*lat1/Slc7a5*; upregulated) and lactate/monocarboxylate (*mct1/Slc16a1*, *mct4/Slc16a4*; both downregulated) transport that were significantly changed in

response to glutamatergic silencing. *Bsg*, which helps target monocarboxylate transporters (Slc16 family) to the plasma membrane was also downregulated further suggesting that BBB aims to limit monocarboxylate transport in response to glutamatergic silencing. Interestingly, the transcytosis pathway regulators *Mfsd2a* and *Cav1* were also downregulated after glutamatergic silencing. There were no changes in LAM expression. The BBB property that was the most robustly affected by silencing was efflux transport with 5 major efflux transporters being upregulated by glutamatergic silencing (*Pgp/Abcb1a*, *BCRP/Abcg2*, *Mrp4/Abcc4*, *Abca3*, *Abcd4*), many of the same efflux transporters that were downregulated by increasing glutamatergic activity.

In total, there were 243 genes that were regulated in opposite directions by activating and silencing neural activity (105 genes directly correlated and 138 genes inversely correlated with the amount of neural activity), suggesting that the absolute mRNA expression level of these brain endothelial genes are regulated by the total amount of glutamatergic activity (Figure 2.2 D, Figure 2.2 E). The 2 most enriched pathways that were directly correlated with neural activity were adherens junctions and focal adhesion providing further evidence that the brain endothelial cells are primed to respond to dynamic changes in blood flow and may undergo structural remodeling to compensate for the sustained alteration in shear stress (Table S2.6). VEGF signaling was inversely correlated with neural activity suggesting that angiogenic signaling is switched off in response to DREADDs-mediated changes in neural activity (Table 2S.5) in the adult brain. Although it has been previously shown that brain angiogenesis is increased in the adult brain after both locomotor exercise(71) and electroconvulsive seizures(72), perhaps differential effects on angiogenesis are dependent on the degree of neural activity perturbation. For example, sensory stimulation was proangiogenic in a critical postnatal period(58) whereas vigorous exercise, persistent auditory stimulation and seizures were antiangiogenic in the same postnatal period(57).

Moreover, although neural activity has been shown to locally increase permeability to IGF-1 into the CNS(73), we found that *Igflr* expression was significantly downregulated after glutamatergic activation and significantly upregulated after glutamatergic silencing (Figure 2.3). However, it was found in that study that the receptor was phosphorylated in response to neural activity and the mechanism did not primarily involve the receptor, but rather cleavage of an IGF binding protein suggesting this phenomenon may be independent of *Igflr* transcription. Of particular interest was the identification that ABC transporters (*Pgp/Abcb1a*, *Mrp4/Abcc4*, *Abca3*, *Abcd4*), a core property of the BBB, and a group of proline and acidic amino acid-rich basic leucine zipper (PAR bZip) family of circadian transcription factors (*Dbp*, *Tef* and *Hlf*) which were both inversely correlated with neural activity (Table 2S.5).

### **Neural activity regulates ABC efflux transporter expression and function**

We found that ABC transporters were one of the top pathways upregulated after glutamatergic silencing and downregulated after glutamatergic activation suggesting that efflux transporter expression is regulated by neural activity (Table 2S.1, Figure 2.4 A). We next aimed to determine whether there were corresponding activity-dependent changes in BBB efflux function. We injected Rhodamine123 (Rh123), a fluorescent small lipophilic molecule that is a substrate for *Pgp (Abcb1a)*(74), 2 hours post-CNO injection into hM3Dq-Activating and hM4Di-Silencing mice paired with littermate controls and measured its fluorescence in the brain and blood. Significantly more Rh123 entered the brains of the hM3Dq-Activating mice relative to hM4Di-Silencing mice, corresponding to the decreased expression of *Pgp/Abcb1a* in the hM3Dq-Activating mice and increased expression in the hM4Di-Silencing mice (Figure 2.4 B). We observed no difference in brain permeability to sodium fluorescein (NaFl), a small hydrophilic molecule that is not a substrate of *Pgp*, between hM3Dq-Activating mice and hM4Di-Silencing

mice (Figure 2.4 C). This indicates that these permeability changes are specific to efflux transport, and not non-specific leakiness of the BBB. Taken together these data demonstrate that neural activity decreases the expression and function of BBB efflux.

## **DISCUSSION**

Here, we report that DREADD-mediated changes in glutamatergic activity robustly regulates brain endothelial cell gene expression. While most BBB properties were largely unaffected by neural activity, efflux transporter expression and function were homeostatically by neural activity.

This work suggests that specific properties of the BBB exhibit plasticity in response to neural activity. There is increased blood flow to localized regions of high neural activity presumably to deliver oxygen and nutrients for the energy-demanding neurons. Functional changes to the BBB involving transport and metabolism can change the local chemical environment and thus potentially modulate local circuit function. Our work demonstrating the activity-dependent downregulation of efflux transport and other studies involving increased permeability to IGF-1 and increased transcytosis suggest that the BBB becomes less stringent after high neural activity perhaps as a mechanism to deliver more nutrients into the energy-demanding areas of the brain parenchyma(73,75). It's also possible that BBB efflux transport becomes less stringent during high neural activity as an evolutionary mechanism to preserve energy as both neuronal action potentials and active efflux transport require vast amounts of ATP.

We identified hundreds of brain endothelial genes, including those involved in metabolism and focal adhesion, that were regulated by neural activity and it will be very interesting to determine how these activity-dependent genes may affect the local neural environment. In addition, it will be interesting to understand the signaling mechanism(s) by which neural activity

regulate(s) brain endothelial transcription. When glutamatergic neurons fire, they change the extracellular environment (e.g. ATP, glutamate, d-serine, potassium) around the neurovascular unit which can have vasoactive effects(76–80), and thus there may be a direct effect of neuronal metabolites on brain endothelial transcription. Astrocytes have been shown to be key mediators of NVC and it is possible that these glial cells may play a role in mediating these neural activity-dependent changes in brain endothelial transcription, as they are physically located in close contact with both neurons and brain blood vessels, actively communicating with both synapses and blood vessels(81). In addition, blood flow is tightly coupled with neural activity in the brain and it is possible that neural activity may regulate brain endothelial transcription through luminal mechanosensation of differential shear stress via TRP channels, *Piezo1*, *GPR68* or other endothelial mechanosensitive mechanisms(82–85). Interestingly, many focal adhesion genes that we found to be increased with neuronal activity have been shown to be regulated by the mechanosensory ion channel *Piezo1* in the endothelium (*Actn1*, *Actn4*, *Flna*, *Flnb*, *Pls3*, *Vcl*, *Tubb2a*, *Tubb2b*, *Tubb4b*)(83).

The experiments described likely identified “homeostatic” changes to brain endothelial cells in response to altering neural activity, as we examined the gene expression changes hours after manipulating neural activity. It would be interesting to identify “dynamic” changes to BBB properties that would occur on the order of seconds to minutes. Such dynamic changes would likely not involve the alteration of the transcriptional profile of the endothelial cells, but perhaps post-translational regulation including the trafficking of key transporters such as Pgp to and from the surface(86–88). In addition, only a single time point was analyzed after neuronal manipulation in this study. Due to the dynamic nature of transcription, it would also be interesting to investigate how neural activity affects brain endothelial transcription at multiple time points. In addition, the

experiments described specifically analyzed glutamatergic activity since it is the major type of excitatory neurotransmission in the brain, but it would be interesting to see how other types of neural activity regulate the brain endothelial cells and determine whether there are circuit-specific and regional-specific activity-dependent changes in the brain endothelial cells. It is also worth noting that although we analyzed brain endothelial transcriptomics and BBB function in the localized areas that we manipulated neural activity, based on previous findings, we expect that these changes should be specific to these localized areas rather than affecting the entire brain vascular network(59,73).

Although there is substantial overlap in neural activity-dependent brain endothelial gene expression changes between our study and Hrvatin et al. 2019, we also newly identify many different genes not found in their study, especially many downregulated genes. However, we think this is primarily due to the fact that their study was done with single cell RNA sequencing (sc-RNAseq) on whole brain tissue (all cell types) and ours was done with bulk RNA sequencing on FACS-purified brain endothelial cells. Not only does sc-RNAseq achieve substantially lower sequencing depth than bulk sequencing, but this shallowness is amplified if the cell type of interest is not purified, especially for endothelial cells which make up ~10% of cells in the brain. Hrvatin et al was interested in the activity-dependent transcriptional changes of all cell types so there was no cell purification performed. Indeed a recent study has shown that enrichment of vascular cells in combination with sc-RNAseq was sufficient to further probe vascular heterogeneity due to increased sequencing depth(89). While we expect that there were likely transcriptional changes in all cell types in our study, we were primarily interested in the endothelial response so we combined endothelial cell purification with deep bulk RNA sequencing to identify gene expression changes not observed in Hrvatin et al. While we did achieve deep sequencing with presumably primarily

microvascular brain endothelial cells, performing sc-RNAseq in this paradigm would also be beneficial in elucidating how different endothelial cells along the zonation of the brain vascular network respond to neural activity(89).

BBB efflux transporters have a broad range of exogenous substrates and thus act as a major obstacle for delivery of small molecule drugs to the CNS(14). They also have endogenous substrates and act as a major extrusion route of waste products and metabolites from the brain into the bloodstream(10). We have previously found that Pgp is important for modulating concentrations of endogenous steroids in the brains of flies and mice and is important for behavior(7). Because our work here shows that the expression and function of Pgp is regulated by neural activity, it is possible that BBB efflux and neural activity exhibit dynamic crosstalk to maintain the brain concentrations of these important neuromodulators. This would implicate the BBB as a dynamic component of the neural circuitry.

## FIGURES

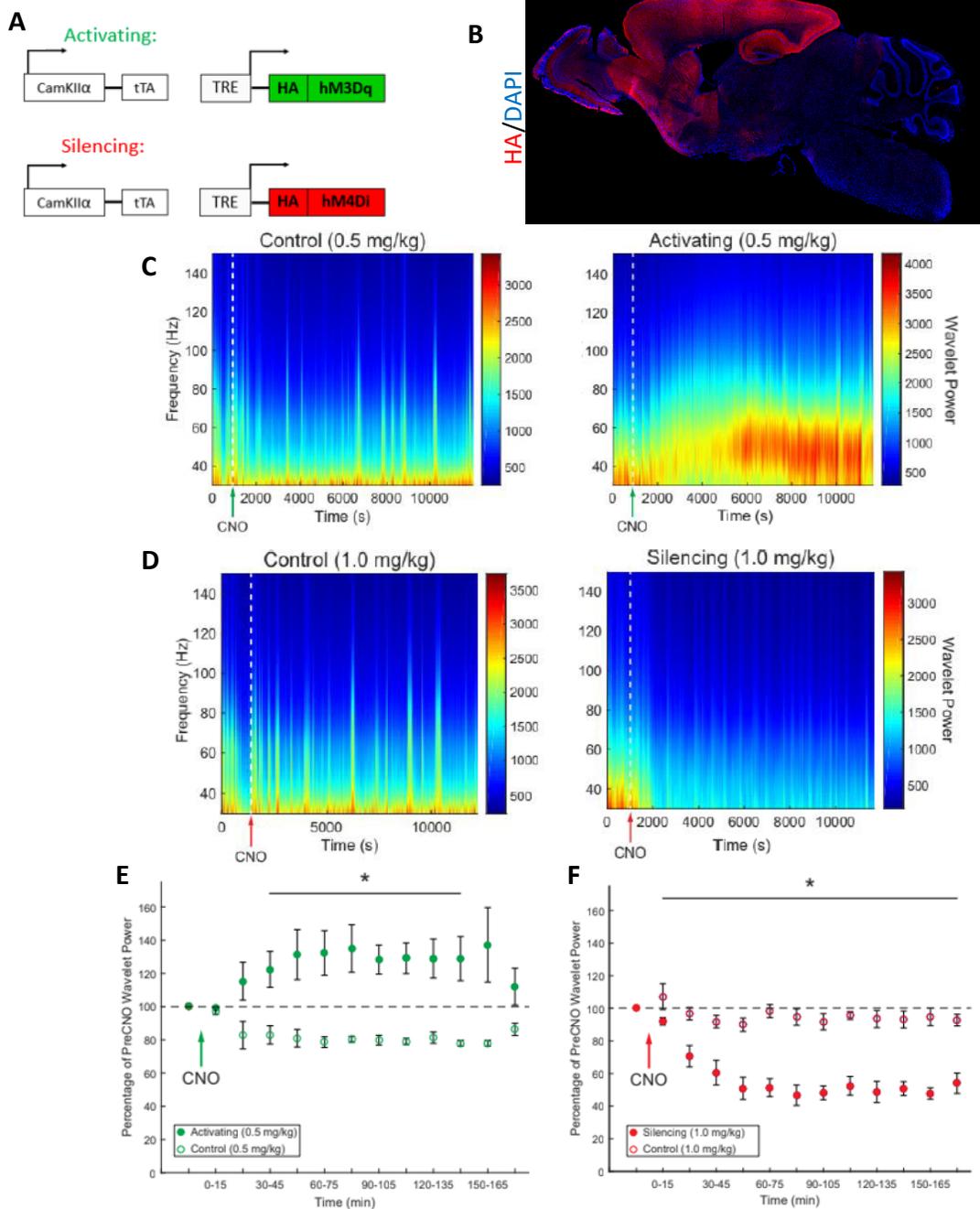
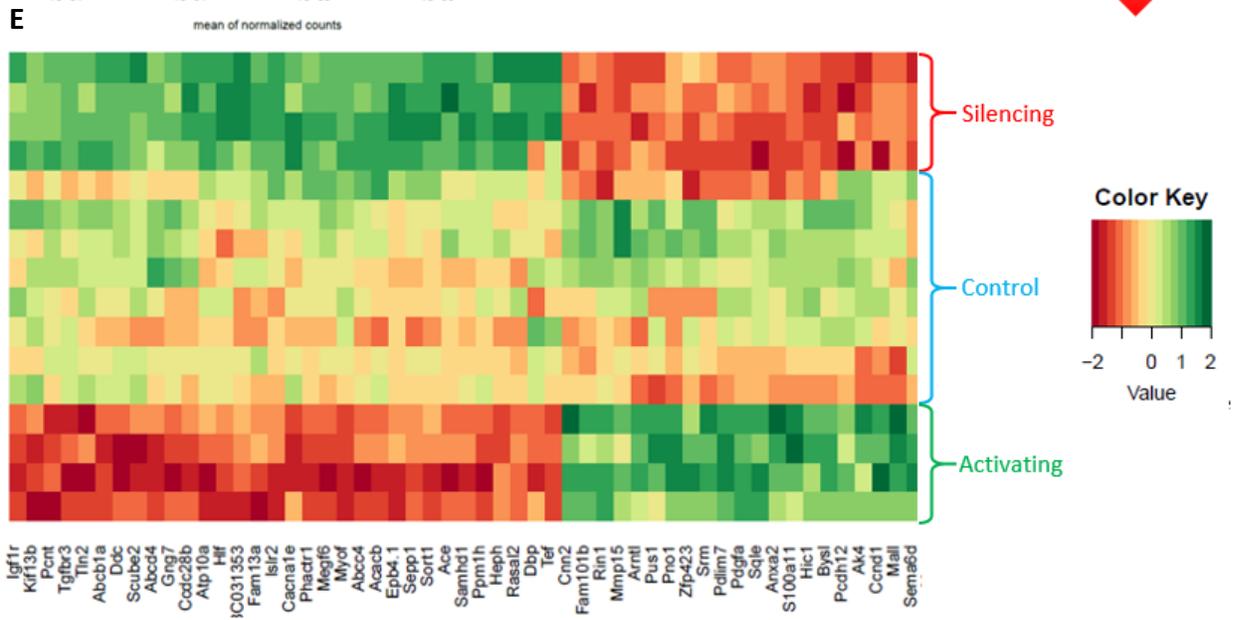
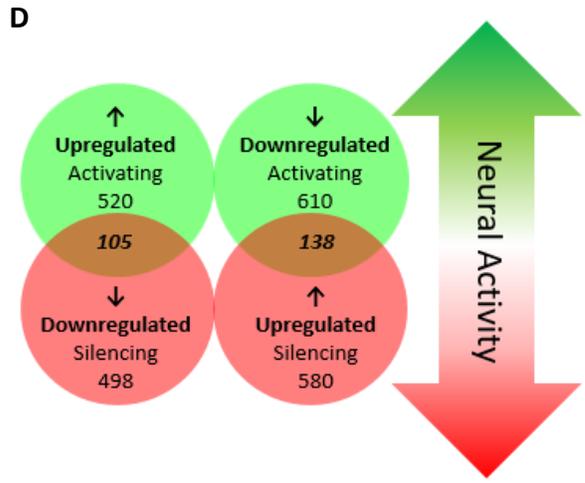
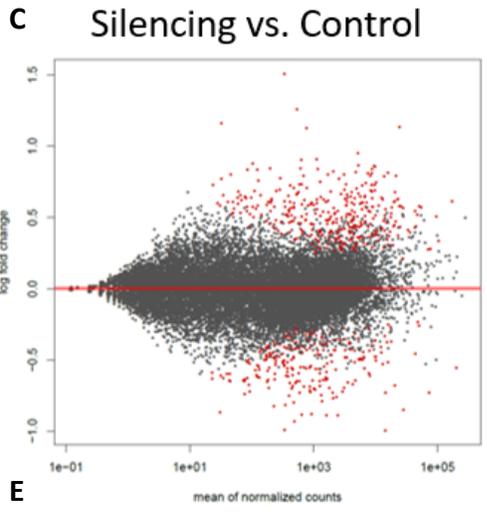
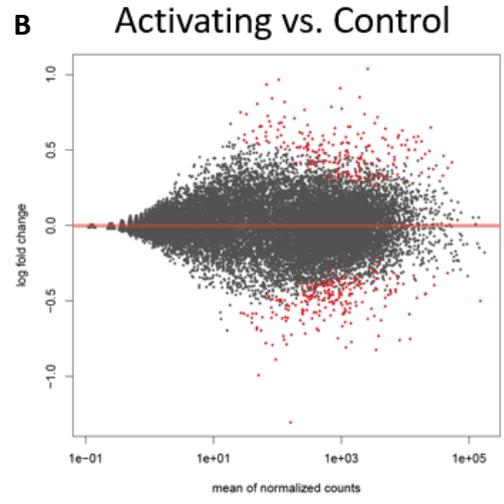
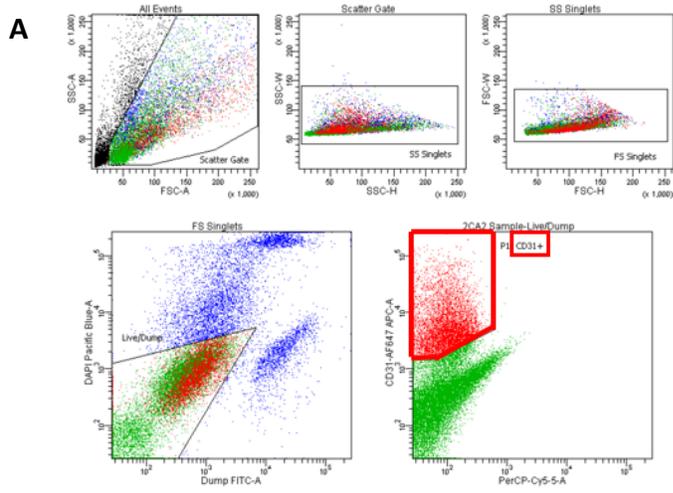


**Figure 2.1: DREADDs as a Tool to Manipulate Glutamatergic Activity *in vivo*.** (A) Schematic representation of the genetic mouse models utilizing DREADDs to activate or silence glutamatergic activity *in vivo*.

(B) Sagittal section of a brain derived from an Activating DREADDs mouse stained for HA (red) and cell nuclei with DAPI (blue).

(C-D) Power density spectrograms depicting gamma local field potential (LFP) power from representative multielectrode array electrophysiological recording sessions from Activating DREADDs mice and controls (C) and Silencing DREADDs mice and control (D). CNO dosages are noted, and delivered when indicated by the green (C) or red (D) arrow on the X-axis. (E-F) Average gamma local field potential (LFP) power as a percentage of the pre-CNO injection baseline for Activating DREADDs mice and controls (E) and Silencing DREADDs mice and control (F).  $n=3$  per group,  $*p<0.05$  by Student's t-test.

**Figure 2.2: DREADDs-Mediated, Neural Activity-Regulated Brain Endothelial Transcriptome.** (A) Representative FACS plot of the gating strategy used to sort brain endothelial cells. First, intact cells were gated using forward and side scatter (top 3 panels). Next, cells were gated against dead cells and (DAPI-positive) and pericytes and immune cells (FITC-positive). Finally, Alexa 647-positive endothelial cells were positively selected. (B) MA plot representing global gene expression changes in brain endothelial cells after glutamatergic activation vs. control. Red dots signify statistically significant changes by Wald Test. n=4 mice per group. (C) MA plot for glutamatergic silencing vs. control. n=4 mice per group. (D) Venn Diagram for statistically significant ( $p < 0.05$  by Wald Test) gene expression changes after glutamatergic activation and silencing. “Neural activity-dependent genes” are the 243 (105 and 138) that were regulated in opposite directions after glutamatergic activation and silencing. (E) Clustering heat map of refined list of neural activity-dependent genes (at least 0.3 log<sub>2</sub> fold change in both directions). Color scale represents arbitrary units of expression. Red represents lower expression and green represents higher expression.



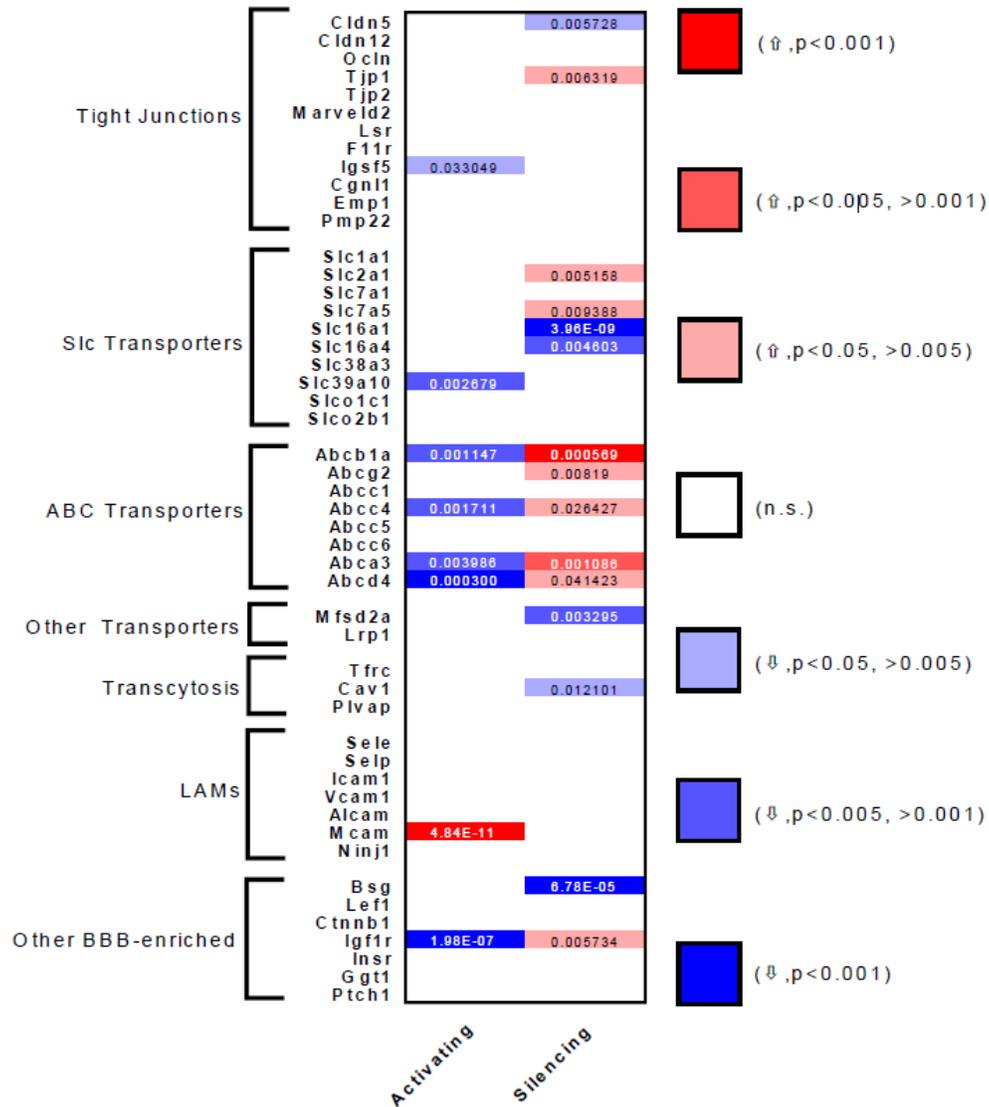


**Figure 2.3: Neural Activity-Regulated BBB Transcriptome.** Heat map for binned p-values and activity-regulated directionality of common BBB genes in Activating vs. Control (left) and Silencing vs. Control (right). Genes were divided into groups for different BBB properties: Tight junctions, Slc transporters, Abc transporters, other transporters, transcytosis, Leukocyte Adhesion Molecules (LAMs), or Other BBB-enriched. Color scale denotes if a given gene was upregulated (↑) (red) or downregulated (↓) (blue) and whether the change was statistically significant by Wald Test (intensity of color). Individual p-values are shown for significantly regulated genes.

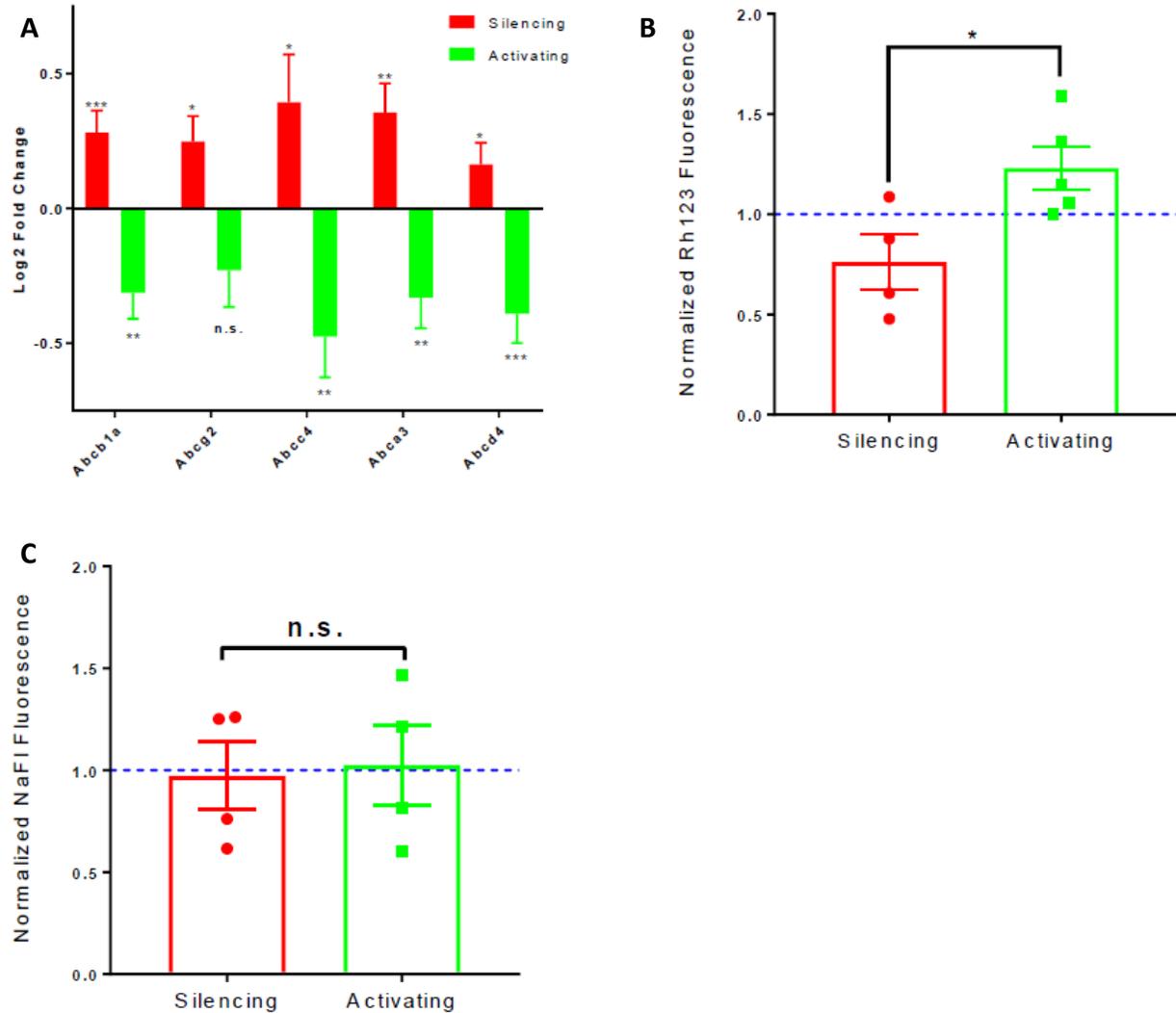


**Figure 2.4: Neural Activity Regulates ABC Transporter Expression and Function.** (A) Log2 fold change of mRNA expression in Activating or Silencing groups relative to respective littermate controls of 5 major BBB-specific ABC transporters after DREADDs-mediated manipulation of glutamatergic activity (~ZT23-ZT24). Data represent mean  $\pm$  SEM (error bars).  $n=4$  per group. \* $p<0.05$ , \*\* $p<0.05$ , \*\*\* $p<0.001$ , n.s. (not significant) by Wald Test. (B) Normalized Rhodamine123 (Rh123) fluorescence of Activating vs. Silencing brains following CNO administration (~ZT3-ZT4). Mutants were paired with littermate control. The rhodamine fluorescence (brain:blood) of each mutant was normalized to the fluorescence of its littermate control (Excitation=505nm, Emission=560nm). Data represents mean  $\pm$  SEM (error bars). Individual data points are shown. \* $p=0.0291$  by Student's t-test. (C) Normalized Sodium Fluorescein (NaFl) fluorescence of Activating vs. Silencing brains following CNO administration (~ZT3-ZT4). Mutants were paired with littermate control. The NaFl fluorescence (brain:blood) of each mutant was normalized to fluorescence of its littermate control (Excitation=480nm, Emission=538nm). Data represents mean  $\pm$  SEM (error bars). Individual data points are shown. n.s. (not significant) by Student's t-test.

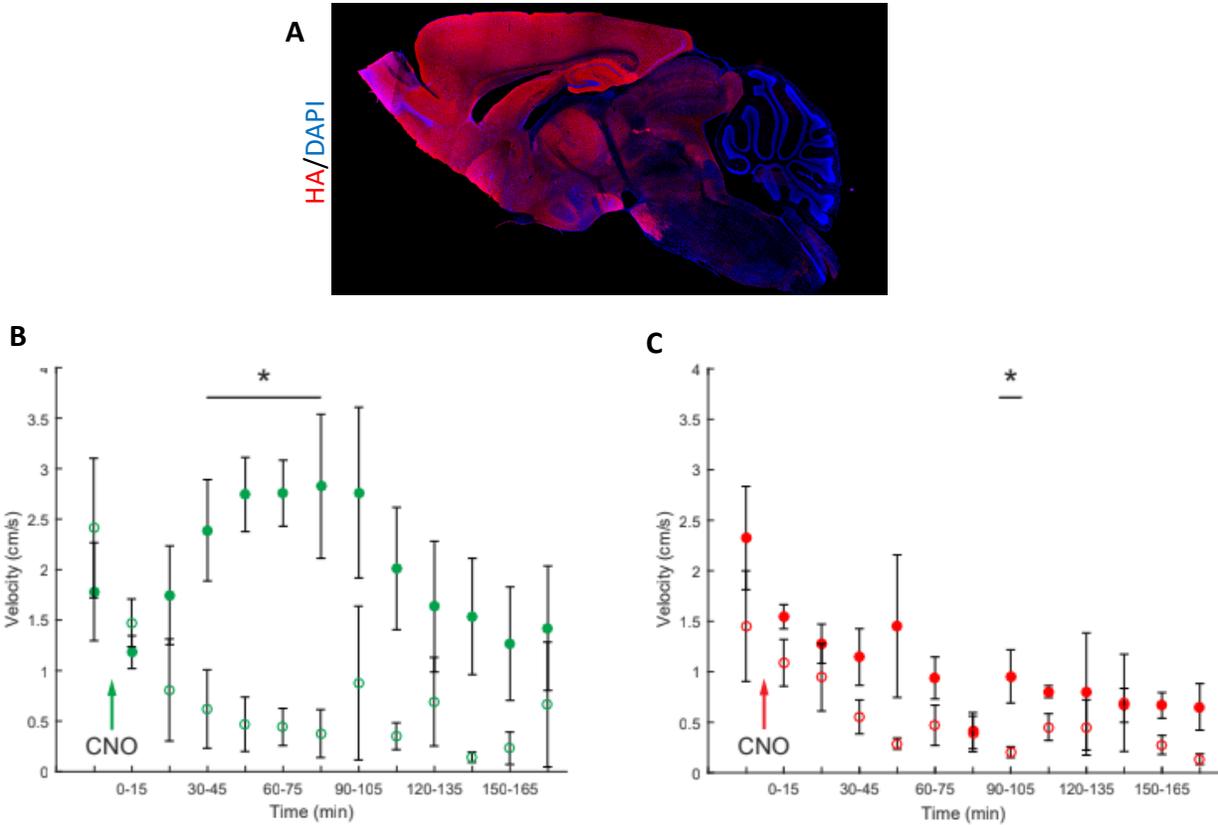
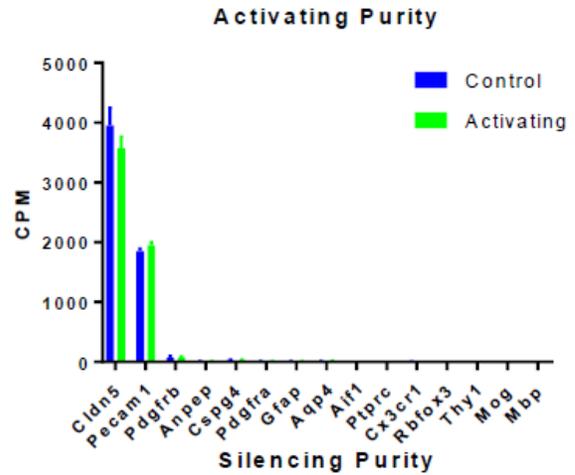


**Figure 2S.1: Further Validation of DREADDs.** (A) Representative sagittal section of Silencing DREADDs mouse brain stained for HA (red) and cell nuclei with DAPI (blue). (B-C) Average velocity of Activating mice vs. paired littermate controls (B) and Silencing mice vs. paired littermate controls (C) over 3 hour recording sessions. n=3 per group, \*p<0.05 by Student's t-test.

**A**

Cell Type	Gene	Control CPM	Activating CPM
Endothelial	Cldn5	3950.45	3569.193
	CD31	1852.826	1947.142
Pericyte	Pdgfrb	71.80941	69.28318
	CD13	8.123434	7.389564
Pericyte/OPCs	NG2	29.28712	29.20847
	Pdgfra	11.84399	10.24598
Astrocytes	GFAP	6.69824	8.634951
	Aqp4	9.345761	14.00008
Microglia	Iba1	0.530904	0.467565
	CD45	0.94533	0.922413
	Cx3cr1	5.016872	5.274231
Neurons	NeuN	0.971562	0.970873
	Thy1	3.092319	3.12039
Oligodendrocytes	Mog	0.107316	0.261564
	Mbp	2.14875	2.286906



**B**

Cell Type	Gene	Control CPM	Silencing CPM
Endothelial	Cldn5	3970.005	2357.484
	CD31	2052.527	1921.881
Pericyte	Pdgfrb	79.26506	94.81409
	CD13	8.777674	9.974195
Pericyte/OPCs	NG2	33.78414	35.34182
	Pdgfra	22.6561	21.91366
Astrocytes	GFAP	12.02751	8.4481
	Aqp4	12.09609	10.32857
Microglia	Iba1	0.305715	0.273614
	CD45	0.894348	0.50944
	Cx3cr1	5.068705	4.107045
Neurons	NeuN	1.066674	1.133582
	Thy1	3.061972	3.14312
Oligodendrocytes	Mog	0.189905	0.127891
	Mbp	2.653085	1.981621

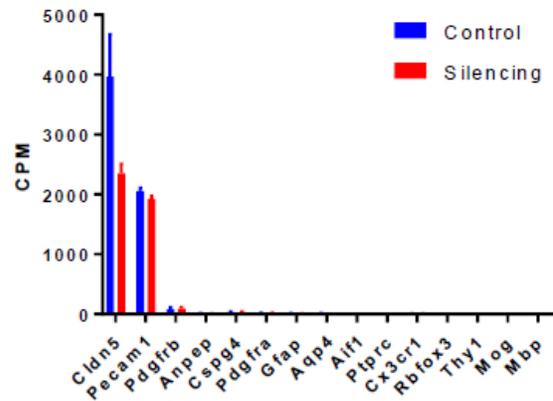


**Figure 2S.2: DREADDs-Mediated, Neural Activity-Regulated Brain Endothelial Transcriptome Cell Purity.** (A-B) The counts per million (CPM) of cell-specific markers in the Activating (A) and Silencing (B) datasets. Raw values for each gene are also listed in the tables (left).

**Table 2S.1: DAVID Pathway Analysis for 748 genes *downregulated* by glutamatergic activation.**

<b>Cluster Number</b>	<b>Gene Functional Annotation</b>	<b>Enrichment Score</b>
1	Oxidoreductase Activity	5.09
2	Endoplasmic Reticulum	4.51
3	Cilium Biogenesis/Degradation	4.12
4	Protein Transport	3.85
5	WD40 repeat-containing domain	3.27
6	Valine, Leucine and Isoleucine Degradation	2.81
7	Peroxisome	2.68
8	Cell projection	2.62
9	Biotin Carboxylation	2.55
10	PIK-related kinase	2.52
11	Lipid Metabolism	2.41
12	Cell Cycle	2.27
13	Protein Kinase Activity	2.2
14	Ciliary Basal Body	2.13
15	Tetratricopeptide repeat	1.93

**Table 2S.2: DAVID Pathway Analysis for 625 genes *upregulated* by glutamatergic activation.**

Cluster Number	Gene Functional Annotation	Enrichment Score
1	Cell-cell Adherens Junction	18.31
2	Actin Filament Binding	10.51
3	Nucleotide Binding	5.82
4	GTP Binding	5.37
5	RNA-binding	4.98
6	Translational Initiation	4.42
7	Protein Transport	3.76
8	Protein Folding	3.58
9	snoRNA Binding	3.43
10	Zinc finger, LIM-type	3.03
11	mRNA splicing	3.02
12	Endosome	2.65
13	Actin Filament Bundle Assembly	2.63
14	Actin Filament Capping	2.62
15	Tubulin	2.51

**Table 2S.3: DAVID Pathway Analysis for 603 genes *downregulated* by glutamatergic *silencing*.**

<b>Cluster Number</b>	<b>Gene Functional Annotation</b>	<b>Enrichment Score</b>
1	Mitochondrion	5.73
2	Cell-cell Adherens Junction	5.68
3	snoRNA Binding	4.28
4	Lipid Metabolism	3.28
5	WD40 repeat-containing domain	3
6	Endoplasmic Reticulum	2.93
7	Box H/ACA snoRNA Binding	2.77
8	Small-Subunit Processome	2.26
9	Ribonucleoprotein	2.23
10	Glycolysis	2.06
11	Heme Biosynthesis	1.86
12	Oxidoreductase	1.84
13	PDZ Domain	1.81
14	Steroid Metabolism	1.68
15	Zinc Finger, LIM Type	1.67

**Table 2S.4: DAVID Pathway Analysis for 718 genes *upregulated* by glutamatergic *silencing*.**

Cluster Number	Gene Functional Annotation	Enrichment Score
1	Pleckstrin Homology Domain	9.02
2	Zinc Ion Binding	7.39
3	Transcriptional Regulation, DNA-binding	6.94
4	GTPase Activation	6.35
5	Guanyl-Nucleotide Exchange Factor Activity	3.95
6	Zinc Finger, PHD type	3.9
7	Src Homology-3 Domain	3.23
8	Phosphotyrosine Interaction Domain	3.17
9	Spectrin Repeat	3.02
10	PDZ Domain	3.01
11	Cell Junction	2.72
12	C2 calcium-dependent membrane targeting	2.53
13	Cell Cycle	2.41
14	Biological Rhythms	2.35
15	SH3	2.17

**Table 2S.5: DAVID Pathway Analysis for 138 genes *upregulated* after glutamatergic *silencing* AND *downregulated* after glutamatergic *activation*.**

<b>Cluster Number</b>	<b>Gene Functional Annotation</b>	<b>Enrichment Score</b>
1	Transcriptional Regulation, DNA-binding	2.93
2	Chromo domain	2.71
3	Cytoskeleton	2.16
4	ABC transporters	1.95
5	Basic-leucine zipper domain, biological rhythms	1.88
6	Chromatin Regulation	1.59
7	C2 calcium-dependent membrane targeting	1.51
8	VEGF Signaling	1.38
9	ATP/Nucleotide Binding	1.38
10	Zinc Finger, PHD type	1.32
11	Phosphatidylinositol signaling	1.2
12	Pleckstrin Homology Domain	1.14
13	Proteoglycans in Cancer	1.13
14	EGF-like Domain	1.1
15	Synaptic Signaling	1.09

**Table 2S.6: DAVID Pathway Analysis for 105 genes *upregulated* after glutamatergic *activation* AND *downregulated* after glutamatergic *silencing*.**

<b>Cluster Number</b>	<b>Gene Functional Annotation</b>	<b>Enrichment Score</b>
1	Cell-cell Adherens Junction	4.95
2	Focal adhesion	4.11
3	RNA-binding	1.89
4	tRNA activity/Protein synthesis	1.24
5	WD40 repeat-containing domain	1.14
6	Ribonucleoprotein	0.99
7	Cell adhesion	0.97
8	Methylation	0.73
9	ATP/Nucleotide Binding	0.7
10	Transcriptional Regulation	0.68
11	Zinc Finger, LIM type	0.58
12	Mitochondrion	0.55
13	Nuclease Activity	0.54
14	Nervous System Development	0.44
15	Endoplasmic Reticulum	0.24

## **MATERIALS AND METHODS**

### **Mouse Strains**

All animal experiments were performed with national and UCSD IACUC guidelines. *CamKIIa-tTA* mice were crossed to *TRE-hM3Dq* mice to generate a tool to activate glutamatergic neurons and *TRE-M4Di* to generate a tool to silence glutamatergic neurons. All mice were kept on a standard 12:12 hour light:dark cycle. Only male mice were used for the transcriptomic experiments. Both male and females were used for all other experiments.

### **Immunohistochemistry**

Mice were anesthetized by i.p. injection of a ketamine/xylazine cocktail and then fixed via transcardial perfusion of D-PBS for 3 minutes, 4% paraformaldehyde (PFA) for 7-10 minutes, and again with D-PBS for 2 minutes using a Dynamax peristaltic pump. Speed was matched to typical cardiac output of a mouse. The brains were then dissected and submersion-fixed in 4% PFA overnight at 4°C. Brains were then submerged in 30% sucrose overnight at 4°C. Brains were then frozen in cryosectioning blocks in a solution consisting of 1:2 30% sucrose: OCT. 40µm sagittal sections were obtained using a cryostat.

Sections were stained floating in solution in the wells of a 12-well cell culture plate. They were blocked in a solution consisting of 5% goat serum and 0.1% Triton X-100 in PBS at room temperature for 45 minutes. They were then incubated in the blocking solution with the primary antibody, Rabbit-anti-HA 1/250 overnight at 4°C. They were then incubated in Goat-anti-Rabbit-Alexa 594 secondary antibody at room temperature for 90 minutes and then mounted on slides with DAPI Fluoromount-G for image processing.

### **Epifluorescence Imaging**

Epifluorescence images of HA-immunostained slides were taken with an Axio Imager D2 (Carl Zeiss) with a 5x Fluor, 0.25 NA using a digital camera (Axiocam HRm, Carl Zeiss).

AxioVision software was used to acquire images. Individual images were stitched together to gain a complete image of a sagittal section of the brain using the photomerge feature of Adobe Photoshop.

### **Multielectrode Array Electrophysiology**

Electrophysiological procedures were performed as described previously(90). Briefly, four-tetrode (bundles of four 17 micron platinum-iridium (90/10%) wires) microdrives were implanted stereotaxically (from bregma: -2.0 mm A/P, +1.8mm M/L, 0.00 mm D/V) into the cortex and hippocampus of adult DREADDs mice and littermate controls. Electrode tips were plated with platinum to reduce electrode impedances to between 150-250 k $\Omega$  at 1 kHz. The mice were given at least 1 week to recover with additional post-operative care administered as needed. For a given recording session, data was collected for 15 minutes while awake behaving mice were in their home cage to establish an internal control of the baseline level of neural activity. The mouse was then injected with the given dose of CNO (0.5 mg/kg or 1.0 mg/kg) intraperitoneally (i.p.). Data was collected for 3 more hours post-injection in the home cage. A preamplifier, tether, and a 32-channel digital data acquisition system (Neuralynx, Inc.) was used. LFP was sampled at 32,000 Hz and filtered between 1 and 1,000 Hz. Wavelet power was calculated by first downsampling by a factor of 25 and filtered between 30-150 Hz. The average gamma power was calculated every 15 minutes beginning with the 15 minutes prior to the CNO injection (“preCNO”), and every 15 minutes following for 3 hours. The percentage of baseline wavelet power was calculated by taking each 15 minute data point and dividing by the preCNO gamma power. Locomotion was tracked via head-mounted LEDs and a camera facing down onto the mouse cage. Average velocity was calculated by taking the instantaneous velocity using the x and y coordinates and averaging over every 15 minutes.

After all recordings were completed, mice were perfused with PBS followed by 4% paraformaldehyde in PBS solution. Brains were post-fixed for an additional 24 hours in 4% paraformaldehyde and then cryoprotected using a 30% sucrose solution for an additional 2 days. Brains were frozen and sliced into 40  $\mu$ m coronal sections on a sliding microtome. Sections were mounted on electrostatic slides and stained with cresyl violet to visualize recording locations for validation of electrode placement.

### **FACS-purification of Brain Endothelial Cells**

For a given experiment, mice were collected in pairs consisting of one DREADDs mouse and one littermate control mouse. Each DREADDs mouse and its littermate control was injected i.p. with the electrophysiologically-verified dose of CNO (0.5mg/kg for Activating mice and 1.0mg/kg for Silencing mice) at approximately ZT23-ZT24. Behavior was closely monitored for 3 hours and the experiment was aborted if behavioral seizures were observed. 3 hours post-injection the mice were live-decapitated using a mouse decapitator (LabScientific, XM-801). Brains were dissected out, the meninges were removed and the cortex and hippocampus were dissected out for further processing. The tissue was then diced using a #10 blade and enzymatically digested in Papain, 1 vial per on a 33° heat-block while being exposed to 95% oxygen, 5% carbon dioxide for 90 minutes. The tissue was then triturated and a second enzymatic digestion was performed in 1.0 mg/ml Collagenase Type 2 and 0.4 mg/ml Neutral Protease on a 33° heat-block while being exposed to 95% oxygen, 5% carbon dioxide for 30 minutes. Myelin was then removed as recommended with myelin removal beads using 30 $\mu$ m filters (MACS Miltenyi Biotec, 130-041-407) and LS columns (MACS Miltenyi Biotec, 130-042-401) on a MidiMACS separator (MACS Miltenyi Biotec, 130-042-302). The remaining single cell suspension was blocked with Rat IgG 1/100 for 20 minutes on ice. The samples were then stained with Rat-anti-CD31-Alexa 647, 1/100,

mouse-anti-CD45-FITC 1/150, rat-anti-CD13-FITC 1/100, rat-anti-CD11b-FITC 1/100, rabbit-anti-NG2-Alexa 488 1/150, and DAPI for 20 minutes at 4°. CD31-positive cells were sorted into Trizol using an ARIA II instrument at the Flow Cytometry Core at the VA Hospital in La Jolla, CA.

### **RNA-sequencing**

RNA was harvested from the FACS-purified brain endothelial cells using the Qiagen RNeasy Microkit. RNA samples were then further processed at the UCSD Genomics Core using standard core procedures. The RNA was tested for quality and concentration using a tape station bioanalyzer. Next, cDNA libraries were made using the TruSeq RNA Library Prep Kit v2. Samples were then sequenced on an Illumina HiSeq4000, 150 based, paired ends.

Sequence reads for all samples were mapped to Ensembl mm9 v67 mouse whole genome using Tophat v 2.0.11 and Bowtie 2 v 2.2.1 with parameters no-coverage-search -m 2 -a 5 -p 7. Alignment files were sorted using SAMtools v.0.1.19. Count tables were generated using HTSeq-0.6.1. Differential expression of genes between control and treated samples, log 2-fold changes between control and treated samples, and statistical analysis including p values and FDR was performed using DESeq2 and Excel.

### **Rhodamine123 Permeability Assay**

Rhodamine123 was dissolved in DMSO to make a stock solution of 10mg/ml. For each experiment, a working solution of 2 mg/ml was made by diluting the stock solution with saline. For a given DREADDs experiment, mice were collected in pairs and injected with CNO at approximately ZT3-ZT4 as described in the FACS-purification section (Activating mice were injected with 0.45mg/kg CNO instead of 0.5mg/kg as they were more susceptible to seizures when also injected with Rhodamine123). 2 hours post-CNO injection, the mice were then injected i.p.

with 25mg/kg Rhodamine123. 3.75 hours post-CNO injection and 15 minutes before the collection, the mice were then anesthetized by i.p. injection of ketamine/xylazine. Blood was collected via cardiac puncture and kept in an EDTA-coated tube rotating until the end of the tissue collection procedure. The mice were then perfused with D-PBS for 3 minutes using a Dynamax peristaltic pump. Brains were dissected, meninges removed and the cortex and hippocampus were then dissected out. The remaining tissue was flash frozen in liquid nitrogen and then stored at -80°C until Rhodamine123 was extracted. The blood samples were then centrifuged. The supernatant (plasma) was collected and stored at -80°C until Rhodamine123 was extracted.

Once Rhodamine123 was ready to be extracted from the collected tissue, the brains were weighed and added to tubes with cold PBS (mass/volume-adjusted). They were then homogenized using a bead beater homogenizer. The homogenized tissue was eluted by centrifugation. The Rhodamine123 extraction was performed on the homogenized brain tissue and plasma as described previously with slight modifications to adjust for input mass and volume(91). Briefly, n-butanol was added to the samples which were then vortexed. These steps were repeated once and the samples were incubated overnight at 4°C rotating. The samples were then vortexed, spun down and the supernatant was collected. The remaining pellet was then washed with an equivalent volume of n-butanol, the samples vortexed, spun down and the supernatant was collected. The samples were then added to a 96-well plate with 4 technical replicates per sample. A standard curve and blanks were also run to ensure that Rhodamine measurements were above the detectable limit. The plate was analyzed on a Tecan Infinite plate reader (Excitation=505nm, Emission=560nm). Brain:Blood ratios were calculated for each sample by taking the average of the technical replicates. To directly compare Activating to Silencing groups, each DREADDs

sample's ratio was then normalized to its paired littermate control sample's ratio to obtain the "Normalized Rhodamine Fluorescence".

### **Sodium Fluorescein Permeability Assay**

Sodium Fluorescein was dissolved in sterile PBS to make 10 mg/ml. For each experiment, a working solution of 2 mg/ml was made by diluting the stock solution with sterile PBS. Tissue collection was carried out identical to rhodamine permeability experiments (dosage was 25 mg/kg).

Brain tissue was homogenized identical the Rhodamine extraction. The brain homogenates were then centrifuged and the resulting supernatant was diluted 1:1 in 2% TCA. Plasma samples were diluted 1:400 in sterile PBS, followed by an additional 1:1 dilution in 2% TCA. Brain and plasma samples were incubated overnight rotating at 4°C. Both sets of samples were then centrifuged and the supernatants were diluted 1:1 in borate buffer, pH 11. The samples were then added to a 96-well plate with 4 technical replicates per sample. A standard curve and blanks were also run to ensure that sodium fluorescein measurements were above the detectable limit. The plate was analyzed on a Tecan Infinite plate reader (Excitation=480nm, Emission=538nm). Data was analyzed identical to the rhodamine experiment.

## **ACKNOWLEDGEMENTS**

This work was in part supported by the UCSD Graduate Training Program in Cellular and Molecular Pharmacology through an institutional training grant from the National Institute of General Medical Sciences, T32 GM007752 and NIH/NINDS R01 NS091281 Diversity Supplement (R.S.P.) This work was also funded by NIH/NINDS R01 NS091281, Rita Allen Foundation, Klingenstein-Simons Foundation, and CureAlz Foundation (R.D.). The authors would like to acknowledge the UCSD Genomics Core and the VA Flow Cytometry Core in La Jolla, CA. The authors have no conflicts of interest to declare.

This chapter is part of a manuscript under revision for publication of the material as it may appear in *Neuron*, 2019, Pulido RS, Munji RN, Chan TC, Quirk CR, Weiner GA, Weger BD, Elmsaouri S, Malfavon M, Gachon F, Leutgeb S, Daneman R. The dissertation author is the primary investigator and first author of this material.

### **CHAPTER THREE:**

The Role of Endothelial Circadian Clock Genes in Mediating Neural Activity-Dependent  
Regulation of Blood-Brain Barrier Efflux and Brain Function

## INTRODUCTION

We identified that the proline and acidic amino acid-rich basic leucine zipper (PAR bZip) family of circadian transcription factors consisting of *Dbp*, *Tef* and *Hlf* are regulated by neural activity (Table 2S.5). Circadian rhythms are intrinsic oscillatory biological processes that are driven by a stereotyped transcriptional feedback loop and govern oscillation of a variety of physiological processes such as sleep, renal activity, cardiovascular function, gastrointestinal tract motility, immune response and metabolism(92). The core circadian transcriptional machinery consists of *Bmal1* and *Clock* in the positive loop which drive transcription of many downstream genes such as the PAR bZip transcription factors, and *per* and *cry* which make up the negative loop and act as negative feedback regulators on *Bmal1* and *Clock*(93–97).

The circadian clock has mostly been studied in the context of the suprachiasmatic nucleus (SCN) of the hypothalamus, the central pacemaker which is entrained by light and synchronizes many of the body's biological rhythms(98,99). However, the core clock transcriptional machinery exists in many non-neuronal cells both in the brain and peripheral tissues, including the vasculature. Our data demonstrates that endothelial circadian genes are tightly regulated by neural activity suggesting that these circadian genes may not only regulate processes controlled by cell intrinsic oscillatory gene networks, but by processes modulated by neuronal activity. Although there has been evidence implicating a significant role of the circadian clock in blood vessel tone of vertebrates and the glial-based BBB in flies, the role of an endothelial circadian clock in the BBB of mammals has not been studied(100–105). Interestingly, global triple knockouts of the PAR bZip transcription factors exhibit aberrant hyperactive neural activity, defective xenobiotic efflux in the liver (downregulation of Pgp (*Abcb1b* in the liver), MRP4 (*Abcc4*) and BCRP

(*Abcg2*)), low circulating endogenous steroids and low blood pressure, but cell-specific roles for these phenotypes have not been explored(106–108). Therefore, it is plausible that endothelial PAR bZip transcription factors are mechanistically mediating the neural activity-dependent regulation of BBB efflux which may reciprocally affect brain function.

## RESULTS

### Neural activity regulates endothelial PAR bZip transcription factors

We had previously demonstrated that neural activity regulates BBB efflux transporter expression and function such that it is upregulated after glutamatergic silencing and downregulated after glutamatergic activation (Chapter 2). The expression of the PAR bZip transcription factors (*Dbp*, *Tef*, *Hlf*) were similarly regulated by neural activity to the ABC efflux transporters in that their expression was decreased after DREADDs activation and increased after DREADDs silencing (Figure 3.1 A), which led us to hypothesize that expression of these clock output genes and ABC efflux transporters may be linked. It is worth noting that both *Arntl* (*Bmal1*) of the positive loop and *Cry1* of the negative loop were regulated in the opposite manner and were positively correlated with neural activity (Figure 3S.1). However, this modulation of the PAR bZip transcription factors could be explained by the expression of *Nr1d2* (REV-ERB $\beta$ ), another major circadian transcription factor in the core clock, whose expression was inversely correlated with neural activity (Figure 3S.1). Interestingly, it has recently been reported that flies exhibit a circadian oscillation of BBB efflux transport(105), suggesting that the activity dependent regulation of BBB efflux may be downstream of these endothelial circadian clock genes.

### PAR bZip transcription factors are required for diurnal rhythmic expression of BBB efflux

We next set out to determine whether there was a diurnal rhythm of BBB efflux in mice, and whether this was controlled by the endothelial-specific circadian genes. Mice are active during their dark period (ZT12-ZT24) and rest during their light period (ZT0-ZT12), thus exhibiting higher excitatory neural activity during the dark period associated with wakefulness and lower excitatory neural activity during the light period associated with sleep(62,109). We observed that there was diurnal oscillation of *Pgp/Abcb1a* transcripts in brains of wildtype mice with a peak

occurring at ZT12 (ZT13 on the fit curve), the end of the resting light period and a trough occurring at ZT0, the end of the active dark period, corresponding with its expression after manipulation of neural activity (Figure 3.1 B). This rhythmic oscillation was largely abolished in the brains of the PAR bZip triple knockout (tKO) mice (Figure 3.1 B). Although there were daily low amplitude changes in the expression of *Abcb1a* in the brains of tKO mice, our statistical framework identified the pattern as non-rhythmic. This suggests that the PAR bZip transcription factors modulate diurnal expression of *Pgp*. Importantly, the PAR bZip triple knockout mice still exhibit relatively normal circadian behavior with respect to locomotor activity(106).

### **Generation and characterization of endothelial-specific, tamoxifen-inducible *Bmal1* conditional knockout**

In order to determine if the circadian clock gene-dependent regulation of BBB efflux transport was specific to its function in endothelial cells, we generated tamoxifen-inducible, endothelial-specific *Bmal1* knockout mice (*VECadherin-CRE<sup>ERT2</sup>; Bmal1<sup>fl/fl</sup>*) with cre-negative littermate controls (*Bmal1<sup>fl/fl</sup>*). *Bmal1* is the master regulator of the positive loop in the circadian transcriptional machinery, and thus deletion of *Bmal1* in endothelial cells will disrupt circadian oscillation of *Dbp*, *Tef* and *Hlf* (Figure 3S.2 A)(94–97). We FACS-purified both endothelial and non-endothelial cell populations from endothelial-specific *Bmal1* conditional knockouts (EC-*Bmal1* cKOs) and littermate controls (*Bmal1<sup>fl/fl</sup>*), purified the genomic DNA, and demonstrated via PCR that we are indeed excising the *Bmal1* gene exclusively in endothelial cells and only in the EC-*Bmal1* cKOs with this genetic strategy (Figure 3S.2 B, Figure 3S.2 C). We also showed via immunofluorescence of brain sections from a *VECadherin-CRE<sup>ERT2</sup>*-driven *tdTomato* reporter mouse that the cre is exclusively active in endothelial cells (Figure 3S.2 D). Moreover, we found that the EC-*Bmal1* cKO mice and littermate controls both have normal diurnal behavior,

displaying a nocturnal eating and drinking schedule (Figure 3S.2 E, Figure 3S.2 F), suggesting that inhibition of the endothelial clock does not interfere with the overall rhythmic activity of the mouse. Therefore, we generated a reliable genetic tool to ablate endothelial circadian clock genes in adulthood.

### **Endothelial circadian clock genes are required for diurnal rhythmic function of BBB efflux**

We next injected Rh123 into EC-Bmal1 cKO and littermate controls at four different time points throughout the day and collected their brains and blood for analysis of Rh123 brain permeability. We observed a rhythmic oscillation of Rh123 permeability that was inversely correlated with the rhythmic expression of *Abcb1a* in wildtype animals (Figure 3.2 A), demonstrating that there is indeed diurnal oscillation of BBB efflux. We observed that at the end of the active dark period (ZT0), there was low expression of Pgp and more Rh123 accumulation in the brain, whereas at the end of the rest light period (ZT12), there was high expression of Pgp and less Rh123 accumulation in the brain. Thus similar to our chemogenetics experiments, the expression and function of BBB efflux inversely correlates with mouse activity. This rhythmic oscillation of Pgp function was inhibited in EC-Bmal1 cKO mice suggesting that the rhythmic oscillation of BBB efflux transport was dependent on proper function of endothelial *Bmal1* (Figure 3.2 A). We did not observe diurnal oscillation of NaFl permeability in either genotype (Figure 3.2 B), suggesting that the diurnal oscillation was specific to BBB efflux, and not paracellular permeability. Taken together this data demonstrates that neural activity regulates the levels of endothelial circadian clock genes, which in turn regulate the levels of Pgp efflux transport.

### **Neural activity regulates BBB efflux *through* endothelial circadian clock genes**

In order to demonstrate the complete epistatic relationship of endothelial circadian clock genes in mediating neural activity-dependent regulation of BBB efflux, we sought to manipulate

activity in EC-Bmal1 cKOs and littermate controls. If endothelial circadian clock genes were indeed the mechanism, we would expect to observe the same neural activity-dependent regulation in the littermate controls we observed in DREADDs mice, but not in the EC-Bmal1 cKOs. In order to manipulate glutamatergic activity in these animals, we injected vehicle or the glutamatergic receptor agonist kainic acid at a subseizure dose into EC-Bmal1 cKOs and littermate controls, FACS-purified the brain endothelial cells from the four groups, and performed RT-qPCR for *Abcb1a*. Kainic acid was sufficient to cause a significant decrease in *p-gp* expression in the littermate controls, similar to what we observed with DREADDs mediated glutamatergic activation, whereas it caused no significant change in *p-gp* expression in the EC-Bmal1 cKOs (Figure 3.3). This suggests that endothelial circadian clock genes are required for neural activity-dependent regulation of BBB efflux.

### **The endothelial circadian clock regulates affect-related behavior**

Our lab has previously shown that *p-gp* is not only important for the transport of xenobiotics but also endobiotics, and that without functional *p-gp*, there is dysregulation of endogenous steroids in the brain and consequently behavioral deficits(7). Since we demonstrated that diurnal *p-gp* expression and function is altered in EC-Bmal1 cKOs, it is plausible that this could have an effect on neurochemical balance and thus affect brain function. In order to assess whether cognitive function was affected, we performed a battery of behavioral tests on EC-Bmal cKOs and littermate controls.

We first tested whether abolishing the clock in endothelial cells would affect learning and memory in the novel object recognition (NOR) test because *Bmal1* global knockouts have been shown to have deficits in long and short term memory(110). The NOR test evaluates the mouse's ability to distinguish a novel object from a familiar object. A mouse with normal learning and

memory skills spends more time exploring a novel object compared to a familiar object, whereas a mouse with impaired learning and memory could spend equal or less time exploring the novel object. We observed no statistically significant difference between EC-Bmal1 cKOs and littermate controls in the discrimination index (Figure 3S.3 A), the ability to discriminate the novel object from the old object, nor in the total amount of time spent exploring the objects (Figure 3S.3 B). This indicates that abolishing the clock in endothelial cells does not affect learning and memory behavior nor general locomotion.

We next wanted to test whether affect-related behavior was affected in the EC-Bmal1 cKOs since we previously observed that disrupted *pgp* causes anxiety(7). In order to test anxiety-related behavior we performed the open field test in which mice are placed in an open arena in which anxious mice will spend more time in the periphery of the field and less anxious mice will spend more time in the middle of the field. Surprisingly, we found that for both EC Bmal1 cKOs and littermate controls spent approximately equivalent amounts of time in the inner portion of the field suggesting that there is no difference in anxiety-related behavior (Figure 3S.3 C). However, we found that EC-Bmal1 cKOs had a significantly greater average immobility time compared to littermate controls in the tail suspension test, a proxy for depression which quantifies learned helplessness (Figure 3.4). This suggests that endothelial circadian clock genes are involved in regulating brain function in the context of affect-related behavior.

## DISCUSSION

Here, we demonstrated that neural activity drives diurnal oscillation of BBB efflux expression and function and that this relationship is dependent on endothelial circadian clock genes. Further, we showed that this pathway is required for behavioral homeostasis and that dysregulation of it causes depressive behavior.

This diurnal oscillation of BBB efflux in mice which is consistent with work done the glial-based BBB of fruit flies, suggesting that there is an evolutionarily conserved mechanism to control the amount of efflux throughout the day(105). The diurnal permeability to Rhodamine in the two organisms are inversely correlated which is consistent with the fact that flies are diurnal and mice are nocturnal when kept on a standard 12:12 hour light:dark cycle. Thus in both cases, the amount of efflux transport decreases with the activity of the organism. This phenomenon has important clinical implications for chronopharmacology, drug treatment that takes the body's circadian rhythm into consideration as time of day variation may affect the efficiency of drug delivery to the CNS and thus efficacy within the brain. Our work further shows that this diurnal oscillation isn't entirely controlled by cell intrinsic gene oscillation, as neuronal activity can modulate the levels and function of efflux through regulation of the circadian genes. This identifies that diurnal oscillatory functions can be modulated by neuronal activity and behavior.

This study also demonstrated the first known example of circadian-related oscillation of the BBB in mammals. Although the brain vasculature has previously been shown to exhibit some oscillatory gene expression(104), it is still unknown to what extent global gene expression oscillates in a circadian gene-dependent manner in brain endothelial cells. It would be interesting to perform gene profiling of brain endothelial cells at various diurnal time points in EC-Bmal cKOs

and littermate controls. This would elucidate which brain endothelial genes exhibit diurnal oscillation and which of those are dependent on expression of endothelial circadian genes.

Interestingly, depression and other mood disorders have considerable evidence linking them to dysregulated circadian rhythms. It has been proposed that disturbances may result from phase shifts in the central pacemaker and its function in regulating body temperature, cortisol and melatonin levels, and rapid-eye-movement sleep(111). Other than phase shifts in SCN output, cerebral vascular disease has also been implicated as possible cause of depression. The “vascular depression” hypothesis proposes cerebrovascular defects have adverse effects on brain circuitry and contribute to the development of late-life depression in elderly people(112). Although the mechanism of this phenomenon is unclear, our work suggests that perhaps dysregulation of endothelial circadian clock genes may impair BBB efflux transport leading to neurochemical imbalance and depression. This may also be an upstream driver of Alzheimer’s pathogenesis (Chapter 5).

## FIGURES

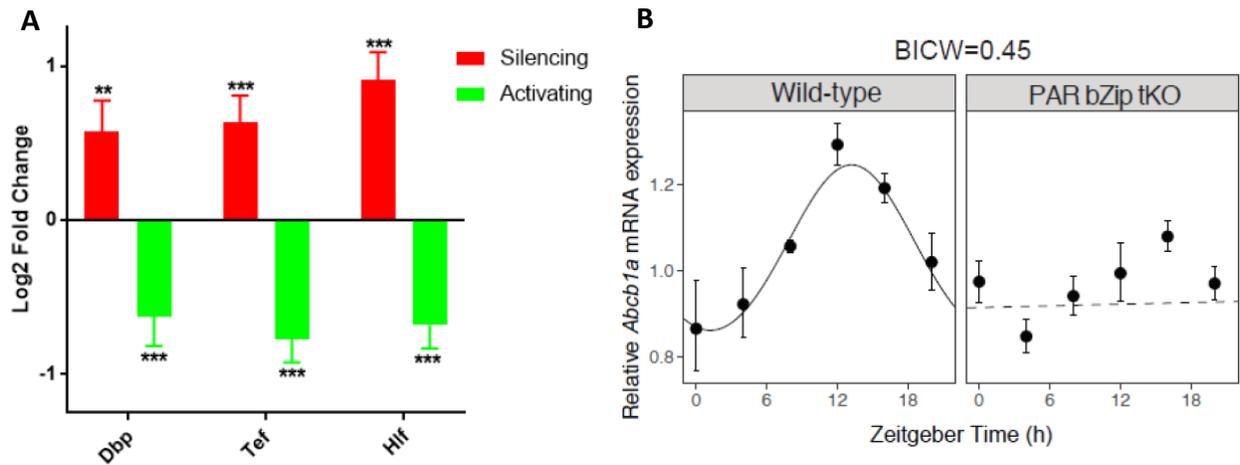


**Figure 3.1: Neural Activity-Regulated Endothelial PAR bZip Transcription Factors are required for Diurnal Rhythmic Expression of Pgp.** (A) Log2 fold change of mRNA expression in Activating or Silencing groups relative to respective littermate controls of 3 PAR bZip transcription factors after DREADDs-mediated manipulation of glutamatergic activity. Data represent mean  $\pm$  SEM (error bars). n=4 mice per group. \*\*p<0.005, \*\*\*p<0.001 by Wald Test. (B) Relative mRNA expression of *Abcb1a* normalized to *GAPDH* across a 24 hour day (12:12 hour dark:light) in Wildtype (left) and PAR bZip triple knockout mice (right). Expression levels represent  $2^{-\Delta\Delta ct}$ . Data represent mean  $\pm$  SEM (error bars). n=4 mice per group. Rhythmicity was assessed by linear regression. Results are represented as lines if the statistical model indicates rhythmicity. Non-rhythmic fits are represented by dashed lines.

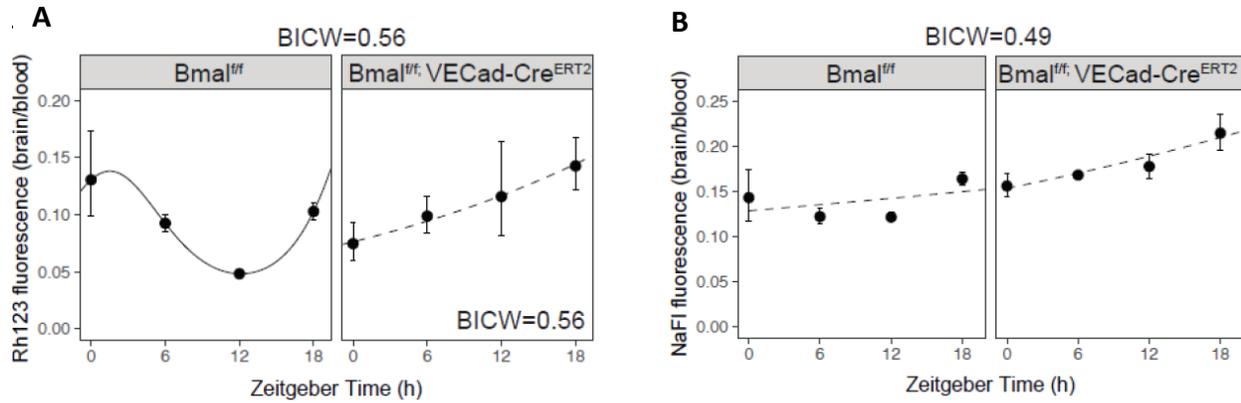


**Figure 3.2: Endothelial Circadian Clock Genes are required for Diurnal Rhythmic Function of BBB Efflux.** (A) Rhodamine123 (Rh123) fluorescence (brain:blood) in littermate controls (left) and endothelial-*Bmal1* knockout mice (right) across a day (Excitation=505nm, Emission=560nm). Data represent mean  $\pm$  SEM (error bars). n=3-7 mice per group. (B) Sodium Fluorescein (NaFl) fluorescence (brain:blood) in littermate controls (left) and endothelial-*Bmal1* knockout mice (right) across a day (Excitation=480nm, Emission=538nm). Data represent mean  $\pm$  SEM (error bars). n=3-6 mice per group. Rhythmicity was assessed by linear regression. Results are represented as lines if the statistical model indicates rhythmicity. Non-rhythmic fits are represented by dashed lines.

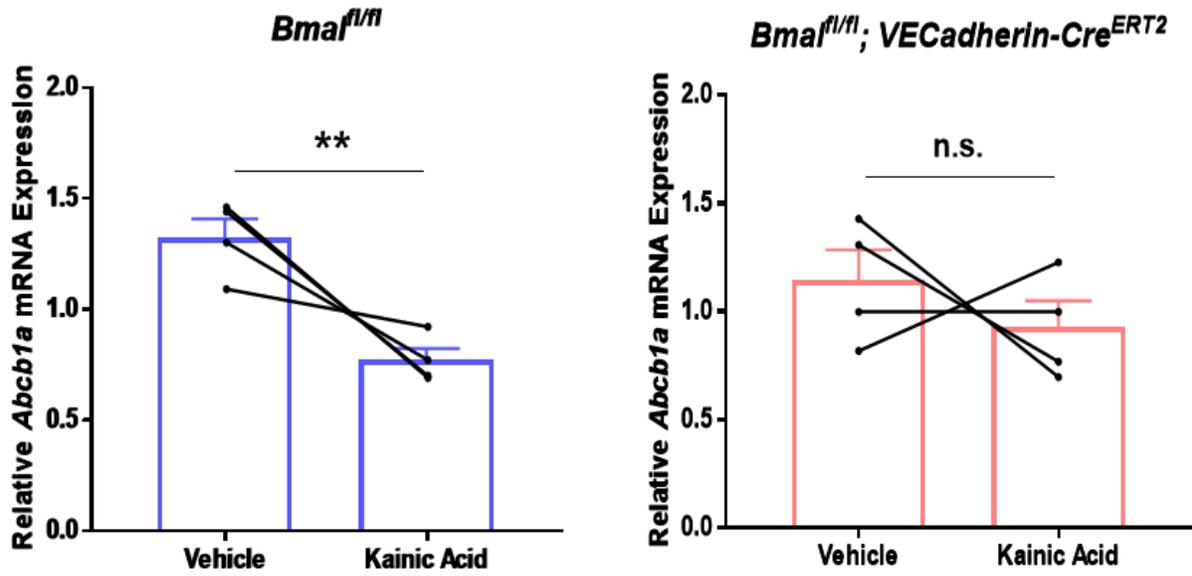


**Figure 3.3: Neural Activity Regulates BBB Efflux through Endothelial Circadian Clock Genes.** Relative mRNA expression of *Abcb1a* normalized to *Rps20* after administration of vehicle or kainic acid in littermate controls (left) endothelial-*Bmal1* knockout mice (right). Expression levels represent  $2^{-\Delta\Delta ct}$ . Data represent mean  $\pm$  SEM (error bars). n=4 mice per group. Individual pairs are shown. \*\*p<0.005 by Paired Student's t-test.

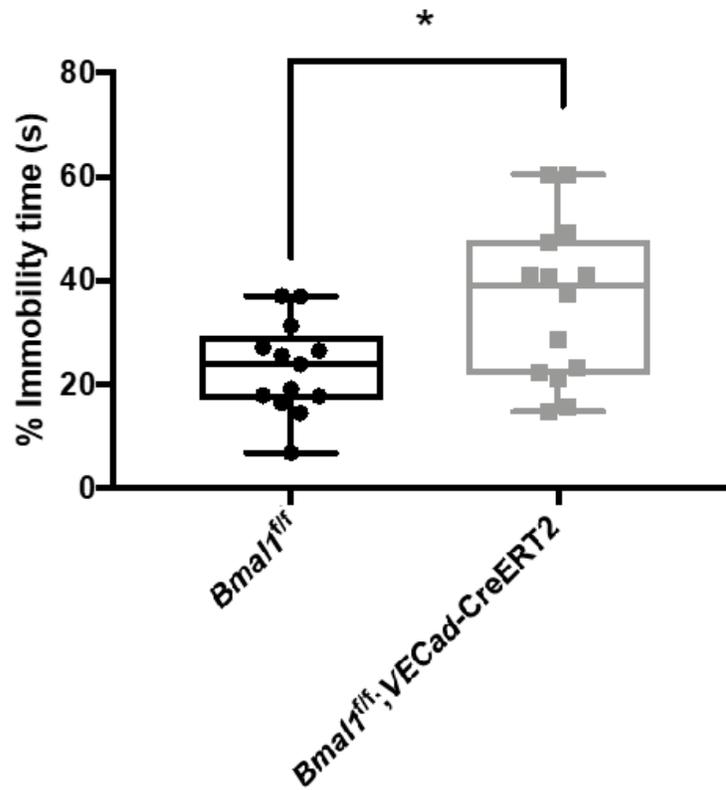


**Figure 3.4: EC-Bmal1 cKOs display Depressive-like Behavior.** The tail suspension test. Data displays total amount of time immobile in littermate controls (left) endothelial-*Bmal1* knockout mice (right). Data represent mean  $\pm$  SEM (error bars).  $n=13$  for *Bmal1<sup>fl/fl</sup>*,  $n=14$  for *Bmal1<sup>fl/fl</sup>; VECad-CreERT2*. Individual replicates are shown.  $p=0.0140$  by Student's t-test.

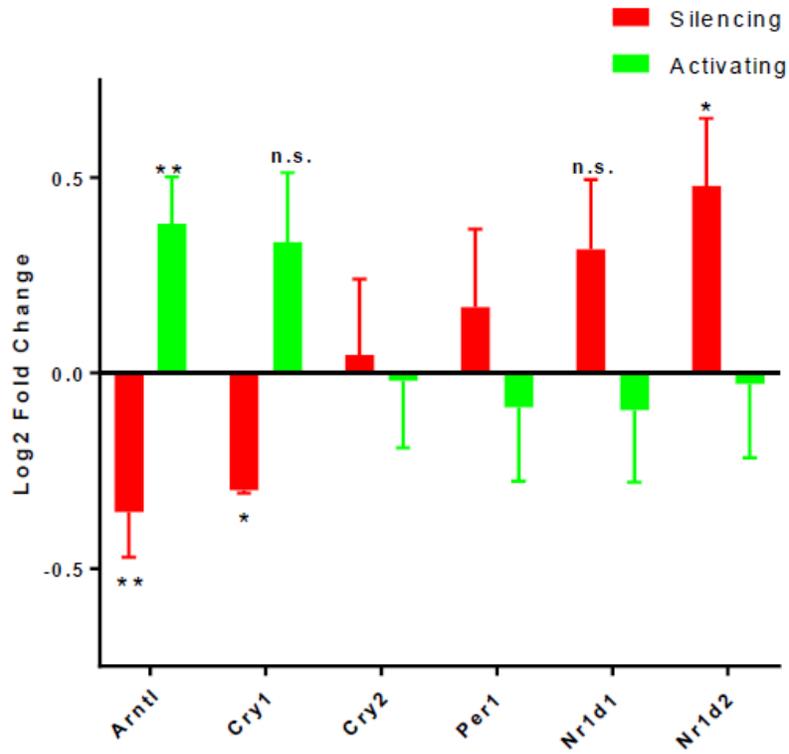
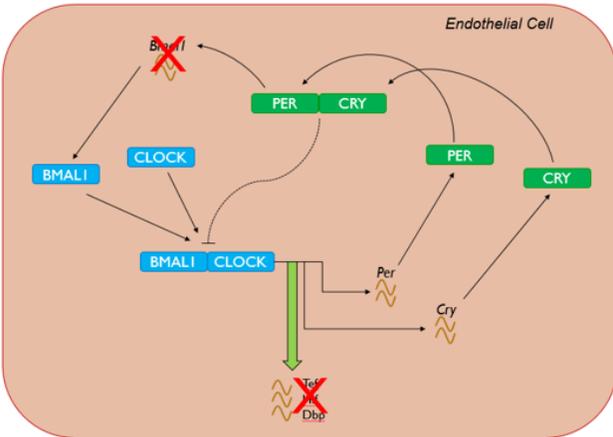
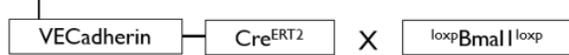


**Figure 3S.1: DREADDs-Mediated, Neural Activity-Regulated Endothelial Circadian Clock Genes.** Log2 fold change of mRNA expression in Activating or Silencing groups relative to respective littermate controls of canonical circadian clock genes in brain endothelial cells after DREADDs-mediated manipulation of glutamatergic activity. Data represent mean  $\pm$  SEM (error bars). n=4 mice per group. \*p<0.05, \*\*p<0.005, n.s. (not significant) by Wald Test.

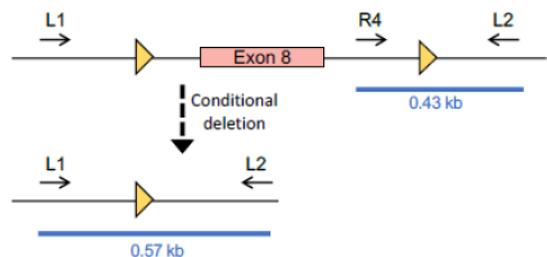
**Figure 3S.2: Generation and Characterization of EC-Bmal cKO Mice.** (A) Schematic of genetic strategy to modulate circadian gene oscillation exclusively in endothelial cells in response to tamoxifen. *Bmal1* floxed mice were mated to VECadherin-Cre<sup>ERT2</sup> mice and injected with tamoxifen at 5 week of age. Ablation of *Bmal1*, the master regulator of the positive loop will ablate typical expression of PAR bZip transcription factors. (B) Schematic of conditional disruption of *Bmal1* and expected PCR product sizes. Yellow triangles represent loxP sites. L1, R4, and L2 represent primers. Adopted from Figure 5A of Storch et al 2007. (C) Schematic of strategy to purify CD31<sup>+</sup> (endothelial) cells CD31<sup>-</sup> (non-endothelial) cells to determine if *Bmal1* was disrupted from the cells' genomes of endothelial-specific *Bmal1* knockout mice and littermate controls. (D) Representative image of section stained with CD31 (green) and endogenous tdTomato fluorescence (red) in VECadherin-Cre<sup>ERT2</sup>; Rosa-lsl-tdTomato mice and wildtype controls in the cortex. (E) Water intake at the end of the dark and light periods across 4 days in endothelial-specific *Bmal1* knockout mice and littermate controls. n=8-9 per group. (F) Chow intake at the end of the dark and light periods across 4 days in endothelial-specific *Bmal1* knockout mice and littermate controls. n=8-9 per group.

**A Tamoxifen-inducible Endothelial-specific**

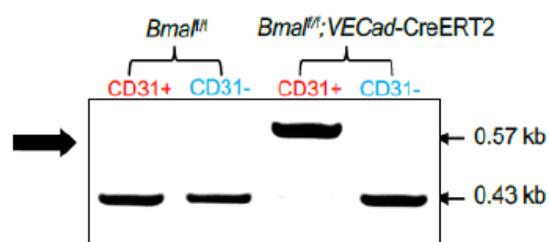
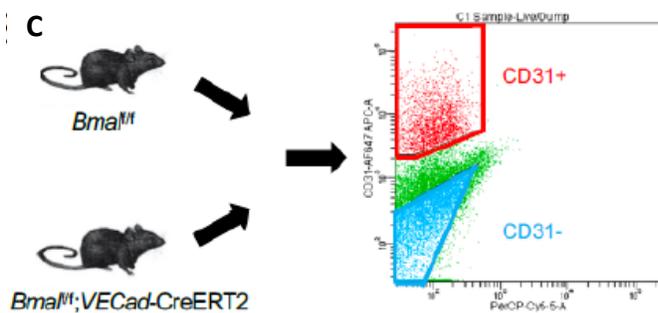
***Bmal1* Knockout:**



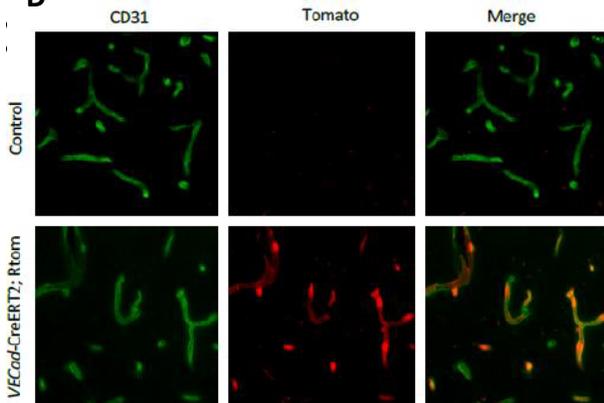
**B**



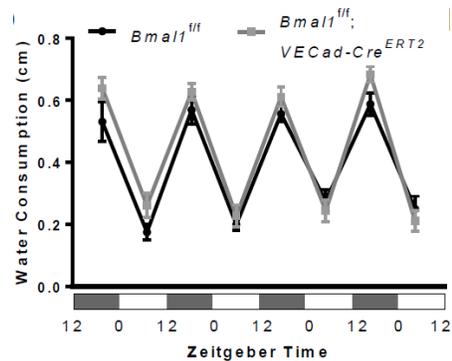
**C**



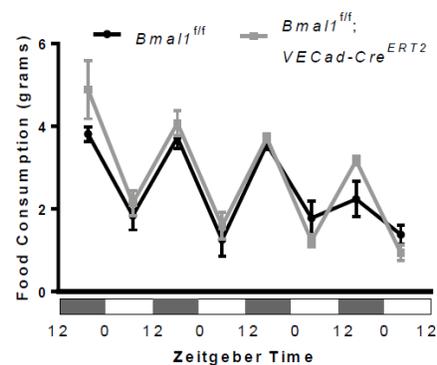
**D**



**E**



**F**



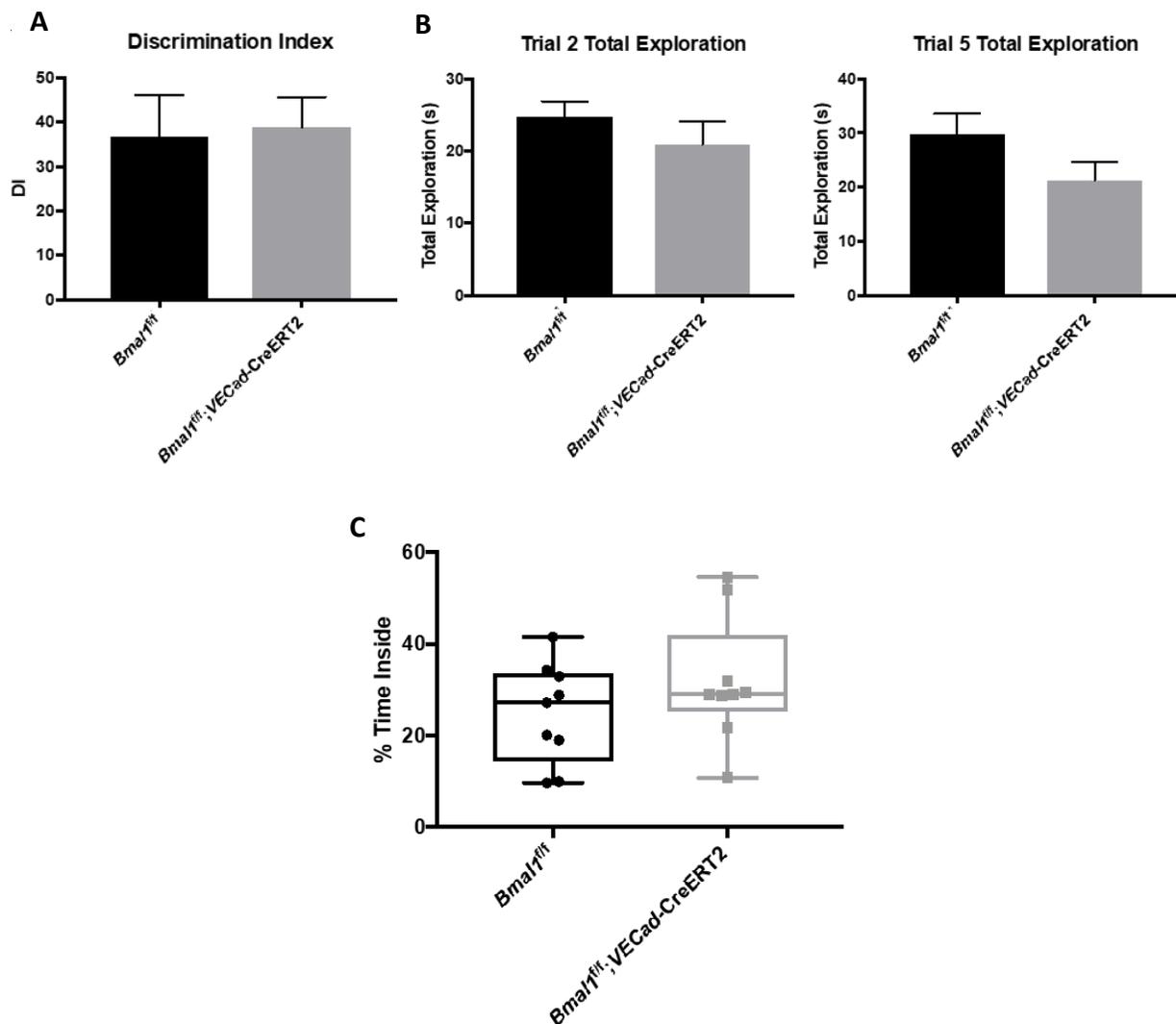


**Figure 3S.3: EC-Bmal cKO Mice do not display Learning and Memory Deficits nor Anxiety-like Behavior.** (A-B) The novel object recognition test. Mice were habituated to the testing box for 5 minutes (Trial 1), then habituated to two identical objects for 5 minutes, x3 trials (Trials 2-4). One object was replaced by a novel object (Trial 5). Mice were scored on how much time they spent exploring each object. (A) Discrimination index was calculated as time spent exploring novel object subtracted by time spent exploring familiar object, divided by total exploration time in trial 5. (B) Total time spent exploring any object in trials 2 and 5. Data is plotted as mean  $\pm$ SEM. n=14 for each condition. (C) The open field test. Mice were placed in the testing arena and scored for amount of time spent inside an inner drawn square, as opposed to around the perimeter of the testing arena. Data is plotted as mean  $\pm$ SEM. n=9 for both conditions.

## MATERIALS AND METHODS

### Mouse Strains

All animal experiments were performed with national and UCSD IACUC guidelines. *Bmal1* floxed mice were crossed to *VECadherin-Cre<sup>ERT2</sup>* mice to generate a tamoxifen-inducible, endothelial-specific, *Bmal1* knockout mice. *Rosa-lsl-tdTomato* mice were crossed to *VECadherin-Cre<sup>ERT2</sup>* mice to generate a tamoxifen-inducible, endothelial-specific, red reporter mouse. Both sets of mice were administered 3 daily intraperitoneal injection of tamoxifen (100µl of 20 mg/ml) at 5 weeks of age and all experiments involving these mice were performed at least 5 weeks post tamoxifen injection. PAR bZip triple knockout mice and corresponding wildtype controls were previously described(106). All mice were kept on a standard 12:12 hour light:dark cycle. Both male and females were used for all experiments.

### Immunohistochemistry

Mice were anesthetized by i.p. injection of a ketamine/xylazine cocktail and then fixed via transcardial perfusion of D-PBS for 3 minutes, 4% paraformaldehyde (PFA) for 7-10 minutes, and again with D-PBS for 2 minutes using a Dynamax peristaltic pump. Speed was matched to typical cardiac output of a mouse. The brains were then dissected and submersion-fixed in 4% PFA overnight at 4°C. Brains were then submerged in 30% sucrose overnight at 4°C. Brains were then frozen in cryosectioning blocks in a solution consisting of 1:2 30% sucrose: OCT. 23µm sagittal sections were obtained using a cryostat and put on slides. They were blocked in a solution consisting of 5% goat serum and 0.1% Triton X-100 in PBS at room temperature for 45 minutes. They were then incubated in the blocking solution with the primary antibody, Rat-anti-HA 1/250 overnight at 4°C. They were then incubated in Goat-anti-Rabbit-Alexa 488 secondary antibody at room temperature for 90 minutes and then mounted on slides with DAPI Fluoromount-G for image processing.

## **Epifluorescence Imaging**

Epifluorescence images were taken with an Axio Imager D2 (Carl Zeiss) with a 5x Fluor, 0.25 NA using a digital camera (AxioCam HRm, Carl Zeiss). AxioVision software was used to acquire 10x images.

## **FACS-purification of Brain Endothelial Cells**

For a given experiment, mice were collected a batch of four mice of the same sex and litter consisting of a pair of EC-Bmal cKOs and a pair of littermate controls. 5 mg of kainic acid was dissolved in 2 ml of saline to obtain a working concentration of 2.5 mg/ml and saline was used as vehicle. One cKO and one littermate control was injected with 15 mg/kg of kainic acid and the other two mice were injected with an equivalent dose of vehicle at approximately ZT23-ZT24. Behavior was closely monitored for 3 hours and the experiment was aborted if behavioral seizures were observed. 3 hours post-injection the mice were live-decapitated using a mouse decapitator (LabScientific, XM-801). Brains were dissected out, the meninges were removed and the cortex and hippocampus were dissected out for further processing. The tissue was then diced using a #10 blade and enzymatically digested in Papain, 1 vial per on a 33° heat-block while being exposed to 95% oxygen, 5% carbon dioxide for 90 minutes. The tissue was then triturated and a second enzymatic digestion was performed in 1.0 mg/ml Collagenase Type 2 and 0.4 mg/ml Neutral Protease on a 33° heat-block while being exposed to 95% oxygen, 5% carbon dioxide for 30 minutes. Myelin was then removed as recommended with myelin removal beads using 30µm filters (MACS Miltenyi Biotec, 130-041-407) and LS columns (MACS Miltenyi Biotec, 130-042-401) on a MidiMACS separator (MACS Miltenyi Biotec, 130-042-302). The remaining single cell suspension was blocked with Rat IgG 1/100 for 20 minutes on ice. The samples were then stained with Rat-anti-CD31-Alexa 647, 1/100, mouse-anti-CD45-FITC 1/150, rat-anti-CD13-FITC 1/100,

rat-anti-CD11b-FITC 1/100, rabbit-anti-NG2-Alexa 488 1/150, and DAPI for 20 minutes at 4°. CD31-positive cells were sorted into Trizol using an ARIA II instrument at the Flow Cytometry Core at the VA Hospital in La Jolla, CA.

### **Rhodamine123 Permeability Assay**

Rhodamine123 was dissolved in DMSO to make a stock solution of 10mg/ml. For each experiment, a working solution of 2 mg/ml was made by diluting the stock solution with saline. For a given diurnal experiment, the mice were injected i.p. with Rhodamine123 1.5 hours before the indicated time. 15 minutes before the collection, the mice were then anesthetized by i.p. injection of ketamine/xylazine. Blood was collected via cardiac puncture and kept in an EDTA-coated tube rotating until the end of the tissue collection procedure. The mice were then perfused with D-PBS for 3 minutes using a Dynamax peristaltic pump. Brains were dissected, meninges removed and the cortex and hippocampus were then dissected out. The remaining tissue was flash frozen in liquid nitrogen and then stored at -80°C until Rhodamine123 was extracted. The blood samples were then centrifuged. The supernatant (plasma) was collected and stored at -80°C until Rhodamine123 was extracted.

Once Rhodamine123 was ready to be extracted from the collected tissue, the brains were weighed and added to tubes with cold PBS (mass/volume-adjusted). They were then homogenized using a bead beater homogenizer. The homogenized tissue was eluted by centrifugation. The Rhodamine123 extraction was performed on the homogenized brain tissue and plasma as described previously with slight modifications to adjust for input mass and volume (91). Briefly, n-butanol was added to the samples which were then vortexed. These steps were repeated once and the samples were incubated overnight at 4°C rotating. The samples were then vortexed, spun down and the supernatant was collected. The remaining pellet was then washed with an equivalent

volume of n-butanol, the samples vortexed, spun down and the supernatant was collected. The samples were then added to a 96-well plate with 4 technical replicates per sample. A standard curve and blanks were also run to ensure that Rhodamine measurements were above the detectable limit. The plate was analyzed on a Tecan Infinite plate reader (Excitation=505nm, Emission=560nm). Brain:Blood ratios were calculated for each sample by taking the average of the technical replicates.

### **Sodium Fluorescein Permeability Assay**

Sodium Fluorescein was dissolved in sterile PBS to make 10 mg/ml. For each experiment, a working solution of 2 mg/ml was made by diluting the stock solution with sterile PBS. Tissue collection was carried out identical to rhodamine permeability experiments (dosage was 25 mg/kg).

Brain tissue was homogenized identical the Rhodamine extraction. The brain homogenates were then centrifuged and the resulting supernatant was diluted 1:1 in 2% TCA. Plasma samples were diluted 1:400 in sterile PBS, followed by an additional 1:1 dilution in 2% TCA. Brain and plasma samples were incubated overnight rotating at 4°C. Both sets of samples were then centrifuged and the supernatants were diluted 1:1 in borate buffer, pH 11. The samples were then added to a 96-well plate with 4 technical replicates per sample. A standard curve and blanks were also run to ensure that sodium fluorescein measurements were above the detectable limit. The plate was analyzed on a Tecan Infinite plate reader (Excitation=480nm, Emission=538nm). Data was analyzed identical to the rhodamine experiment.

### **RT-qPCR**

Brain homogenate RNA from PAR bZip triple knockout mice and respective littermate controls was purified as described previously(106). Approximately 100 mg of frozen brain was

grinded in extraction buffer (3.9 M Guanidium thiocyanate, 0.03 M Sodium citrate, 0.2 M Sodium acetate, 1% (v/v) 2-Mercaptoethanol) using a Polytron PT 2500 E homogenizer. An equal volume of phenol (saturated in H<sub>2</sub>O) and 0.5 volume of chloroform/isoamylalcohol (49:1 (v/v)) were added to the homogenate. The mixture was vigorously vortexed subsequently. Phase separation was accomplished by a centrifugation step at 4°C 12,000 g for 20 min. RNA of the aqueous phase was precipitated at -20°C during at least 20 min using an equal volume of isopropanol. The precipitate was pelleted by centrifugation at 12,000 g for 15 min at 4°C. Subsequently, the pellet was resuspended in 4M LiCl and subsequently re-pelleted during a centrifugation step of 12,000 g for 15 min at 4°C. The pellet was washed with 75% ethanol with a subsequent centrifugation at 12,000 g for 15 min at 4°C. The washed pellet was then dried at room temperature and dissolved in RNase/DNase free water. RNA from FACS-purified brain endothelial cells was purified from trizol using the QIAGEN RNeasy Micro Kit. RNA was reverse transcribed to cDNA using iScript Reverse Transcription Supermix. qPCR was performed using SYBR Green Master Mix with Primetime qPCR primers from Integrated DNA Technologies. Relative gene expression of *Abcb1a* was calculated using the  $\Delta\Delta C_t$  method normalizing to *GAPDH* for the PAR bZip tKO samples and *Rps20* for the FACS-purified brain endothelial cells.

### **Validation of Endothelial-Specific Bmal1 Knockout**

Endothelial cells and non-endothelial cell populations were FACS-purified from the brains of *VECadherin-Cre<sup>ERT2</sup>; Bmal1<sup>fl/fl</sup>* mice and littermate controls (*Bmal1<sup>fl/fl</sup>*). The cell populations were lysed with Proteinase K in DirectPCR Lysis Reagent, then incubated rotating overnight at 55°C. Lysates were incubated at 85°C for 45 minutes to inhibit the Proteinase K. Multiplex PCR was performed using primers L1, L2 and R4 as described previously(113).

### **Rhythmic Behavior**

Mice were single-housed with ad libitum access to food and water in a standard 12:12 hour light-dark cycle. Food intake was measured as weight of food in grams to the nearest 0.1 gram. Daily spillage of food has been shown to not be more than 0.1g and therefore considered negligible(114). Water intake was measured as the displacement of water in a cylindrical tube fixed with a drinking spout. Measurements were taken at ZT0 and ZT12 every day over a period of 4 days.

### **Rhythmicity Analysis**

Rhythmic analysis between different conditions was performed as described previously with minor modifications(115). Briefly, we applied multiple linear regressions on the data and subsequently performed a model selection using the Bayesian information criterion (BIC). The function was defined as  $y(t) = \mu + \gamma \cdot t + \alpha \cos((2\pi/24 \text{ h})t) + \beta \sin((2\pi/24 \text{ h})t) + \text{noise}$ , where  $y$  is the log transformed signal,  $\mu$  is the mean,  $t$  is *Zeitgeber* time,  $\gamma$  is a coefficient to account for non-periodic time-dependent changes and  $\alpha$  and  $\beta$  are the coefficients of the cosine and sine functions. To compare rhythmicity between the wild-type and KO mouse models, we generated five different models with differing  $\alpha$  and  $\beta$  accounting for rhythmic and non-rhythmic patterns in each condition. Each of the models were fitted to the data using linear regression and model complexity was subsequently controlled by a BIC based model selection(116). Schwarz weight ( $w_j$ ) was used to assess the confidence of all fitted models. The model with the highest BIC weight (BICW) was only considered to reflect the measurements if a threshold of 0.4 was reached.

### **Novel object recognition (NOR) test**

Mice were acclimated to the testing room with for 30 minutes prior to experiment. All NOR tests were performed with minimal ambient lighting to minimize anxiety-inducing stressors. The mice were allowed one 5 minute habituation period inside the testing box, define as Trial 1.

They were allowed three consecutive 5 minute habituation periods inside the box with two identical objects, defined as Trials 2-4. After Trial 4, one object was switched for a novel object of different shape, color, and material. Investigative behavior towards an object was defined as head oriented toward the object within 1.0 cm, sniffing of the object, or deliberate contact with the object (deliberate contact with the object but head orientated away was not scored as investigative). Videos were scored manually by an experimenter blind to genotype. Discrimination index (DI) was calculated as time spent exploring novel object subtracted by time spent exploring the old object, divided by the total exploration time.

### **Open field test**

Mice were acclimated to the testing room with for 30 minutes prior to experiment. The testing box contained an inner concentric square drawn on the floor that delineated inside versus outside. Mice were placed in the testing box for a single 5 minute period. Time inside was defined as more than half of the body inside the inner square. Half of the body inside the inner square was only considered “inside” if the head was orientated toward the center of the square. Videos were scored manually by an experimenter blind to genotype.

### **Tail suspension test**

Mice were acclimated to the testing room with for 30 minutes prior to experiment. Mice were fitted with a short tube covering the tail to prevent tail-climbing, and then were suspended by the tail with tape such that they cannot touch the ground or nearby surfaces. The mice were suspended for a single 6 minute period in which immobility (as opposed to escape-orientated behavior) was characterized by complete lack of movement, other than movement necessary to breathe. Videos were scored manually by an experimenter blind to genotype.

## **ACKNOWLEDGEMENTS**

This work was in part supported by the UCSD Graduate Training Program in Cellular and Molecular Pharmacology through an institutional training grant from the National Institute of General Medical Sciences, T32 GM007752 and NIH/NINDS R01 NS091281 Diversity Supplement (R.S.P.) This work was also funded by NIH/NINDS R01 NS091281, Rita Allen Foundation, Klingenstein-Simons Foundation, and CureAlz Foundation (R.D.). The authors would like to acknowledge the UCSD Genomics Core and the VA Flow Cytometry Core in La Jolla, CA. The authors have no conflicts of interest to declare.

This chapter is part of a manuscript under revision for publication of the material as it may appear in *Neuron*, 2019, Pulido RS, Munji RN, Chan TC, Quirk CR, Weiner GA, Weger BD, Elmsaouri S, Malfavon M, Gachon F, Leutgeb S, Daneman R. The dissertation author is the primary investigator and first author of this material.

## **CHAPTER FOUR:**

Behaviorally Motivated Changes in Neural Activity Regulate Molecular Properties of the Brain Vasculature

## INTRODUCTION

We identified hundreds of brain endothelial genes that were significantly regulated by DREADDs-mediated changes in glutamatergic activity, suggesting that the brain vasculature exhibits molecular plasticity in response to neural activity (Chapter 2). However, although these chemogenetic approaches are reliable and precise, DREADDs is an artificial method to manipulate neural activity and may not have robust physiological relevance. Therefore, we sought to ask whether behaviorally motivated changes in neural activity would also illicit similar changes in brain endothelial gene expression. We hypothesized that there would be a large degree of coherence between the two datasets, demonstrating that our neural activity-dependent changes in brain endothelial cells are physiologically relevant and that the brain vasculature and neurons may be under constant communication to maintain brain homeostasis under typical physiological conditions.

## **RESULTS**

### **A paradigm that manipulates neural activity through volitional behavior**

In order to manipulate neural activity through volitional behavior, we utilized a behavioral paradigm in which whisker somatosensation induces robust firing of the neurons in the barrel cortex(117). Mice with whiskers intact were habituated to and permitted to explore a large, environmentally-enriched cage (+Whisker) while mice with their whiskers shaved off were habituated to and allowed to explore a large empty cage (-Whisker) with both conditions in the dark for 3 hours. To verify that the +Whisker paradigm could increase neural activity in the barrel cortex compared to the –Whisker paradigm, we immunostained for the early immediate gene, cFos, and found that the +Whisker group had significantly more cFos+ cells in the barrel cortex in comparison to the –Whisker group (Figure 4.1 A, Figure 4.1 B). This indicates that this behavioral paradigm is sufficient to induce a robust increase in neuronal activity in the barrel cortex.

### **The brain endothelial transcriptome in response to behaviorally motivated changes in neural activity**

Next, we performed RNA sequencing on FACS-purified brain endothelial cells from the barrel cortex of the two groups (+Whisker and –Whisker) and found that 727 genes were significantly upregulated and 508 genes were significantly downregulated (Figure 4.1 C, Figure 4S.1). Pathways uniquely regulated by whisker stimulation include downregulation of genes involved in the lysosome and glycolysis and upregulation of genes involved in the Src Homology-3 Domain and the Rap1 Signaling Pathway (Table 4S.1, Table 4S.2).

### **Comparison of brain endothelial response to behaviorally motivated changes vs. DREADDs-mediated changes in neural activity**

We next compared the significant changes observed through chemogenetics with those observed through the whisker stimulation paradigm. When we looked at the brain endothelial gene expression changes after DREADDs-mediated glutamatergic activation in our whisker stimulation dataset, we found a high degree of correlation ( $r=0.718141$ ), suggesting that the neural activity-regulated gene expression changes in brain endothelial cells that we identified by DREADDs-mediated glutamatergic activation are physiologically relevant and represent a robust transcriptomic signature in the brain endothelial cells in response to activity (Figure 4.2 A). There was a large overlap of enriched pathways between the two experiments. Specifically, pathways involving adherens junctions and the cytoskeleton were also upregulated after whisker-mediated increase in neural activity (Table 4S.2). In addition, pathways involving metabolism were also downregulated after whisker-mediated increase in neural activity (Table 4S.1). Whisker stimulation also decreased expression of the same 5 ABC efflux transporters and the PAR bZip circadian clock-regulated transcription factors, and had an overall similar effect on endothelial clock genes suggesting that physiologically relevant changes in neural activity regulate BBB efflux and the endothelial circadian clock (Figure 4.2 C, Figure 4S.2).

Interestingly, when we looked at the brain endothelial gene expression changes after DREADDs-mediated glutamatergic silencing in our whisker stimulation dataset, they were not inversely correlated ( $r=0.049543$ ) suggesting that silencing of neural activity is potentially an active form of signaling to the brain vasculature, rather than a lack of signaling from neural activity (Figure 4.2 B, Figure 4.2 D).

Although our DREADDs glutamatergic activation and whisker stimulation datasets were overall highly correlated, their effects on the BBB were slightly different perhaps due to the difference in robustness of neuronal firing in the two paradigms as well as the difference in the

brain region analyzed (Figure 4S.3). In the behavioral paradigm there was significant upregulation of two TJ genes (*Marveld2* and *F11r*). Because TJs are involved in preventing paracellular diffusion of ions and molecules, perhaps there is upregulation of TJs as a structural response to higher shear stress similar to what occurs for adherens junctions. There was upregulation of the two LAMs, *Sele* and *Vcam1* after whisker stimulation, which similar to DREADDs-mediated glutamatergic activation, could be a shear stress-dependent response rather than an inflammatory response. Interestingly *Slc1a1*, a glutamate transporter, was significantly upregulated after whisker stimulation which may be a mechanism for modulating glutamate levels in response to the increased glutamatergic neuronal activity in the barrel cortex. *Slc2a1*, which transports glucose into the brain, was also significantly upregulated after whisker stimulation which may be a mechanism for providing more energy for the brain since neural activity is a highly energy-demanding process. *Slc16a1*, *Slc16a4*, *Slc38a3* and *Slco2b1* were also significantly changed after whisker stimulation. *Lrp1* which is sits on the abluminal side of brain endothelial cells and is involved in extruding waste products such as A $\beta$  from the brain parenchyma, was significantly downregulated after whisker stimulation.

We also examined the expression of 155 Slc transporters (expressed above a threshold of 10 average CPM across all samples) and 65 were significantly changed in at least one of the 3 experiments (Figure 4S.4). 6 genes were significantly regulated in the same direction after DREADDs-mediated glutamatergic activation and whisker-mediated increase in neural activity (*Slc12a2*, *Slc12a9*, *Slc20a1*, *Slc25a24*, *Slc5a3*, *Slc9a3r2*). The substrates and cellular localization of many of these transporters are unknown but these transporters may have important roles in regulating the endothelial intracellular and brain parenchymal extracellular chemical and ionic

environments. These data suggest that brain endothelial cells may plastically change expression of these transporters as a mechanism to meet neuronal circuit-specific energy and nutrient demands.

Taken together, these data suggest that physiological changes in neural activity and DREADDs-mediated changes in neural activity regulate the brain vasculature in a similar manner.

## DISCUSSION

Here, we demonstrate that changes in neural activity through volitional behavior is sufficient to cause robust transcriptional changes in the brain vasculature of the barrel cortex. We further showed that these changes in the brain endothelium are highly similar to those in response to our chemogenetic paradigm. This suggests that our activity-dependent changes in the brain vasculature are sensitive to standard physiological changes in neural activity. And specifically, this suggests that neural activity, which is on average higher during wakefulness and lower during sleep, acts as a homeostat to regulate diurnal oscillation of endothelial circadian genes which in turn modulate BBB efflux transport.

Unlike the full cortex and hippocampus we collected our DREADDs paradigm, the barrel cortex that we collected in our behavioral paradigm is a much smaller brain region and the overall change in neural activity was much more physiologically relevant. However, we still observed a large amount of gene expression changes in the brain endothelial cells suggesting that neural activity can regulate the brain vasculature on a local level, rather than needing to affect a large portion of the entire vascular network. However, similar to the *CamkII $\alpha$* -driven DREADDs, whisker stimulation primarily activates glutamatergic pyramidal neurons. Therefore, it is unclear whether this phenomenon occurs only in the context of glutamatergic neurotransmission, or whether the metabolic demand of neuronal firing regardless of neurotransmitter is sufficient to induce these changes in the vasculature. In addition, the barrel cortex is part of the larger cortical region that was activated in our DREADDs paradigm, so it is also unclear whether this phenomenon occurs in other brain regions, and whether there are neuronal circuit-specific changes. More studies manipulating other brain regions, neurons releasing other neurotransmitters, and

more precise neuronal circuits are needed to address these questions and expand on our understanding of neuronal communication to the brain vasculature.

## FIGURES

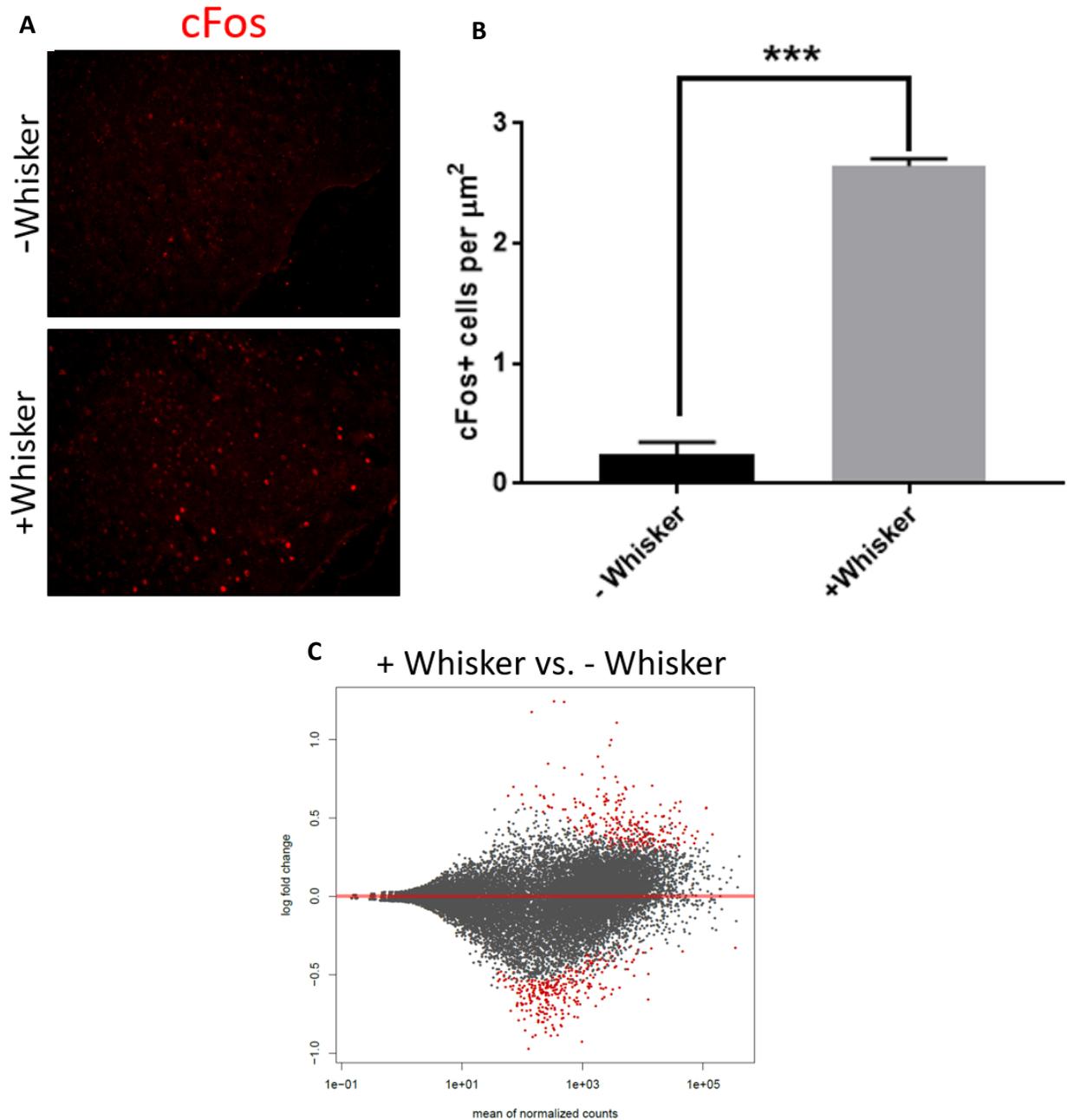
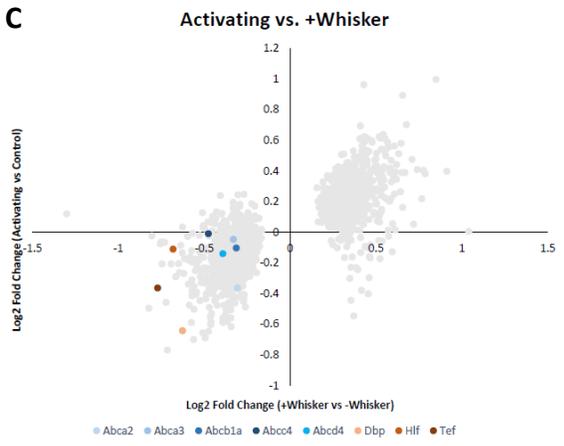
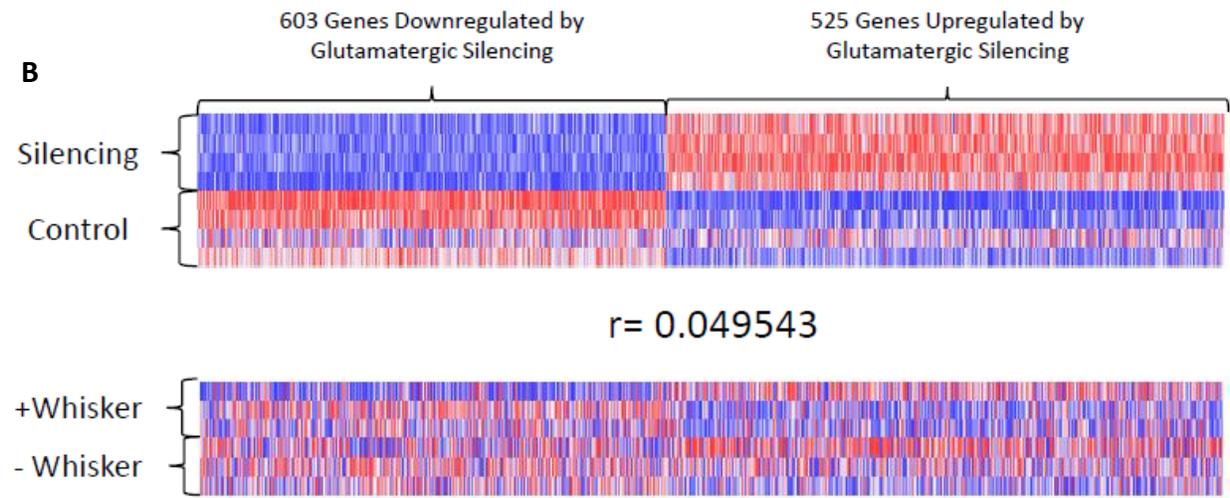
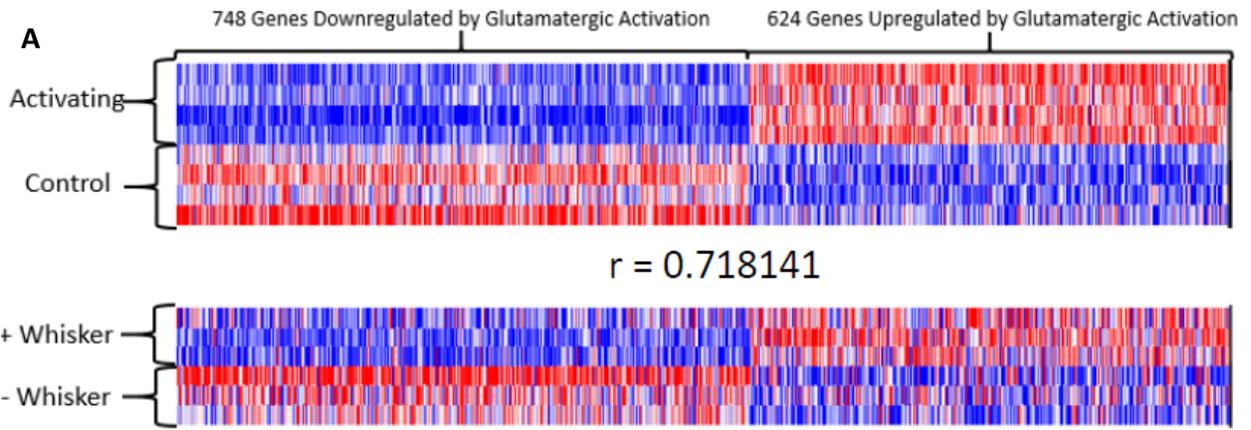


**Figure 4.1: Behaviorally motivated, Neural Activity-Regulated Brain Endothelial Transcriptome.** (A) Representative sections of barrel cortex in whisker-shaven, environmentally-null mice (top) vs. whisker-intact, environmentally-enriched mice (bottom) stained for cFos (red). (B) Quantification of cFos+ cells per  $\mu\text{m}^2$  in barrel cortex of “-Whisker” vs. “+Whisker” mice. Data represent mean  $\pm$  SEM (error bars).  $n=3$  per group. \*\*\* $p<0.001$  by Student’s t-test. (C) MA plot for +Whisker vs. -Whisker.  $n=3$  mice per group.

**Figure 4.2: Comparison of brain endothelial response to behaviorally motivated changes vs. DREADDs-mediated changes in neural activity.** (A) Heat maps of genes significantly regulated by DREADDs-mediated glutamatergic activation in the Activating mice and paired littermate controls (top) and +Whisker mice and –Whisker mice (bottom). Color scale represents arbitrary units of expression. Blue represents lower expression and red represents higher expression. Pearson Correlation Coefficient shown. (B) Heat maps of genes significantly regulated by DREADDs-mediated glutamatergic silencing in the Silencing mice and paired littermate controls (top) and +Whisker mice and –Whisker mice (bottom). Color scale represents arbitrary units of expression. Blue represents lower expression and red represents higher expression. Pearson Correlation Coefficient shown. (C) XY scatter plot of genes significantly regulated by DREADDs-mediated glutamatergic activation in the Activating mice and +Whisker mice based on log<sub>2</sub> fold change. The majority of genes cluster in the top right (upregulated in both) or bottom left (downregulated in both) quadrants. ABC transporter and bZip transcription factor genes are shown as colored dots. (D) XY scatter plot of genes significantly regulated by DREADDs-mediated glutamatergic silencing in the Silencing mice and +Whisker mice based on log<sub>2</sub> fold change.



Cell Type	Gene	- Whisker CPM	+ Whisker CPM
Endothelial	Cldn5	2744.506	2636.557
	CD31	1909.85	2069.65
Pericyte	Pdgfrb	42.30872	29.67534
	CD13	3.326646	3.371701
Pericyte/OPCs	NG2	26.77481	16.53828
OPCs	Pdgfra	12.37082	8.088497
Astrocytes	GFAP	7.464317	3.141213
	Aqp4	18.34414	6.350982
Microglia	Iba1	0.337592	0.571674
	CD45	0.718816	1.186568
	Cx3cr1	6.682205	8.118941
Neurons	NeuN	0.465649	0.194224
	Thy1	1.881724	1.046022
Oligodendrocytes	Mog	0.230766	0.07517
	Mbp	2.825719	0.801201

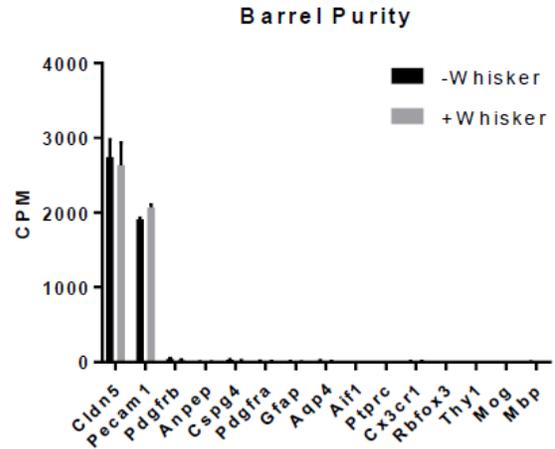


**Figure 4S.1: Behaviorally Motivated, Neural Activity-Regulated Brain Endothelial Transcriptome Cell Purity.** The counts per million (CPM) of cell-specific markers in the Barrel dataset. Raw values for each gene are also listed in the tables (left).

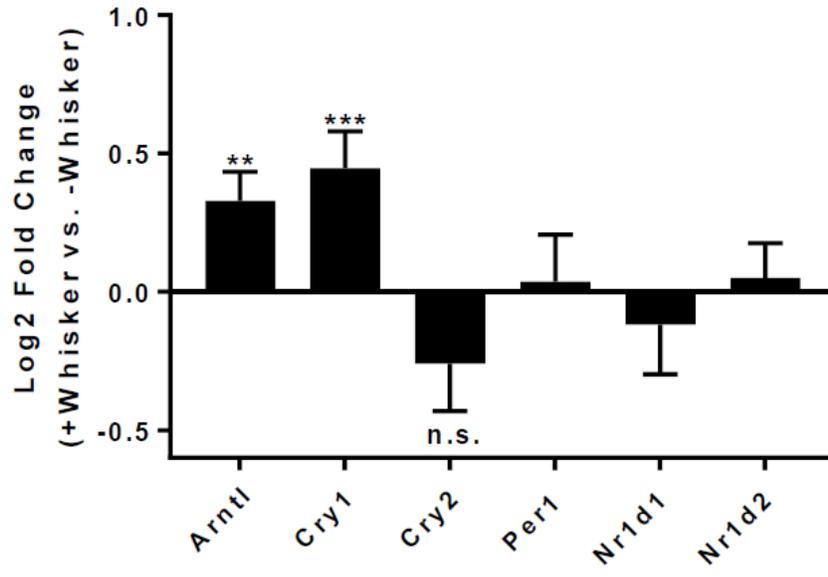


**Figure 4S.2: Behaviorally Motivated, Neural Activity-Regulated Endothelial Circadian Clock Genes.** Log<sub>2</sub> fold change of mRNA expression in +Whisker mice relative to -Whisker mice of canonical circadian clock genes in brain endothelial cells. Data represent mean ± SEM (error bars). n=3 mice per group. \*\*p<0.005, \*\*\*p<0.001, n.s. (not significant) by Wald Test.

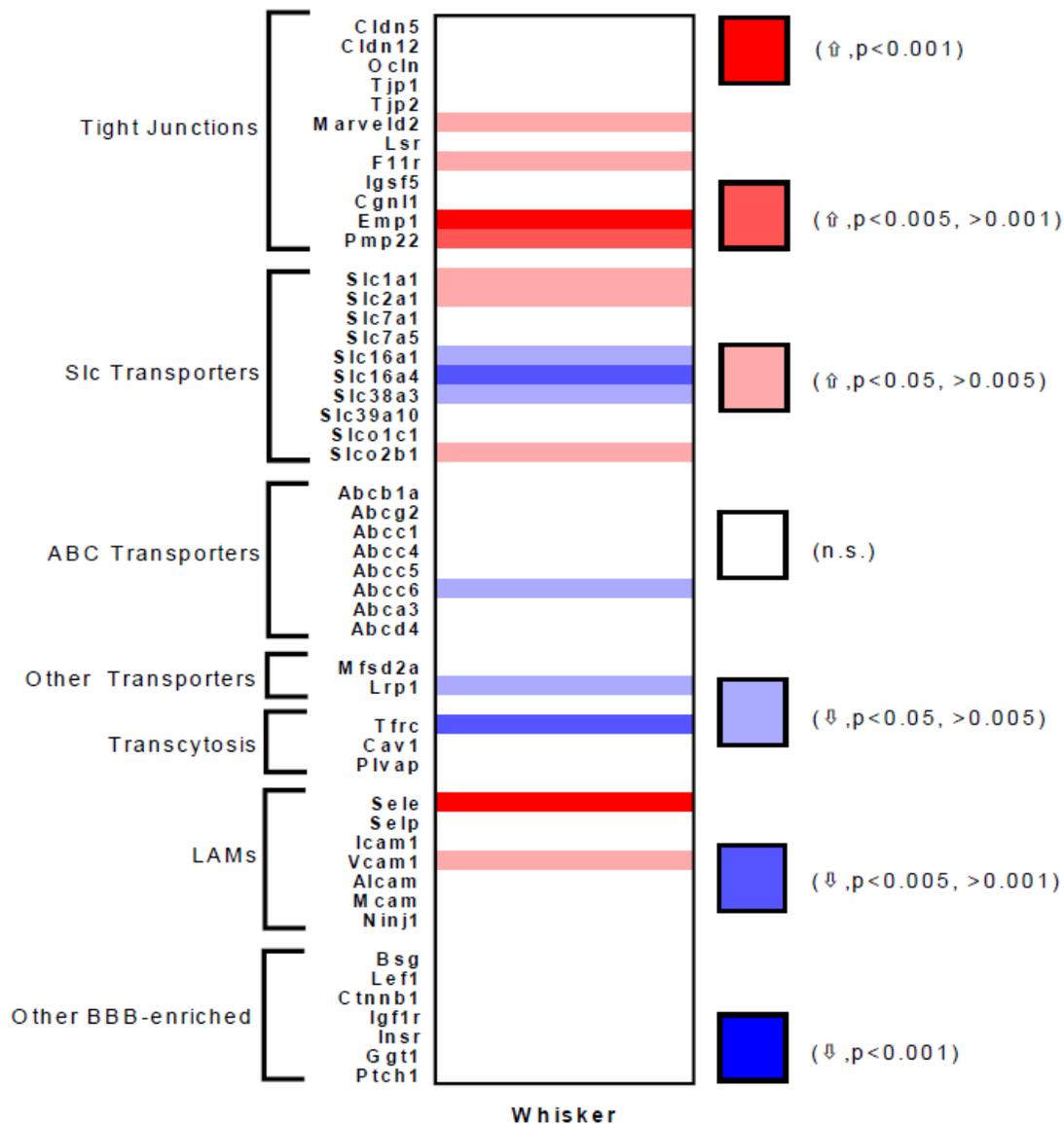


**Figure 4S.3: Behaviorally Motivated, Neural Activity-Regulated BBB Transcriptome.** Heat map for binned p-values and activity-regulated directionality of common BBB genes in Barrel experiment. Genes were divided into groups for different BBB properties: Tight junctions, Slc transporters, Abc transporters, other transporters, transcytosis, Leukocyte Adhesion Molecules (LAMs), or Other BBB-enriched. Color scale denotes if a given gene was upregulated ( $\uparrow$ ) (red) or downregulated ( $\downarrow$ ) (blue) and whether the change was statistically significant by Wald Test (intensity of color).

**Figure 4S.4. Neural Activity-Regulated Slc Transporter Transcriptome**

Heat map for binned p-values and activity-regulated directionality of Slc transporters (>10 average CPM) in Activating vs. Control (left), Silencing vs. Control (middle) and +Whisker vs. -Whisker (right). Color scale denotes if a given gene was upregulated (↑) (red) or downregulated (↓) (blue) and whether the change was statistically significant by Wald Test (intensity of color).

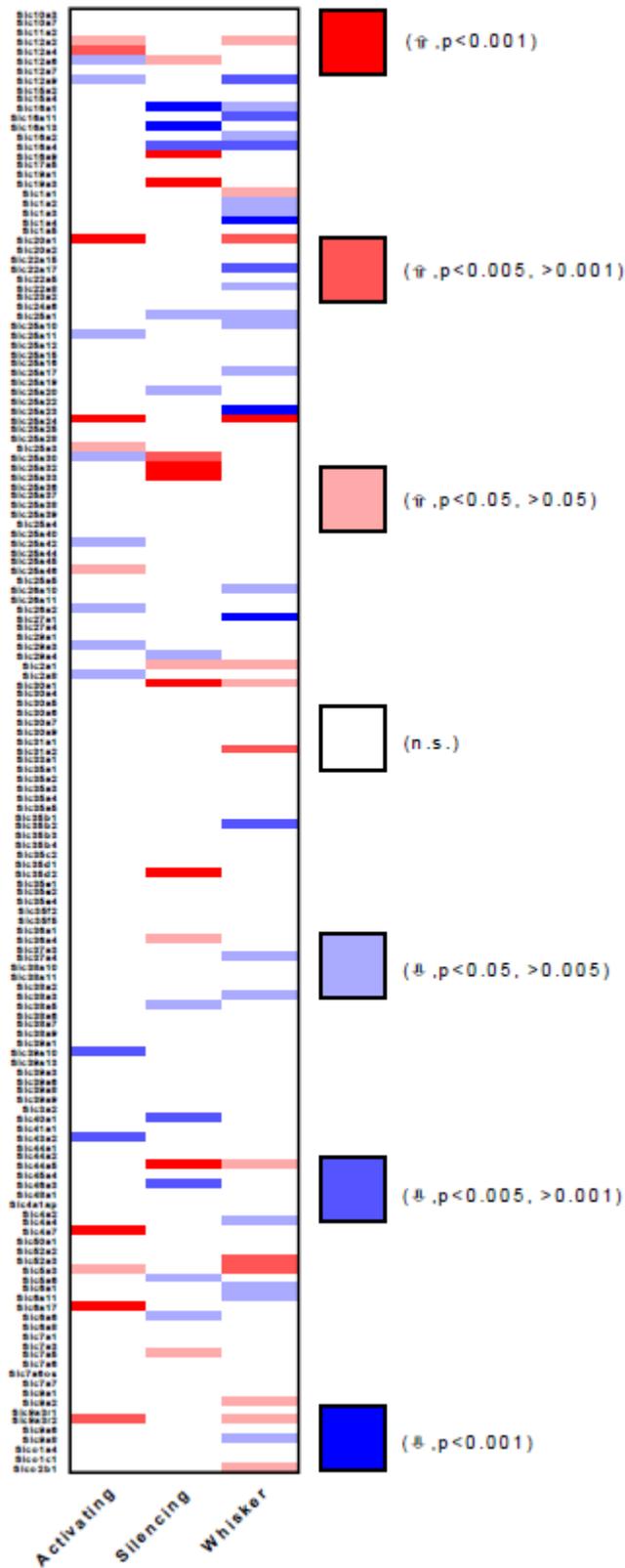


**Table 4S.1: DAVID Pathway Analysis for 508 genes *downregulated* by *whisker stimulation*.**

<b>Cluster Number</b>	<b>Gene Functional Annotation</b>	<b>Enrichment Score</b>
1	Oxidoreductase Activity	5
2	Mitochondrion	4.26
3	Transmembrane	4.1
4	Lysosome	4.1
5	Glycolysis	3.66
6	Endoplasmic Reticulum	3.48
7	Lipid Metabolism	3.41
8	Peroxisome	3.32
9	Cilium Biogenesis/Degradation	3.12
10	Disulfide Bond	2.67
11	Tryptophan Metabolism	2.47
12	Cell Projection	2.47
13	Aldehyde Dehydrogenase Activity	2.47
14	Pyridoxal Phosphate	2.36
15	Biotin Carboxylation	2.29

**Table 4S.2: DAVID Pathway Analysis for 727 genes upregulated by whisker stimulation.**

Cluster Number	Gene Functional Annotation	Enrichment Score
1	Cell-cell Adherens Junction	15.42
2	Protein Folding	10.03
3	Actin-Binding	6.91
4	Nucleotide-Binding	6.69
5	GTPase Activity	5.25
6	Src Homology-3 Domain	4.76
7	Rap1 Signaling Pathway	3.88
8	SH2 Domain	3.72
9	Endosome	3.63
10	Chaperone Tailless Complex Polypeptide 1	3.2
11	14-3-3 Domain	2.68
12	Endoplasmic Reticulum	2.67
13	Beta Tubulin	2.42
14	Ankyrin Repeat-Containing Domain	2.11
15	Fc gamma R-mediated phagocytosis	2.06

## **MATERIALS AND METHODS**

### **Mouse Strains**

All animal experiments were performed with national and UCSD IACUC guidelines. Animals were C57/BL6 wildtype. All mice were kept on a standard 12:12 hour light:dark cycle. Only male mice were used for the transcriptomic experiment.

### **Immunohistochemistry**

Mice were anesthetized by i.p. injection of a ketamine/xylazine cocktail and then fixed via transcardial perfusion of D-PBS for 3 minutes, 4% paraformaldehyde (PFA) for 7-10 minutes, and again with D-PBS for 2 minutes using a Dynamax peristaltic pump. Speed was matched to typical cardiac output of a mouse. The brains were then dissected and submersion-fixed in 4% PFA overnight at 4°C. Brains were then submerged in 30% sucrose overnight at 4°C. Brains were then frozen in cryosectioning blocks in a solution consisting of 1:2 30% sucrose: OCT. 12µm sagittal sections were obtained using a cryostat and cross referenced with a brain atlas to ensure sections included the barrel cortex. Sections were put on slides and blocked with % donkey serum + 0.1% Triton X-100 in PBS at room temperature for 45 minutes. They were then incubated in the blocking solution with the primary antibody, Goat-anti-cFos 1/250 overnight at 4°C. They were then incubated in Goat-anti-Rabbit-Alexa 594 secondary antibody at room temperature for 90 minutes and then mounted on slides with DAPI Fluoromount-G for image processing.

### **Epifluorescence Imaging**

Epifluorescence images of HA-immunostained slides were taken with an Axio Imager D2 (Carl Zeiss) with a 5x Fluor, 0.25 NA using a digital camera (Axiocam HRm, Carl Zeiss). AxioVision software was used to acquire 10x images.

### **cFos Image Analysis**

Once the barrel cortex was identified, cFos-positive cells were quantified using ImageJ. The following functions were used in sequential order: “Threshold Adjustment,” “Convert to Mask,” “Fill Holes,” “Watershed,” “Analyze particles”. Then “# cFos+ cells per  $\mu\text{m}^2$ ” was calculated by (Total # cFos-positive)/ (Area). Three images (technical replicates) were averaged for each mouse (biological replicates).

### **Barrel Cortex Activity Behavior Experiment**

The design of this experiment was based off previously described work with minor modifications(117). Briefly, for each experiment, 10 C57/BL6 mice were separated into 2 groups, 5 mice in the “+Whisker” group and 5 mice in the “-Whisker” group. All mice underwent “Habituation Period 1” for 7 days in which they were weighed, monitored and handled once daily. The mice then underwent “Habituation Period 2” for 5 days in which each group explored an empty standard rat cage for 30 minutes in the dark daily. Then, on the last day of Habituation Period 2 (Day 11), all mice were transiently anesthetized (2-3 minutes) with 1-3% isoflurane and the whiskers were clipped from the -Whisker mice using an electric hair trimmer. On the Test Day (Day 12), mice were added to their respective habituated rat cages in the dark at approximately ZT23 for a duration of 3 hours. The +Whisker mice had an enriched environment with novel objects which they were encouraged to explore with their whiskers due to the absence of light. Objects were switched and rearranged every 30 minutes to maintain novelty and exploration. - Whisker mice were kept in their empty habituated rat cage. Mice were then live-decapitated using a mouse decapitator.

The barrel cortex was then dissected out using a mouse brain matrix. A single coronal cut was made where the olfactory bulb meets the cortex. Two more posterior coronal cuts were made at 3mm intervals. The barrel cortex was then dissected from the 3mm coronal section by making

cuts overlaid on a scaled-down image of the mouse brain atlas coronal section containing the barrel cortex. The meninges were removed from the dissected barrel cortex and the remaining tissue was pooled together from the 5 mice from each group. The pooled tissue was then processed further for FACS-purification as described below.

### **FACS-purification of Brain Endothelial Cells**

Once the barrel cortices from the groups were processed and pooled, the tissue was then diced using a #10 blade and enzymatically digested in Papain, 1 vial per on a 33° heat-block while being exposed to 95% oxygen, 5% carbon dioxide for 90 minutes. The tissue was then triturated and a second enzymatic digestion was performed in 1.0 mg/ml Collagenase Type 2 and 0.4 mg/ml Neutral Protease on a 33° heat-block while being exposed to 95% oxygen, 5% carbon dioxide for 30 minutes. Myelin was then removed as recommended with myelin removal beads using 30µm filters (MACS Miltenyi Biotec, 130-041-407) and LS columns (MACS Miltenyi Biotec, 130-042-401) on a MidiMACS separator (MACS Miltenyi Biotec, 130-042-302). The remaining single cell suspension was blocked with Rat IgG 1/100 for 20 minutes on ice. The samples were then stained with Rat-anti-CD31-Alexa 647, 1/100, mouse-anti-CD45-FITC 1/150, rat-anti-CD13-FITC 1/100, rat-anti-CD11b-FITC 1/100, rabbit-anti-NG2-Alexa 488 1/150, and DAPI for 20 minutes at 4°. CD31-positive cells were sorted into Trizol using an ARIA II instrument at the Flow Cytometry Core at the VA Hospital in La Jolla, CA.

### **RNA-sequencing**

RNA was harvested from the FACS-purified brain endothelial cells using the Qiagen RNeasy Microkit. RNA samples were then further processed at the UCSD Genomics Core using standard core procedures. The RNA was tested for quality and concentration using a tape station

bioanalyzer. Next, cDNA libraries were made using the TruSeq RNA Library Prep Kit v2. Samples were then sequenced on an Illumina HiSeq4000, 150 based, paired ends.

Sequence reads for all samples were mapped to Ensembl mm9 v67 mouse whole genome using Tophat v 2.0.11 and Bowtie 2 v 2.2.1 with parameters no-coverage-search -m 2 -a 5 -p 7. Alignment files were sorted using SAMtools v.0.1.19. Count tables were generated using HTSeq-0.6.1. Differential expression of genes between control and treated samples, log 2-fold changes between control and treated samples, and statistical analysis including p values and FDR was performed using DESeq2 and Excel.

## **ACKNOWLEDGEMENTS**

This work was in part supported by the UCSD Graduate Training Program in Cellular and Molecular Pharmacology through an institutional training grant from the National Institute of General Medical Sciences, T32 GM007752 and NIH/NINDS R01 NS091281 Diversity Supplement (R.S.P.) This work was also funded by NIH/NINDS R01 NS091281, Rita Allen Foundation, Klingenstein-Simons Foundation, and CureAlz Foundation (R.D.). The authors would like to acknowledge the UCSD Genomics Core and the VA Flow Cytometry Core in La Jolla, CA. The authors have no conflicts of interest to declare.

This chapter is part of a manuscript under revision for publication of the material as it may appear in *Neuron*, 2019, Pulido RS, Munji RN, Chan TC, Quirk CR, Weiner GA, Weger BD, Elmsaouri S, Malfavon M, Gachon F, Leutgeb S, Daneman R. The dissertation author is the primary investigator and first author of this material.

## **CHAPTER FIVE:**

Discussion of Implications in Brain Waste Clearance and Alzheimer's disease

Here, we report that neural activity regulates brain endothelial cell gene expression, and specifically that neural activity inhibits the expression of BBB ABC efflux transporters and PAR bZip circadian clock-regulated transcription factors. We further show that there is a diurnal oscillation to BBB efflux transporter expression and function, which is abolished by endothelial-specific deletion of one of the main circadian clock regulators *Bmal1*. In particular, we found that there is overall less BBB efflux during the dark period when mice are more active and more BBB efflux during the light period when mice are at rest. We also demonstrate that acute regulation of BBB efflux by neural activity is abolished by endothelial-specific deletion of endothelial *Bmal1*. Lastly, we show that the detrimental consequence of disrupting this endothelial circadian-dependent pathway is depressive behavior (Figure 5.1).

These results demonstrate that the expression and function of efflux at the BBB is modulated by activity and is dependent on the expression of circadian clock genes within the endothelial cells. Although there may be endogenous oscillation of endogenous oscillation of endothelial circadian clock genes which mediate diurnal oscillatory BBB efflux, it appears that neural activity may be able to override this endogenous oscillation and converge on the endothelial bZip transcription factors to regulate efflux transport.

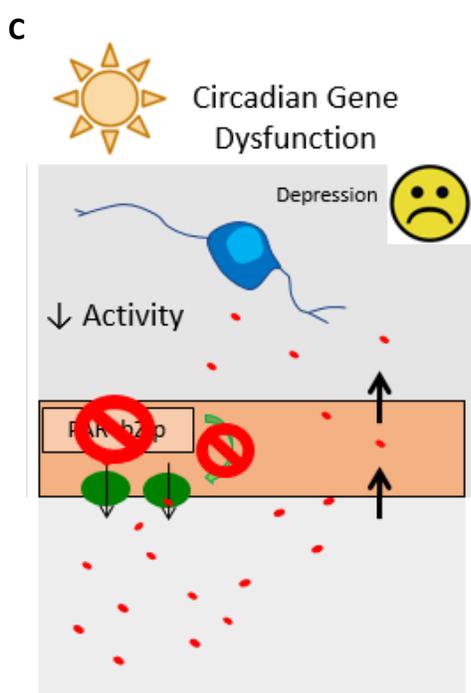
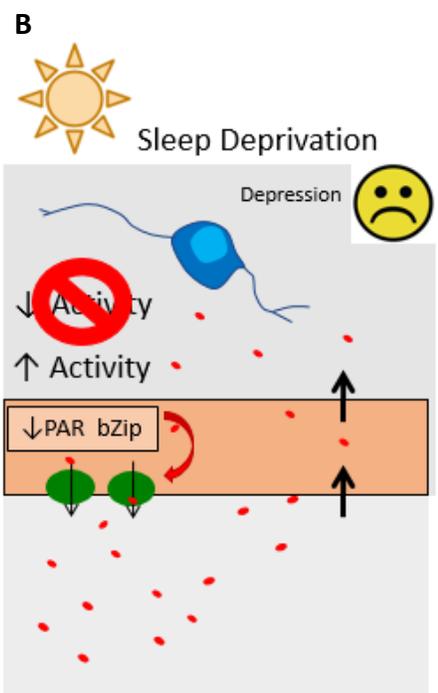
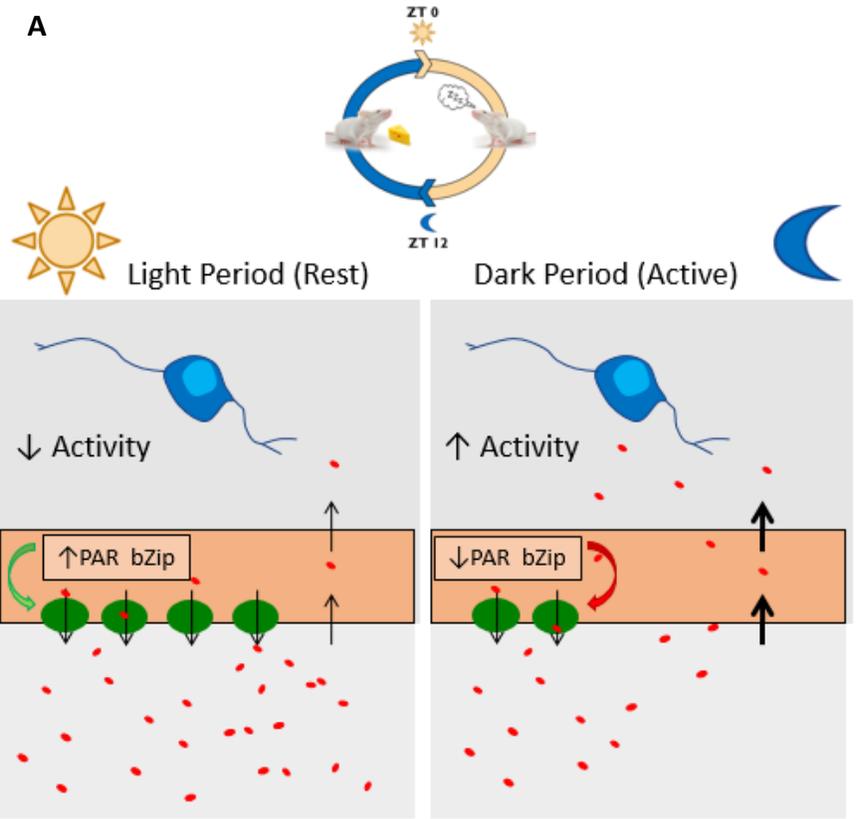
Our work also has substantial clinical implications in the context of waste clearance from the brain and Alzheimer's disease (AD). Our finding that BBB efflux inversely correlates with neuronal activity is consistent with previous studies that there is increased clearance of waste products such as amyloid beta ( $A\beta$ ) from the brain during sleep(118). Although the results from that study specifically implicated a role of the glymphatic system, there has been an abundance of literature expanding on our knowledge of the BBB's role, and specifically Pgp's, in waste clearance and Alzheimer's disease(10). Alzheimer's patients have been shown to have decreased

Pgp function in the brain(119,120). A $\beta$  has been shown to be cleared from the brain to the blood abluminally via LRP1 and luminally via pgp(36,121). It is also well-established that there is a substantial relationship between aberrant hyperactive neural activity and buildup of A $\beta$  plaques in both mouse models of AD and humans with AD, although a mechanistic role for pgp or the vasculature has not been explored in this context(60–66). We found that increased neural activity downregulates expression of both *Abcb1a* and *LRP1*. Thus, it is plausible that proper circadian balance of activity-dependent regulation of BBB efflux is important for clearing waste products such as A $\beta$  from the brain during sleep when activity is lower and BBB efflux transport is higher, and that BBB efflux may work synergistically with other brain clearance pathways during sleep. Interestingly, sleep has been shown to regulate PAR bZip transcription factor expression in the brain through modulation of *Bmal1* activity(95,96,122). In addition, circadian rhythm is often disrupted in patients with Alzheimer’s disease(123). Depression is also a common comorbidity in Alzheimer’s disease(124).

Based on our findings, it appears that an increase in Pgp expression and function occurs during sleep in control subjects and may be critical for waste clearance during sleep. And this increase in Pgp expression/function did not occur in our circadian mutants. Moreover, neural activity appears to be able to override this oscillatory phenomenon. Therefore, it is plausible that substantial disruption of this pathway, whether it be through imbalance of net neural activity in sleep/wakefulness or dysfunction of endothelial circadian clock genes can lead to neurochemical imbalance and depression. Taken together, these findings suggest that disruption of circadian-dependent and neural activity-modulated BBB efflux may be an upstream driver of Alzheimer’s pathogenesis.

## FIGURES

**Figure 5.1: Model of neural activity-dependent expression of endothelial circadian clock-regulated PAR bZip transcription factors which regulate BBB efflux transport and maintain neurochemical balance.** (A) Mice are more active during the night vs. day and thus exhibit more neural activity during the night. The expression of the PAR bZip transcription factors in brain endothelial cells is inversely regulated by the amount of glutamatergic activity in the brain and their expression regulates the expression and function of BBB efflux transporters. Therefore, there is more BBB efflux during the day/rest period vs. the night/active period in mice, which is important for waste clearance during sleep (day) and maintenance of neurochemical balance. However, if there is disruption of this pathway through sleep deprivation (B) or endothelial circadian gene dysfunction (C), there is improper waste clearance, neurochemical imbalance and depression.



## **APPENDIX A:**

### **Signaling Mechanisms of Neural Activity-Dependent Regulation of the Brain Vasculature**

## INTRODUCTION

We demonstrated that both chemogenetic and behaviorally-motivated changes in neural activity robustly regulate brain endothelial gene expression. However, the signaling mechanism(s) by which neuronal activity may be signaling to the vasculature in this context remains elusive. The cells in the NVU dynamically interact with each other to maintain brain homeostasis(38). Cellular signaling mechanisms of neurovascular communication has been extensively studied in the context of NVC and BBB function. Although NVC is much more dynamic than the neural activity-dependent regulation of brain endothelial gene expression that we identified and signaling for development/maintenance of the BBB is more “all or nothing,” we can still gain insight from these studies to hypothesize how neural activity signals to brain endothelial cells to regulate gene expression.

First, it is possible that neural activity regulates brain endothelial gene expression by directly interacting with endothelial cells. When glutamatergic neurons fire, they change the extracellular environment (e.g. ATP, glutamate, d-serine, potassium) around the neurovascular unit which can have vasoactive effects(77–80,125). Thus, there may be a direct effect of neuronal metabolites on brain endothelial gene expression.

Second, astrocytes, the most abundant glial cell in the brain, are physically located between neurons and CNS blood vessels, sending out thousands of processes interacting with both synapses and blood vessels. Not only are they essential for neuronal communication(126) and BBB maintenance(46), but they have been shown to be potentially key mediators of NVC(81). Although somewhat disputed, one of the major forms of astrocytic signaling in the context of NVC is thought to be through calcium waves which seem to occur in response to neuronal firing, propagate to other astrocytes through gap junctions and potentially release vasoactive signaling molecules(127).

Therefore, it is possible that astrocytic calcium signaling may play role in mediating these neural activity-dependent changes in brain endothelial gene expression.

Third, mural cells consisting of pericytes on capillaries and smooth muscle cells on larger blood vessels, tightly wrap around the abluminal surface of endothelial cells. They regulate blood flow primarily through physical contraction in response to molecules secreted by neurons and astrocytes(128), but could also be acting as mediators in relaying neuronal activity to the brain endothelial cells through release of signaling molecules.

Lastly, blood flow is tightly coupled with neural activity in the brain and it is possible that neural activity may regulate brain endothelial transcription through luminal mechanosensation of differential shear stress via TRP channels, *Piezo1*, *GPR68* or other endothelial mechanosensitive mechanisms(82–85).

In this work, we sought to understand the contribution of astrocytic signaling in mediating neural activity-dependent regulation of brain endothelial gene expression. We manipulated astrocytic calcium signaling *in vivo* and looked at global gene expression changes in brain endothelial cells.

## RESULTS

We hypothesized that one mechanism by which neural activity may be regulating brain endothelial gene expression is through astrocytic calcium signaling. Therefore, we wanted to use a tool to manipulate astrocytic calcium signaling *in vivo*. We used hM3Dq-DREADDs to increase astrocytic calcium signaling via Gq-GPCR-mediated calcium influx(129). We injected mice expressing *Rls1-hM3Dq* and *Glast-CreERT2* and cre-negative littermate controls with tamoxifen at 3 weeks of age to induce expression of Gq-DREADDs exclusively in astrocytes in adulthood (Figure A.1 A). The DREADDs were abundantly expressed in astrocytes throughout the brain including the cortex and hippocampus, the regions in which we identified the neural activity-dependent changes (Figure A.1 B).

In order to determine a mechanistic role for astrocytic calcium signaling in mediating neural activity-dependent regulation of brain endothelial gene expression, we injected these DREADDs mice and littermate controls with CNO, waited 3 hours after injection (same time course as our neuronal DREADDs experiments), FACS-purified the brain endothelial cells from the cortex and hippocampus, and performed RNA sequencing (Figure AS.1). There were 572 genes significantly upregulated and 157 genes significantly downregulated by DREADDs-mediated astrocytic calcium signaling. Zinc, DNA and RNA binding were the three top upregulated pathways (Table A.1). Focal adhesion was also a top upregulated pathway which may be a response to a potential increase in blood flow similar to what occurs after increased neuronal activity (Table A1).

Surprisingly, the ribosomal protein pathway was by far the most enriched downregulated pathway (Table A.2). Over 36 genes in brain endothelial cells encoding for ribosomal subunits were significantly downregulated in response to DREADDs-mediated astrocytic calcium

signaling. Interestingly, downregulation of ribosomal transcription has previously been observed as a regulatory aspect of cellular differentiation(130–132). However, it is unclear why brain endothelial cells would differentiate in response to astrocytic signaling.

DREADDs-mediated astrocytic calcium signaling had a mild effect on BBB genes with no obvious pattern (Figure A.2 A). Of note, *Cldn5*, the major tight junction protein, was significantly downregulated. In addition, LAT1 (*Slc7a5*) and *DDC* which are both important for regulating dopamine precursors in the brain were also downregulated suggesting that perhaps dynamic astrocytic regulation of the BBB may play a role in neurotransmitter homeostasis.

Surprisingly, when we looked at the brain endothelial gene expression changes after DREADDs-mediated glutamatergic activation or silencing in our astrocyte dataset, there was very minimal correlation (Figure A.2 B, Figure A.2 C). This suggests that astrocytic calcium signaling likely does not play a mechanistic role in mediating neural activity-dependent regulation of brain endothelial gene expression.

## DISCUSSION

We aimed to investigate potential signaling mechanisms by which neural activity regulates brain endothelial gene expression. To assess a mechanistic role of astrocytes, we used chemogenetics to manipulate calcium signaling in astrocytes *in vivo* and performed gene profiling on FACS-purified brain endothelial cells. We found that there was negligible coherence between the gene expression changes in our chemogenetic manipulation of glutamatergic neurons and our chemogenetic manipulation of astrocytes, suggesting that astrocytic calcium plays a minimal mechanistic role, if at all.

However, we cannot definitively rule out a mechanistic role for astrocytes because it is possible that using DREADDs to manipulate astrocytes *in vivo* does not adequately recapitulate normal physiological activity. In fact, an ongoing issue in astrocyte biology is finding the ideal tools to manipulate astrocytes *in vivo*(133). Many tools aren't precise enough or have been developed primarily for neuronal manipulation. A potential way to still answer this question without manipulating astrocytes directly, could be to manipulate neural activity in control mice and mice in which astrocytic calcium signaling is ablated, and gene profile brain endothelial cells. If astrocytic calcium signaling was responsible for a given neural activity-dependent brain endothelial gene expression change, we would expect that the gene expression would not change in the absence of astrocytic calcium signaling. However, there are caveats to obtaining complete ablation of calcium signaling in astrocytes that may confound this result(134).

The most robust result of this study was that a large cassette of ribosomal genes in brain endothelial cells were downregulated in response to DREADDs-mediated astrocytic calcium signaling. Since downregulation of ribosomal genes has been linked to cellular differentiation(130–132), it is possible that astrocytic calcium signaling regulates brain endothelial

cell differentiation and angiogenesis. However, it is interesting that there were no downregulated angiogenesis-related genes, which are well characterized. It would be interesting to follow this up with functional experiments to validate that this is occurring on a functional level. One way to investigate this *in vitro* would be to co-culture astrocytes and brain endothelial cells, induce astrocytic calcium signaling and determine if it is sufficient to increase brain endothelial differentiation. However, it is possible that this downregulation of brain endothelial ribosomal transcription may be an artifact of an artificial tool of manipulating astrocytes that has no physiological basis.

In this study, we only tested one potential signaling mechanism of neural activity-dependent regulation of brain endothelial gene expression. There are many other potential signaling mechanisms by which neural activity could regulate brain endothelial gene expression. It is known that neuronal firing changes the extracellular composition around the NVU which can have vasoactive effects(77–80,125). One way to test this *in vitro*, would be to apply varying concentrations of known neuronal metabolites, such as potassium, glutamate, d-serine, and ATP to brain endothelial cell cultures to determine if they are sufficient to induce expected brain endothelial gene expression changes.

Blood flow, which is downstream of other cellular signaling mechanisms in the NVU, is tightly coupled to neural activity in the brain(55). Therefore, it is plausible that neural activity may regulate brain endothelial gene expression through luminal mechanosensation of differential shear stress which the vasculature is readily equipped to sense with a variety of mechanosensitive mechanisms. One way to determine if mechanosensation of shear stress is sufficient to induce neural activity-dependent changes in brain endothelial gene expression *in vitro*, would be to apply different forces and types of shear stress on cultured brain endothelial cells and analyze gene

expression. If a certain shear stress paradigm was sufficient to induce an expected brain endothelial gene expression change, one could then determine if certain mechanosensory proteins (such as TRP channels, *Piezo1*, *GPR68*, etc.) are necessary for this process, by manipulating neural activity in genetic knockouts and controls and determining if the expected neural activity-dependent regulation is abolished in the knockouts.

It is also possible that there are biochemical mechanisms with unknown molecules secreted by one or multiple cell types in the NVU in response to neuronal firing. In order to assess this, one could generate an *in vitro* reconstitution co-culture consisting of neurons, astrocytes, pericytes and brain endothelial cells to determine if expected brain endothelial gene expression changes occurred after neuronal activity modulation. If this was the case, biochemical and size fractionation could be applied onto the media to reveal key signaling molecules.

It is important to note that all of these potential signaling mechanisms are not mutually exclusive, but may be intertwined and complement each other. Specific mechanisms may regulate specific cassettes of genes in brain endothelial cells. There may also be limitations to standard *in vitro* models and it may be necessary to use more physiologically relevant models, such as brain-on-a-chip microfluidic cultures or brain organoids, which recapitulate both blood flow and cellular aspects of the NVU(135,136).

## FIGURES

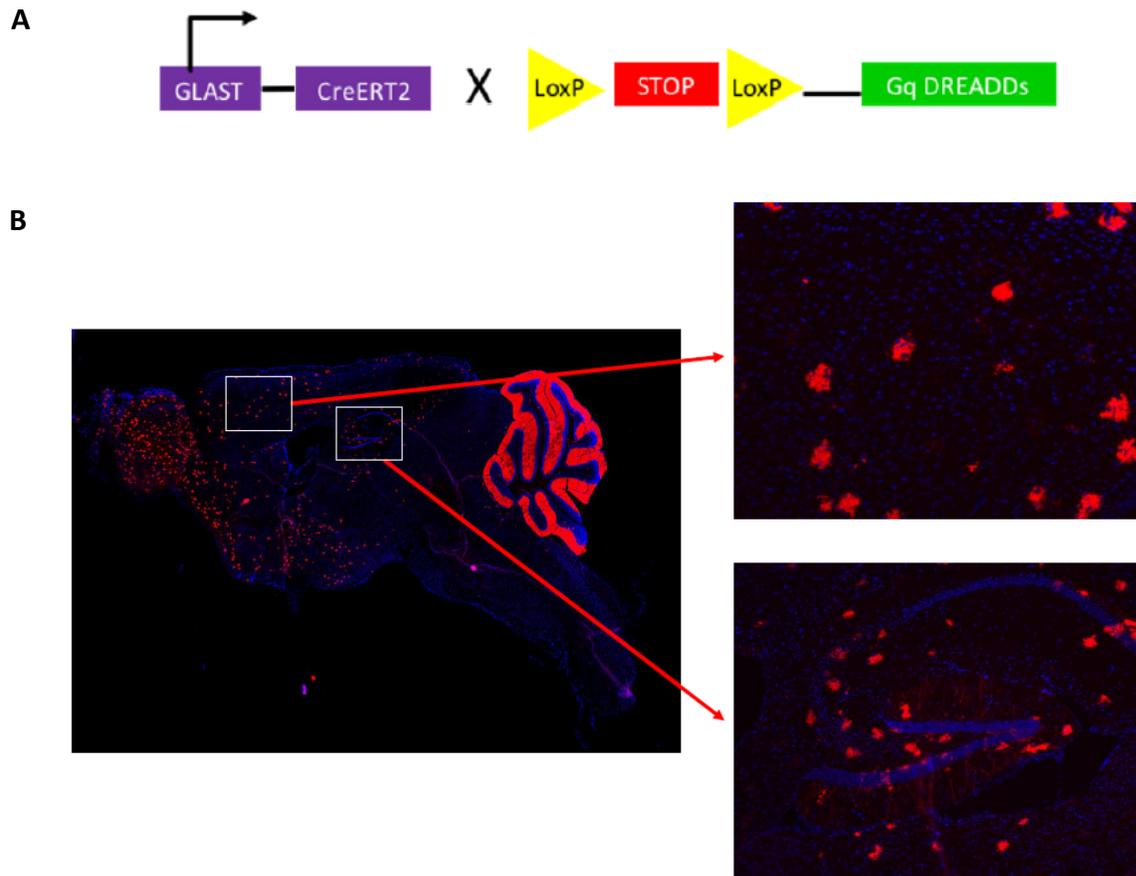


**Figure A.1: Astrocyte Gq-DREADDs.** (A) Schematic representation of the genetic mouse models utilizing DREADDs to activate or silence glutamatergic activity *in vivo*. (B) Sagittal section of a brain derived from an Astrocyte Gq-DREADDs mouse stained for HA (red) and cell nuclei with DAPI (blue). Top inset is a 20x magnification of the cortex and bottom inset is a 10x magnification of the hippocampus.

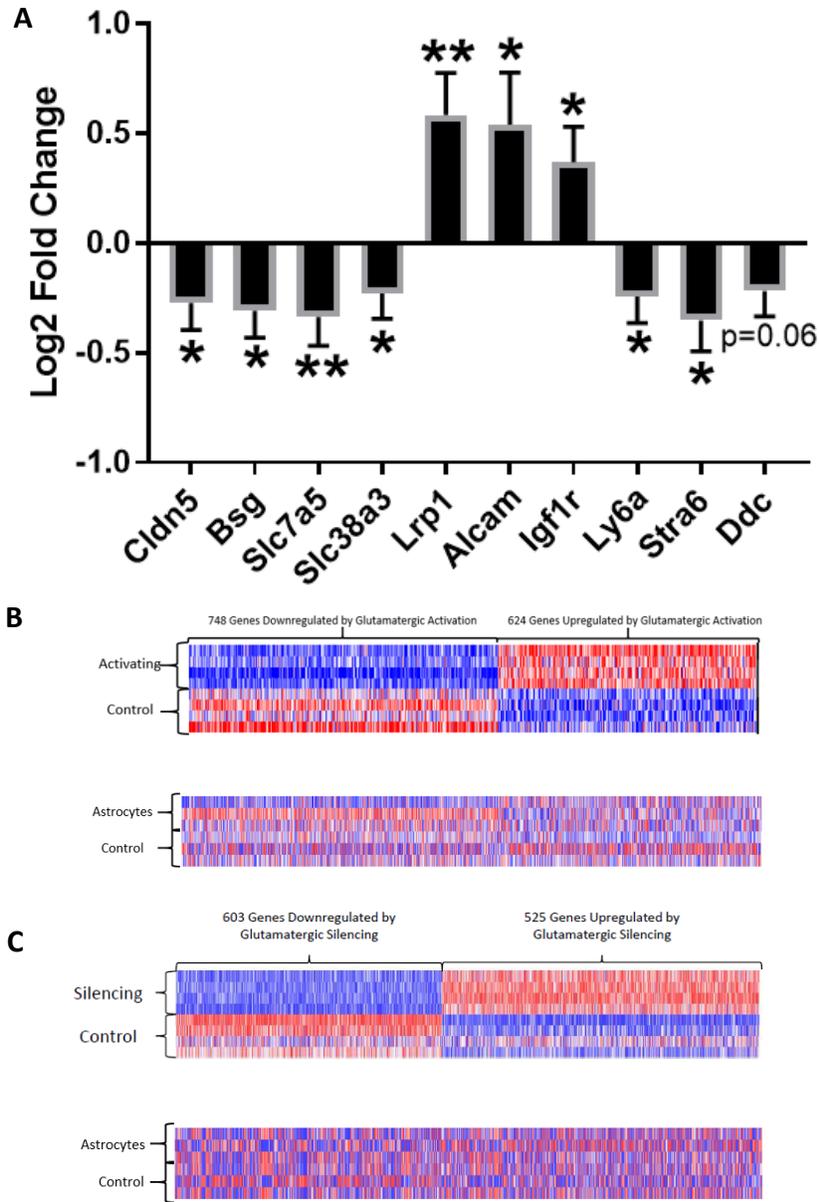


**Figure A.2: Astrocyte Gq-DREADDs RNA sequencing.** (A) Log<sub>2</sub> fold change of mRNA expression in Astrocyte Gq-DREADDs relative to respective littermate controls of BBB-specific genes after CNO administration. Data represent mean ± SEM (error bars). n=3 per group. \*p<0.05, \*\*p<0.005 by Wald Test. (B) Heat maps of genes significantly regulated by DREADDs-mediated glutamatergic activation in the Activating mice and paired littermate controls (top) and Astrocyte Gq-DREADDs mice paired littermate controls mice (bottom). Color scale represents arbitrary units of expression. Blue represents lower expression and red represents higher expression. (C) Heat maps of genes significantly regulated by DREADDs-mediated glutamatergic silencing in the Activating mice and paired littermate controls (top) and Astrocyte Gq-DREADDs mice paired littermate controls mice (bottom). Color scale represents arbitrary units of expression. Blue represents lower expression and red represents higher expression.

**Table A.1: DAVID Pathway Analysis for 572 genes *upregulated* by astrocytic calcium signaling.**

<b>Pathway</b>	<b>Enrichment Score</b>
Zinc ion binding	9.25
DNA binding	7.33
RNA binding	6.11
Pleckstrin homology domain	4.78
Bromodomain	4.61
Helicase activity	4.36
ATP binding	4.12
DNA repair	4.03
Focal adhesion	3.69
Rho GTPase activation protein	3.57

**Table A.2: DAVID Pathway Analysis for 157 genes *downregulated* by astrocytic calcium signaling.**

<b>Pathway</b>	<b>Enrichment Score</b>
Ribosomal Protein	25.84
rRNA-binding	5.27
Ribosomal small subunit assembly	5.16
Mitochondrial inner membrane	5.16
Mitochondrial Matrix	2.95
Mitochondrial respiratory chain complex	2.05
Mitochondrial outer membrane	1.89
Haptoglobin binding	1.79
Ribosomal protein, zinc-binding domain	1.41
Regulation of translation	1.21

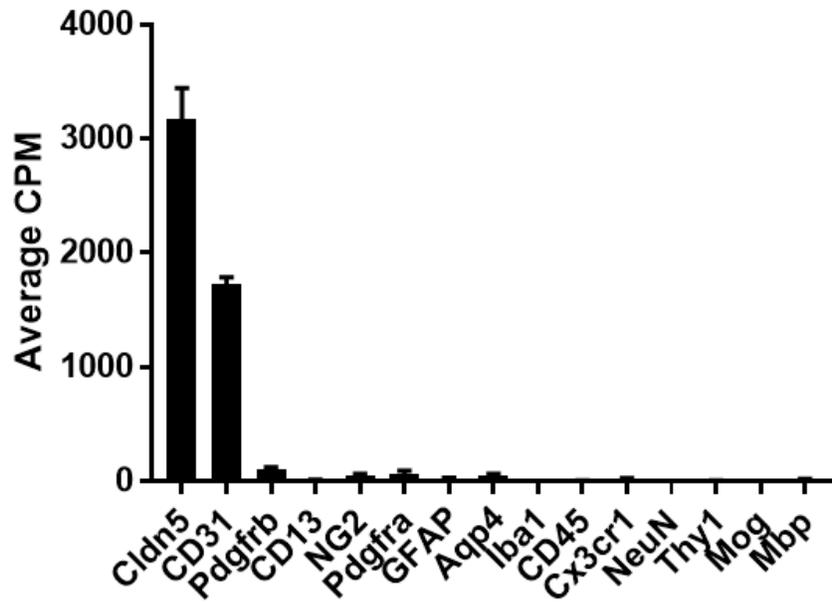


**Figure AS.1: Astrocytic Calcium-Regulated Brain Endothelial Transcriptome Cell Purity.** The counts per million (CPM) of cell-specific markers from all samples in the astrocyte dataset.

## **MATERIALS AND METHODS**

### **Mouse Strains**

All animal experiments were performed with national and UCSD IACUC guidelines. *Glast-CreERT2* mice were crossed to *Rls1-hM3Dq* mice to generate a tool to activate calcium signaling in astrocytes in response to tamoxifen administration. Mice were injected with 3 daily intraperitoneal injections of 100  $\mu$ l 20 mg/ml tamoxifen at 3 weeks and collected at 3-4 months of age. All mice were kept on a standard 12:12 hour light:dark cycle. Only male mice were used.

### **Immunohistochemistry**

Mice were anesthetized by i.p. injection of a ketamine/xylazine cocktail and then fixed via transcardial perfusion of D-PBS for 3 minutes, 4% paraformaldehyde (PFA) for 7-10 minutes, and again with D-PBS for 2 minutes using a Dynamax peristaltic pump. Speed was matched to typical cardiac output of a mouse. The brains were then dissected and submersion-fixed in 4% PFA overnight at 4°C. Brains were then submerged in 30% sucrose overnight at 4°C. Brains were then frozen in cryosectioning blocks in a solution consisting of 1:2 30% sucrose: OCT. 40 $\mu$ m sagittal sections were obtained using a cryostat.

Sections were stained floating in solution in the wells of a 12-well cell culture plate. They were blocked in a solution consisting of 5% goat serum and 0.1% Triton X-100 in PBS at room temperature for 45 minutes. They were then incubated in the blocking solution with the primary antibody, Rabbit-anti-HA 1/250 overnight at 4°C. They were then incubated in Goat-anti-Rabbit-Alexa 594 secondary antibody at room temperature for 90 minutes and then mounted on slides with DAPI Fluoromount-G for image processing.

### **Epifluorescence Imaging**

Epifluorescence images of HA-immunostained slides were taken with an Axio Imager D2 (Carl Zeiss) with a 5x Fluor, 0.25 NA using a digital camera (Axiocam HRm, Carl Zeiss). AxioVision software was used to acquire images. Individual images were stitched together to gain a complete image of a sagittal section of the brain using the photomerge feature of Adobe Photoshop.

### **FACS-purification of Brain Endothelial Cells**

For a given experiment, mice were collected in pairs consisting of one DREADDs mouse and one littermate control mouse. Each DREADDs mouse and its littermate control was injected i.p. with the electrophysiologically-verified dose of CNO(137) (1.0mg/kg) at approximately ZT23-ZT24. 3 hours post-injection the mice were live-decapitated using a mouse decapitator (LabScientific, XM-801). Brains were dissected out, the meninges were removed and the cortex and hippocampus were dissected out for further processing. The tissue was then diced using a #10 blade and enzymatically digested in Papain, 1 vial per on a 33° heat-block while being exposed to 95% oxygen, 5% carbon dioxide for 90 minutes. The tissue was then triturated and a second enzymatic digestion was performed in 1.0 mg/ml Collagenase Type 2 and 0.4 mg/ml Neutral Protease on a 33° heat-block while being exposed to 95% oxygen, 5% carbon dioxide for 30 minutes. Myelin was then removed as recommended with myelin removal beads using 30µm filters (MACS Miltenyi Biotec, 130-041-407) and LS columns (MACS Miltenyi Biotec, 130-042-401) on a MidiMACS separator (MACS Miltenyi Biotec, 130-042-302). The remaining single cell suspension was blocked with Rat IgG 1/100 for 20 minutes on ice. The samples were then stained with Rat-anti-CD31-Alexa 647, 1/100, mouse-anti-CD45-FITC 1/150, rat-anti-CD13-FITC 1/100, rat-anti-CD11b-FITC 1/100, rabbit-anti-NG2-Alexa 488 1/150, and DAPI for 20 minutes at 4°.

CD31-positive cells were sorted into Trizol using an ARIA II instrument at the Flow Cytometry Core at the VA Hospital in La Jolla, CA.

### **RNA-sequencing**

RNA was harvested from the FACS-purified brain endothelial cells using the Qiagen RNeasy Microkit. RNA samples were then further processed at the UCSD Genomics Core using standard core procedures. The RNA was tested for quality and concentration using a tape station bioanalyzer. Next, cDNA libraries were made using the TruSeq RNA Library Prep Kit v2. Samples were then sequenced on an Illumina HiSeq4000, 150 based, paired ends.

Sequence reads for all samples were mapped to Ensembl mm9 v67 mouse whole genome using Tophat v 2.0.11 and Bowtie 2 v 2.2.1 with parameters no-coverage-search -m 2 -a 5 -p 7. Alignment files were sorted using SAMtools v.0.1.19. Count tables were generated using HTSeq-0.6.1. Differential expression of genes between control and treated samples, log 2-fold changes between control and treated samples, and paired statistical analysis including p values and FDR was performed using DESeq2 and Excel.

## **APPENDIX B:**

The Role of the Mechanosensitive Ion Channel *Piezol* in Barrier Development

## INTRODUCTION

Although blood flow and the BBB are two well-studied fields, little is known about whether blood flow can regulate the BBB. The majority of work done on blood flow in the brain vasculature has been done in the context of NVC(55). Many of the unique properties of the BBB are extrinsically regulated by the microenvironment of the CNS. However, it is unknown whether CNS endothelial cells possess unique mechanisms of integrating common signals that all endothelial cells are exposed to such as blood flow. Recent breakthroughs on how endothelial cells transduce mechanosensory information from blood flow can shed new light on this(138,139).

The Piezo receptor is a collection of pore-forming subunits that form a membrane-bound ion channel which opens in response to mechanosensation, allowing positively charged ions to flow into a cell and illicit downstream functional signaling. Most vertebrates have two channel isoforms, *Piezo1* and *Piezo2*, which are necessary for mechanical responses in a diverse array of cell types across a wide range of tissues that undergo functional mechanosensation. The unique trimeric propeller-like structure of the Piezo channel enables its ability to be activated by a diverse array of mechanical stimuli(140). In general, *Piezo1* tends to be localized to nonsensory tissue experiencing fluid pressure and flow such as blood vessels, whereas *Piezo2* tends to be localized to sensory tissue experiencing touch sensation.

*Piezo1* is highly expressed in endothelial cells throughout the body(139). Endothelial-specific deletion of *Piezo1* in development is embryonic lethal suggesting that it is essential for vascular development(83,141). It was shown that presence of *Piezo1* is essential during development for sensing mechanical shear stress for endothelial cell alignment in the direction of blood flow. This mechanism is also preserved in lymphatic endothelial cells(142). Endothelial-

specific deletion in adulthood causes high systemic blood pressure due to impaired endothelial nitric oxide synthase (eNOS) signaling(143).

Although *Piezo1* has been shown to play crucial roles in endothelial cells in both development and adulthood, its function specifically in CNS endothelial cells has not been investigated thoroughly. CNS endothelial cells have much more specialized functions in maintaining brain homeostasis through the BBB and dynamic NVC. It is plausible that *Piezo1*-mediated mechanosensation of blood flow may regulate these CNS endothelial-specific functions. The major limitation to understanding a CNS endothelial-specific role from these studies is that the investigators used Cre recombinase that is downstream of a pan-endothelial promoter to genetically ablate *Piezo1*. Therefore, the effects of genetically ablating *Piezo1* in peripheral endothelial cells may convolute its effect on CNS endothelial cells. In this study we wanted to investigate whether *Piezo1* is important for development and maintenance of CNS endothelial barrier properties. We utilized a genetic tool to ablate *Piezo1* exclusively in CNS endothelial cells during postnatal development and adulthood and assessed blood-retinal barrier (BRB) function.

## RESULTS

In order to investigate the role of Piezo1 specifically in CNS endothelial cells and whether it is required for development and maintenance of barrier properties, we utilized mice expressing *Slco1c1-CreERT2*, a CNS endothelial cell-specific, tamoxifen-sensitive cre recombinase. We then crossed it to Piezo1-floxed mice to genetically ablate Piezo1 in CNS endothelial cells in response to tamoxifen administration. The BBB forms embryonically(47,48) whereas the BRB forms postnatally(144). Therefore, in order to reliably ablate Piezo1 expression in CNS vascular development we injected tamoxifen into Piezo1 conditional knockouts (cKOs) and littermate controls at P2-P4 during retinal angiogenesis and barrierogenesis and asked whether Piezo1 was required for functional BRB development. At P9, there was significantly more extravascular leakage of Sulfo-NHS-Biotin in the retinas of Piezo1 cKOs compared to littermate controls (Figure B.1 A, Figure B.1 C). This suggests that Piezo1 is required for barrierogenesis in the developing retinal vasculature. However, there was difference in extravascular leakage between cKOs and littermate controls when tamoxifen was injected in adulthood after postnatal development (Figure A.1 B, Figure A.1 D). This suggests that Piezo1 is not required for BRB maintenance in adulthood.

## DISCUSSION

Here, we genetically ablate the mechanosensitive cation channel Piezo1 exclusively in CNS endothelial cells during postnatal development and demonstrate that it is required for BRB development, but not BRB maintenance. This elucidates a potentially novel pathway in which mechanosensation of shear stress during development regulates barrier formation.

Extravascular biotin leakage suggests that there is BRB dysfunction specifically related to transcellular or paracellular pathways. Therefore, it is plausible that Piezo1 is required for development of tight junctions or suppression of transcytosis. It would be interesting to investigate markers of these two barrier properties through immunofluorescence or electron microscopy to determine which aspect(s) of the BRB are regulated by Piezo1 in development.

It is also possible that a similar mechanism from peripheral endothelial deletion is responsible for the BRB leakage. It was shown that there was impaired shear stress-mediated focal adhesion and cell alignment in the absence of Piezo1(83,141). If endothelial focal adhesion is impaired, this could potentially affect adherens junctions which compose a minor barrier in all endothelial cells(68,69). If adherens junctions were disrupted, this would undoubtedly permit paracellular extravascular leakage.

Although unlikely, it is also possible that Piezo1 has an unknown non-mechanosensory role that is required for BRB development. We did not directly test shear-stress in our experiments. Therefore, *in vitro* studies that combine shear stress and barrier function would be required to confirm the role of blood flow.

In addition, it would be interesting to investigate whether Piezo1 is also required for BBB development. Unfortunately, we cannot reliably administer tamoxifen embryonically so a non-tamoxifen-inducible *Slco1c1*-Cre would be required to address this.

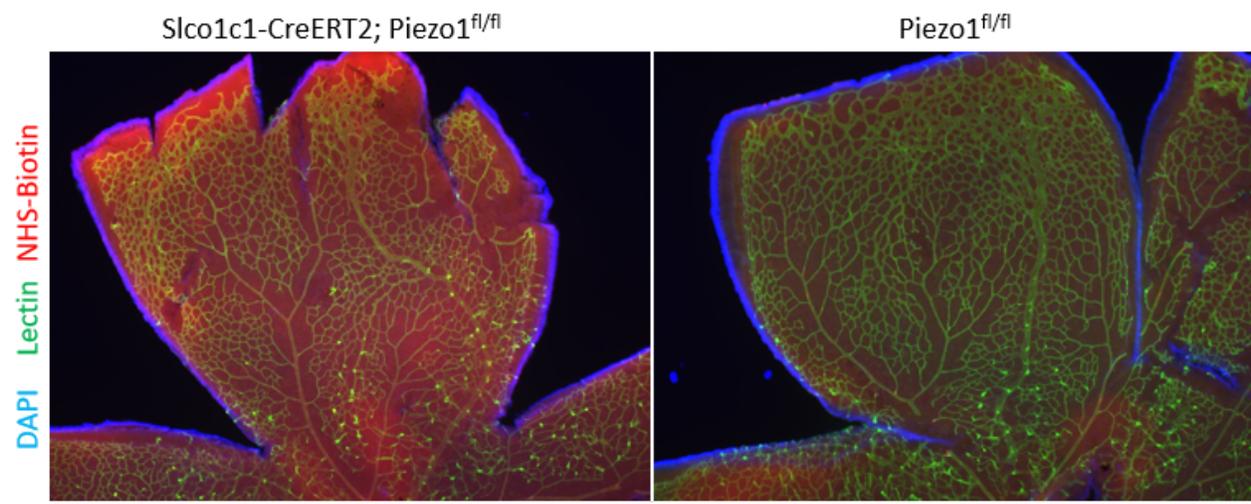
More studies are needed to understand how blood flow regulates barrier properties in CNS vasculature. Understanding these molecular mechanisms may elucidate clinically relevant information for diseases that involve both blood flow and the BBB such as stroke and epilepsy.

## FIGURES

**Figure B.1: CNS endothelial Piezo1 is required for BRB development, but not BRB maintenance.** (A-B) Representative images of retinas after PFA-fixed perfusion of NHS-Biotin which was visualized with streptavidin-Alexa594 staining. (A) To assess BRB function during postnatal development, Piezo1 cKO mice (left) and littermate controls (right) were injected with tamoxifen P2-P4 and the NHS-Biotin leakage assay was performed at P9. (B) To assess BRB function during adulthood, Piezo1 cKO mice (left) and littermate controls (right) were injected with tamoxifen at 6 weeks of age and the NHS-Biotin leakage assay was performed at 12 weeks of age. (C-D) Quantification of extravascular NHS-Biotin accumulation by fluorescence microscopy of the two experiments. Leakage was calculated as the amount of signal outside the Lectin-defined vasculature. \*\*\* $p < 0.001$ , n.s. (not significant) by Student's t-test.

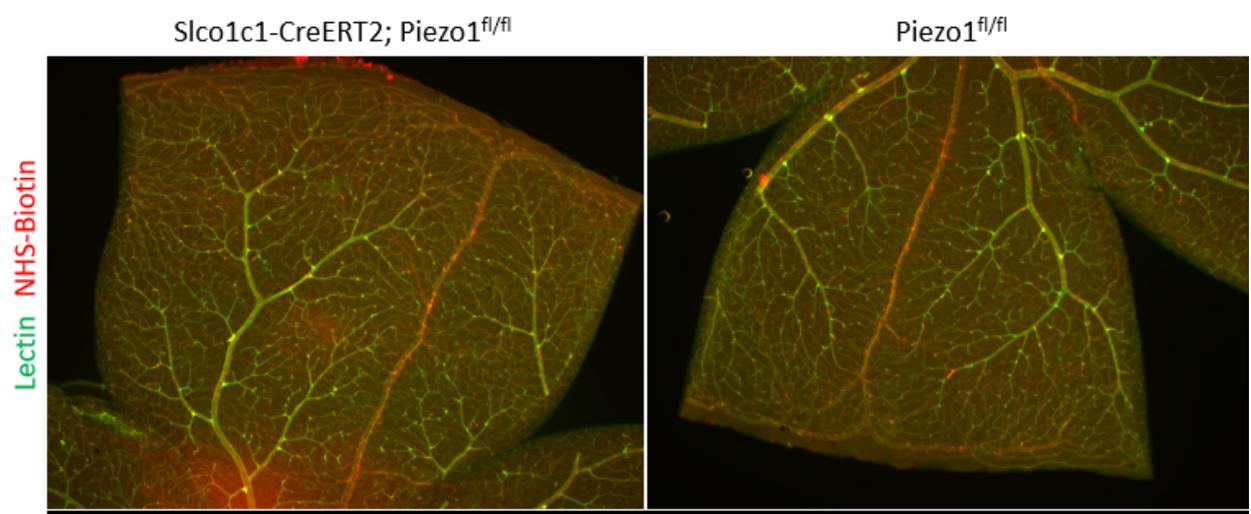
A

Tamoxifen P2-P4 → Analyze P9

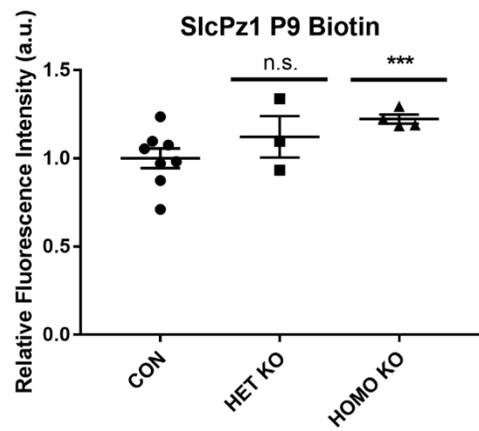


B

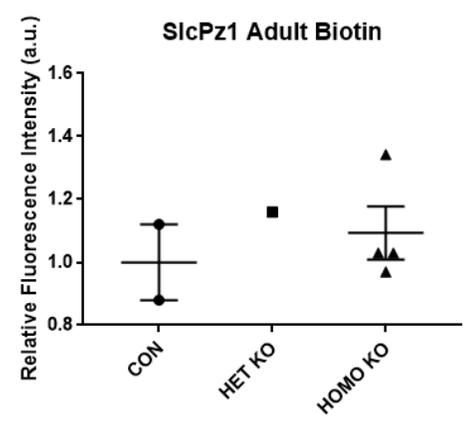
Tamoxifen 6 weeks → Analyze 12 weeks



C



D



## **MATERIALS AND METHODS**

### **Mouse Strains**

All animal experiments were performed with national and UCSD IACUC guidelines. *Slco1c1-CreERT2* mice were crossed to *Piezo1<sup>fl/fl</sup>* mice to generate a tamoxifen-inducible, CNS endothelial-specific Piezo1 conditional knockout mouse line. To ablate Piezo1 during postnatal development, mice were injected with 3 daily intraperitoneal injections of 30  $\mu$ l 2 mg/ml tamoxifen at P2-P4 and retinas were collected at P9. To ablate Piezo1 in adulthood, mice were injected with 3 daily intraperitoneal injections of 100  $\mu$ l 20 mg/ml tamoxifen at 6 weeks of age and retinas were collected at 12 weeks of age. All mice were kept on a standard 12:12 hour light:dark cycle.

### **Retina collection for barrier analysis**

Mice were deeply anesthetized using aketamine/xylazine mixture and then sequentially transcardially perfused with 0.25 mg/mL EZ-Link Sulfo-NHS–Biotin in PBS followed by 4% PFA in PBS. The whole eyes were fixed in 4% PFA in 1 $\times$  PBS at room temperature for 10 min, then transferred to 1 $\times$  PBS on ice. The retinas were dissected out and post-fixed in 4% PFA for 45 min to 1 h then washed in PBS and stored in PBS plus azide at 4 $^{\circ}$  in the dark.

### **Immunofluorescence**

Whole-mount fixed retinas were washed in PBS then blocked for 30 min in 0.2% bovine serum albumin, 5% serum, and 0.3% TritonX-100, then incubated in primary antibody in blocking buffer overnight at 4 $^{\circ}$  with gentle rocking. Retinas were then washed in 0.3% Triton X-100 three times, and incubated with secondary antibodies in 0.3% Triton X-100 for 2–4 h at room temperature, protected from light with gentle rocking. They were then washed in 0.3% Triton X-100 twice, 1x PBS twice, and then mounted on slides with Fluoromount-G with DAPI. Fluorescein conjugated *bandeiraea simplicifolia* lectin was used to label blood vessels. Streptavidin conjugated to Alexa-594 was used to label biotin.

## REFERENCES

1. Aird WC. Phenotypic Heterogeneity of the Endothelium. *Circ Res*. 2007;
2. Gloor SM, Wachtel M, Bolliger MF, Ishihara H, Landmann R, Frei K. Molecular and cellular permeability control at the blood-brain barrier. *Brain Res Rev*. 2001;36(2–3):258–64.
3. LL Rubin JS. The cell biology of the blood-brain barrier. *Annu Rev Neurosci*. 1999;11–28.
4. Saunders NR, Ek CJ, Habgood MD, Dziegielewska KM. Barriers in the brain: a renaissance? *Trends Neurosci*. 2008;31(6):279–86.
5. Zlokovic B V. The Blood-Brain Barrier in Health and Chronic Neurodegenerative Disorders. *Neuron*. 2008;57(2):178–201.
6. Daneman R, Zhou L, Agalliu D, Cahoy JD, Kaushal A, Barres BA. The mouse blood-brain barrier transcriptome: A new resource for understanding the development and function of brain endothelial cells. *PLoS One*. 2010;5(10).
7. Hindle SJ, Munji RN, Dolgih E, Gaskins G, Orng S, Ishimoto H, Soung A, DeSalvo M, Kitamoto T, Keiser MJ, Jacobson MP, Daneman R, Bainton RJ. Evolutionarily Conserved Roles for Blood-Brain Barrier Xenobiotic Transporters in Endogenous Steroid Partitioning and Behavior. *Cell Rep*. 2017;21(5):1304–16.
8. Alvarez JI, Cayrol R, Prat A. Disruption of central nervous system barriers in multiple sclerosis. *Biochim Biophys Acta - Mol Basis Dis*. 2011;1812(2):252–64.
9. Sandoval KE, Witt KA. Blood-brain barrier tight junction permeability and ischemic stroke. *Neurobiol Dis* [Internet]. 2008;32(2):200–19.
10. Sweeney MD, Kisler K, Montagne A, Toga AW, Zlokovic B V. The role of brain vasculature in neurodegenerative disorders. *Nature Neuroscience*. 2018.
11. Pardridge WM. Blood-brain barrier delivery. *Drug Discovery Today*. 2007.
12. Pardridge WM. Drug transport in brain via the cerebrospinal fluid. *Fluids and Barriers of the CNS*. 2011.
13. Hanson LR, Frey WH. Intranasal delivery bypasses the blood-brain barrier to target therapeutic agents to the central nervous system and treat neurodegenerative disease. In: *BMC Neuroscience*. 2008.
14. Cordon-Cardo C, O'Brien JP, Casals D, Rittman-Grauer L, Biedler JL, Melamed MR, Bertino JR. Multidrug-resistance gene (P-glycoprotein) is expressed by endothelial cells at blood-brain barrier sites. *Proc Natl Acad Sci U S A*. 1989;86(2):695–8.
15. Lee HJ, Engelhardt B, Lesley J, Bickel U, Pardridge WM. Targeting rat anti-mouse transferrin receptor monoclonal antibodies through blood-brain barrier in mouse. *J Pharmacol Exp Ther*. 2000;
16. Niewoehner J, Bohrmann B, Collin L, Urich E, Sade H, Maier P, Rueger P, Stracke JO,

- Lau W, Tissot AC, Loetscher H, Ghosh A, Freskgård PO. Increased Brain Penetration and Potency of a Therapeutic Antibody Using a Monovalent Molecular Shuttle. *Neuron*. 2014;
17. Kanodia JS, Gadkar K, Bumbaca D, Zhang Y, Tong RK, Luk W, Hoyte K, Lu Y, Wildsmith KR, Couch JA, Watts RJ, Dennis MS, Ernst JA, Scarce-Levie K, Atwal JK, Ramanujan S, Joseph S. Prospective design of anti-transferrin receptor bispecific antibodies for optimal delivery into the human brain. *CPT Pharmacometrics Syst Pharmacol*. 2016;
  18. Hynynen K, Jolesz FA. Demonstration of potential noninvasive ultrasound brain therapy through an intact skull. *Ultrasound Med Biol*. 1998;
  19. Lipsman N, Meng Y, Bethune AJ, Huang Y, Lam B, Masellis M, Herrmann N, Heyn C, Aubert I, Boutet A, Smith GS, Hynynen K, Black SE. Blood–brain barrier opening in Alzheimer’s disease using MR-guided focused ultrasound. *Nat Commun*. 2018;
  20. Furuse M. Molecular basis of the core structure of tight junctions. Vol. 2, Cold Spring Harbor perspectives in biology. 2010.
  21. Amasheh S, Schmidt T, Mahn M, Florian P, Mankertz J, Tavalali S, Gitter AH, Schulzke JD, Fromm M. Contribution of claudin-5 to barrier properties in tight junctions of epithelial cells. *Cell Tissue Res*. 2005;
  22. Hou J, Gomes AS, Paul DL, Goodenough DA. Study of claudin function by RNA interference. *J Biol Chem*. 2006;
  23. Balda MS, Whitney JA, Flores C, González S, Cereijido M, Matter K. Functional dissociation of paracellular permeability and transepithelial electrical resistance and disruption of the apical-basolateral intramembrane diffusion barrier by expression of a mutant tight junction membrane protein. *J Cell Biol*. 1996;
  24. Martin-Padura I, Lostaglio S, Schneemann M, Williams L, Romano M, Fruscella P, Panzeri C, Stoppacciaro A, Ruco L, Villa A, Simmons D, Dejana E. Junctional adhesion molecule, a novel member of the immunoglobulin superfamily that distributes at intercellular junctions and modulates monocyte transmigration. *J Cell Biol*. 1998;
  25. Williams LA, Martin-Padura I, Dejana E, Hogg N, Simmons DL. Identification and characterization of human junctional adhesion molecule (JAM). *Mol Immunol*. 1999;
  26. Aurrand-Lions M, Johnson-Leger C, Wong C, Du Pasquier L, Imhof BA. Heterogeneity of endothelial junctions is reflected by differential expression and specific subcellular localization of the three JAM family members. *Blood*. 2001;
  27. Knipp GT, Ho NFH, Barsuhn CL, Borchardt RT. Paracellular diffusion in Caco-2 cell monolayers: Effect of perturbation on the transport of hydrophilic compounds that vary in charge and size. *J Pharm Sci*. 1997;
  28. Sohet F, Lin C, Munji RN, Lee SY, Ruderisch N, Soung A, Arnold TD, Derugin N, Vexler ZS, Yen FT, Daneman R. LSR/angulin-1 is a tricellular tight junction protein involved in blood-brain barrier formation. *J Cell Biol*. 2015;
  29. Hallmann R, Mayer DN, Berg EL, Broermann R, Butcher EC. Novel mouse endothelial

- cell surface marker is suppressed during differentiation of the blood brain barrier. *Dev Dyn*. 1995;202(4):325–32.
30. Engelhardt B. Immune cell entry into the central nervous system: involvement of adhesion molecules and chemokines. *J Neurol Sci*. 2008;274(1–2):23–6.
  31. Daneman R, Zhou L, Kebede AA, Barres BA. Pericytes are required for blood-brain barrier integrity during embryogenesis. Vol. 468, *Nature*. 2010. p. 562–6.
  32. Betz AL, Goldstein GW. Polarity of the blood-brain barrier: neutral amino acid transport into isolated brain capillaries. *Science* (80- ). 1978;202(4364):225–7.
  33. Cornford EM, Hyman S, Swartz BE. The human brain GLUT1 glucose transporter: Ultrastructural localization to the blood-brain barrier endothelia. *J Cereb Blood Flow Metab*. 1994;
  34. Kido Y, Tamai I, Okamoto M, Suzuki F, Tsuji A. Functional clarification of MCT1-mediated transport of monocarboxylic acids at the blood-brain barrier using in vitro cultured cells and in vivo BUI studies. *Pharm Res*. 2000;
  35. Kanai Y, Segawa H, Miyamoto KI, Uchino H, Takeda E, Endou H. Expression cloning and characterization of a transporter for large neutral amino acids activated by the heavy chain of 4F2 antigen (CD98). *J Biol Chem*. 1998;
  36. Cirrito JR, Deane R, Fagan AM, Spinner ML, Parsadanian M, Finn MB, Jiang H, Prior JL, Sagare A, Bales KR, Paul SM, Zlokovic B V., Piwnicka-Worrns D, Holtzman DM. P-glycoprotein deficiency at the blood-brain barrier increases amyloid- $\beta$  deposition in an Alzheimer disease mouse model. *J Clin Invest*. 2005;
  37. Stewart PA, Wiley MJ. Developing nervous tissue induces formation of blood-brain barrier characteristics in invading endothelial cells: A study using quail-chick transplantation chimeras. *Dev Biol*. 1981;84(1):183–92.
  38. Muoio V, Persson PB, Sendeski MM. The neurovascular unit - concept review. *Acta Physiologica*. 2014.
  39. Janzer RC, Raff MC. Astrocytes induce blood-brain barrier properties in endothelial cells. Vol. 325, *Nature*. 1987. p. 253–7.
  40. Arthur FE, Shivers RR, Bowman PD. Astrocyte-mediated induction of tight junctions in brain capillary endothelium: an efficient in vitro model. *Dev Brain Res*. 1987;
  41. Raub TJ. Signal transduction and glial cell modulation of cultured brain microvessel endothelial cell tight junctions. *Am J Physiol Physiol*. 2017;
  42. Rist RJ, Romero IA, Chan MWK, Couraud PO, Roux F, Abbott NJ. F-actin cytoskeleton and sucrose permeability of immortalised rat brain microvascular endothelial cell monolayers: Effects of cyclic AMP and astrocytic factors. *Brain Res*. 1997;
  43. Igarashi Y, Utsumi H, Chiba H, Yamada-Sasamori Y, Tobioka H, Kamimura Y, Furuuchi K, Kokai Y, Nakagawa T, Mori M, Sawada N. Glial cell line-derived neurotrophic factor induces barrier function of endothelial cells forming the blood-brain barrier. *Biochem*

- Biophys Res Commun. 1999;
44. Lee SW, Kim WJ, Choi YK, Song HS, Son MJ, Gelman IH, Kim YJ, Kim KW. SSeCKS regulates angiogenesis and tight junction formation in blood-brain barrier. *Nat Med.* 2003;
  45. Wosik K, Cayrol R, Dodelet-Devillers A, Berthelet F, Bernard M, Moumdjian R, Bouthillier A, Reudelhuber TL, Prat A. Angiotensin II Controls Occludin Function and Is Required for Blood Brain Barrier Maintenance: Relevance to Multiple Sclerosis. *J Neurosci.* 2007;
  46. Alvarez JI, Dodelet-Devillers A, Kebir H, Ifergan I, Fabre PJ, Terouz S, Sabbagh M, Wosik K, Bourbonnière L, Bernard M, Van Horssen J, De Vries HE, Charron F, Prat A. The hedgehog pathway promotes blood-brain barrier integrity and CNS immune quiescence. *Science* (80- ). 2011;
  47. Bauer HC, Steiner M, Bauer H. Embryonic development of the CNS microvasculature in the mouse: new insights into the structural mechanisms of early angiogenesis. In 1992.
  48. Bauer HC, Bauer H, Lametschwandtner A, Amberger A, Ruiz P, Steiner M. Neovascularization and the appearance of morphological characteristics of the blood-brain barrier in the embryonic mouse central nervous system. *Dev Brain Res.* 1993;
  49. Armulik A, Genové G, Mäe M, Nisancioglu MH, Wallgard E, Niaudet C, He L, Norlin J, Lindblom P, Strittmatter K, Johansson BR, Betsholtz C. Pericytes regulate the blood-brain barrier. *Nature.* 2010;
  50. Ben-Zvi A, Lacoste B, Kur E, Andreone BJ, Mayshar Y, Yan H, Gu C. Mfsd2a is critical for the formation and function of the blood-brain barrier. *Nature* [Internet]. 2014;509(7501):507–11.
  51. Nguyen LN, Ma D, Shui G, Wong P, Cazenave-Gassiot A, Zhang X, Wenk MR, Goh ELK, Silver DL. Mfsd2a is a transporter for the essential omega-3 fatty acid docosahexaenoic acid. *Nature.* 2014;509(7501):503–6.
  52. Weidenfeller C, Svendsen CN, Shusta E V. Differentiating embryonic neural progenitor cells induce blood-brain barrier properties. *J Neurochem.* 2007;
  53. Daneman R, Agalliu D, Zhou L, Kuhnert F, Kuo CJ, Barres BA. Wnt/beta-catenin signaling is required for CNS, but not non-CNS, angiogenesis. *Proc Natl Acad Sci U S A.* 2009;106(2):641–6.
  54. Wang Y, Rattner A, Zhou Y, Williams J, Smallwood PM, Nathans J. Norrin/Frizzled4 signaling in retinal vascular development and blood brain barrier plasticity. *Cell.* 2012;
  55. Roy CS, Sherrington CS. On the Regulation of the Blood-supply of the Brain. *J Physiol.* 1890;
  56. Nersesyan H, Herman P, Erdogan E, Hyder F, Blumenfeld H. Relative changes in cerebral blood flow and neuronal activity in local microdomains during generalized seizures. *J Cereb Blood Flow Metab.* 2004;24(9):1057–68.
  57. Whiteus C, Freitas C, Grutzendler J. Perturbed neural activity disrupts cerebral

- angiogenesis during a postnatal critical period. *Nature*. 2014;
58. Lacoste B, Comin CH, Ben-Zvi A, Kaeser PS, Xu X, Costa LF, Gu C. Sensory-Related Neural Activity Regulates the Structure of Vascular Networks in the Cerebral Cortex. *Neuron*. 2014;
  59. Hrvatin S, Hochbaum DR, Nagy MA, Cicconet M, Robertson K, Cheadle L, Zilionis R, Ratner A, Borges-Monroy R, Klein AM, Sabatini BL, Greenberg ME. Publisher Correction: Single-cell analysis of experience-dependent transcriptomic states in the mouse visual cortex. *Nature Neuroscience*. 2018;
  60. Palop JJ, Chin J, Roberson ED, Wang J, Thwin MT, Bien-Ly N, Yoo J, Ho KO, Yu GQ, Kreitzer A, Finkbeiner S, Noebels JL, Mucke L. Aberrant Excitatory Neuronal Activity and Compensatory Remodeling of Inhibitory Hippocampal Circuits in Mouse Models of Alzheimer's Disease. *Neuron*. 2007;
  61. Busche MA, Eichhoff G, Adelsberger H, Abramowski D, Wiederhold KH, Haass C, Staufenbiel M, Konnerth A, Garaschuk O. Clusters of hyperactive neurons near amyloid plaques in a mouse model of Alzheimer's disease. *Science* (80- ). 2008;
  62. Bero AW, Yan P, Roh JH, Cirrito JR, Stewart FR, Raichle ME, Lee JM, Holtzman DM. Neuronal activity regulates the regional vulnerability to amyloid- $\beta$  2 deposition. *Nat Neurosci*. 2011;
  63. Yuan P, Grutzendler J. Attenuation of  $\beta$ -Amyloid Deposition and Neurotoxicity by Chemogenetic Modulation of Neural Activity. *J Neurosci*. 2016;
  64. Dickerson BC, Salat DH, Greve DN, Chua EF, Rand-Giovannetti E, Rentz DM, Bertram L, Mullin K, Tanzi RE, Blacker D, Albert MS, Sperling RA. Increased hippocampal activation in mild cognitive impairment compared to normal aging and AD. *Neurology*. 2005;
  65. Elman JA, Oh H, Madison CM, Baker SL, Vogel JW, Marks SM, Crowley S, O'Neil JP, Jagust WJ. Neural compensation in older people with brain amyloid- $\beta$  deposition. *Nat Neurosci*. 2014;
  66. Palmqvist S, Schöll M, Strandberg O, Mattsson N, Stomrud E, Zetterberg H, Blennow K, Landau S, Jagust W, Hansson O. Earliest accumulation of  $\beta$ -amyloid occurs within the default-mode network and concurrently affects brain connectivity. *Nat Commun*. 2017;
  67. Alexander GM, Rogan SC, Abbas AI, Armbruster BN, Pei Y, Allen John A., Nonneman RJ, Hartmann J, Moy SS, Nicoletis MA, McNamara JO, Roth BL. Remote control of neuronal activity in transgenic mice expressing evolved G protein-coupled receptors. *Neuron*. 2009;63(1):27–39.
  68. Miao H, Hu YL, Shiu YT, Yuan S, Zhao Y, Kaunas R, Wang Y, Jin G, Usami S, Chien S. Effects of flow patterns on the localization and expression of VE-cadherin at vascular endothelial cell junctions: In vivo and in vitro investigations. *J Vasc Res*. 2005;
  69. Galbraith GG, Skalak R, Chien S. Shear stress induces spatial reorganization of the endothelial cell cytoskeleton. *Cell Motil Cytoskeleton*. 1998;40(4):317–30.

70. Polacheck WJ, Kutys ML, Yang J, Eyckmans J, Wu Y, Vasavada H, Hirschi KK, Chen CS. A non-canonical Notch complex regulates adherens junctions and vascular barrier function. *Nature*. 2017;
71. Isaacs KR, Anderson BJ, Alcantara AA, Black JE, Greenough WT. Exercise and the brain: Angiogenesis in the adult rat cerebellum after vigorous physical activity and motor skill learning. *J Cereb Blood Flow Metab*. 1992;
72. Newton SS, Girgenti MJ, Collier EF, Duman RS. Electroconvulsive seizure increases adult hippocampal angiogenesis in rats. *Eur J Neurosci*. 2006;
73. Nishijima T, Piriz J, Duflot S, Fernandez AM, Gaitan G, Gomez-Pinedo U, Verdugo JMG, Leroy F, Soya H, Nuñez A, Torres-Aleman I. Neuronal Activity Drives Localized Blood-Brain-Barrier Transport of Serum Insulin-like Growth Factor-I into the CNS. *Neuron*. 2010;67(5):834–46.
74. Sohet F, Daneman R. Genetic mouse models to study blood-brain barrier development and function. *Fluids and Barriers of the CNS*. 2013.
75. Sadeghian H, Lacoste B, Qin T, Toussay X, Rosa R, Oka F, Chung DY, Takizawa T, Gu C, Ayata C. Spreading depolarizations trigger caveolin-1-dependent endothelial transcytosis. *Ann Neurol*. 2018;
76. Longden TA, Dabertrand F, Koide M, Gonzales AL, Tykocki NR, Brayden JE, Hill-eubanks D, Nelson MT. Capillary K<sup>+</sup>-sensing initiates retrograde hyperpolarization to increase local cerebral blood flow. 2017;(October 2016).
77. Lemaistre JL, Sanders SA, Stobart MJ, Lu L, Knox JD, Anderson HD, Anderson CM. Coactivation of NMDA receptors by glutamate and D-serine induces dilation of isolated middle cerebral arteries. *J Cereb Blood Flow Metab*. 2011;32(3):537–47.
78. Hogan-cann AD, Anderson CM. Physiological Roles of Non- Neuronal NMDA Receptors. *Trends Pharmacol Sci*. 2016;xx:1–18.
79. Anwar Z, Albert JL, Gubby SE, Boyle JP, Roberts J a, Webb TE, Boarder MR. Regulation of cyclic AMP by extracellular ATP in cultured brain capillary endothelial cells. *Br J Pharmacol*. 1999;128(2):465–71.
80. Mohamed LA, Markandaiah SS, Bonanno S, Pasinelli P, Trotti D. Excess glutamate secreted from astrocytes drives upregulation of P-glycoprotein in endothelial cells in amyotrophic lateral sclerosis. *Exp Neurol*. 2019;(March):0–1.
81. Petzold GC, Murthy VN. Role of astrocytes in neurovascular coupling. Vol. 71, *Neuron*. 2011. p. 782–96.
82. Ranade SS, Qiu Z, Woo S-H, Hur SS, Murthy SE, Cahalan SM, Xu J, Mathur J, Bandell M, Coste B, Li Y-SJ, Chien S, Patapoutian A. Piezo1, a mechanically activated ion channel, is required for vascular development in mice. *Proc Natl Acad Sci*. 2014;111(28):10347–52.
83. Li J, Hou B, Tumova S, Muraki K, Bruns A, Ludlow MJ, Sedo A, Hyman AJ, McKeown L, Young RS, Yuldasheva NY, Majeed Y, Wilson LA, Rode B, Bailey MA, Kim HR, Fu

- Z, Carter DAL, Bilton J, Imrie H, Ajuh P, Dear TN, Cubbon RM, Kearney MT, Prasad RK, Evans PC, Ainscough JFX, Beech DJ. Piezo1 integration of vascular architecture with physiological force. *Nature*. 2014;515(7526):279–82.
84. Xu J, Mathur J, Vessières E, Hammack S, Nonomura K, Favre J, Grimaud L, Petrus M, Francisco A, Li J, Lee V, Xiang F li, Mainquist JK, Cahalan SM, Orth AP, Walker JR, Ma S, Lukacs V, Bordone L, Bandell M, Laffitte B, Xu Y, Chien S, Henrion D, Patapoutian A. GPR68 Senses Flow and Is Essential for Vascular Physiology. *Cell*. 2018;
  85. Baeyens N, Schwartz MA. Biomechanics of vascular mechanosensation and remodeling. *Mol Biol Cell*. 2016;
  86. McCaffrey G, Staatz WD, Sanchez-Covarrubias L, Finch JD, Demarco K, Laracuent ML, Ronaldson PT, Davis TP. P-glycoprotein trafficking at the blood-brain barrier altered by peripheral inflammatory hyperalgesia. *J Neurochem*. 2012;
  87. Noack A, Noack S, Hoffmann A, Maalouf K, Buettner M, Couraud PO, Romero IA, Weksler B, Alms D, Römermann K, Naim HY, Löscher W. Drug-induced trafficking of P-glycoprotein in human brain capillary endothelial cells as demonstrated by exposure to mitomycin C. *PLoS One*. 2014;
  88. Tome ME, Herndon JM, Schaefer CP, Jacobs LM, Zhang Y, Jarvis CK, Davis TP. P-glycoprotein traffics from the nucleus to the plasma membrane in rat brain endothelium during inflammatory pain. *J Cereb Blood Flow Metab*. 2016;
  89. Vanlandewijck M, He L, Mäe MA, Andrae J, Ando K, Del Gaudio F, Nahar K, Lebouvier T, Laviña B, Gouveia L, Sun Y, Raschperger E, Räsänen M, Zarb Y, Mochizuki N, Keller A, Lendahl U, Betsholtz C. A molecular atlas of cell types and zonation in the brain vasculature. *Nature*. 2018;
  90. Koenig J, Linder AN, Leutgeb JK, Leutgeb S. The spatial periodicity of grid cells is not sustained during reduced theta oscillations. *Science* (80- ). 2011;
  91. Banes AJ, Link GW, Beckman WC, Camps JL, Powers SK. High-performance liquid chromatographic quantitation of rhodamines 123 and 110 from tissues and cultured cells. *J Chromatogr A*. 1986;356(C):301–9.
  92. Richards J, Gumz ML. Invited Review EB 2012: Mechanism of the Circadian Clock in Physiology. *Am J Physiol Regul Integr Comp Physiol*. 2013;
  93. Ripperger JA, Schibler U. Circadian regulation of gene expression in animals. *Current Opinion in Cell Biology*. 2001.
  94. Ripperger JA, Shearman LP, Reppert SM, Schibler U. CLOCK, an essential pacemaker component, controls expression of the circadian transcription factor DBP. *Genes Dev*. 2000;
  95. Mongrain V, La Spada F, Curie T, Franken P. Sleep loss reduces the dna-binding of bmal1, clock, and npas2 to specific clock genes in the mouse cerebral cortex. *PLoS One*. 2011;
  96. Curie T, Mongrain V, Dorsaz S, Mang GM, Emmenegger Y, Franken P. Homeostatic and

- Circadian Contribution to EEG and Molecular State Variables of Sleep Regulation. *Sleep*. 2013;
97. Ripperger JA, Schibler U. Rhythmic CLOCK-BMAL1 binding to multiple E-box motifs drives circadian Dbp transcription and chromatin transitions. *Nat Genet*. 2006;
  98. Welsh DK, Logothetis DE, Meister M, Reppert SM. Individual neurons dissociated from rat suprachiasmatic nucleus express independently phased circadian firing rhythms. *Neuron*. 1995;
  99. Brancaccio M, Edwards MD, Patton AP, Smyllie NJ, Chesham JE, Maywood ES, Hastings MH. Cell-autonomous clock of astrocytes drives circadian behavior in mammals. *Science* (80- ). 2019;192(January):187–92.
  100. Curtis AM, Cheng Y, Kapoor S, Reilly D, Price TS, FitzGerald GA. Circadian variation of blood pressure and the vascular response to asynchronous stress. *Proc Natl Acad Sci*. 2007;
  101. Anea CB, Zhang M, Chen F, Ali MI, Hart CMM, Stepp DW, Kovalenkov YO, Merloiu AM, Pati P, Fulton D, Rudic RD. Circadian Clock Control of Nox4 and Reactive Oxygen Species in the Vasculature. *PLoS One*. 2013;
  102. Richards J, Diaz AN, Gumz ML. Clock genes in hypertension: Novel insights from rodent models. *Blood Pressure Monitoring*. 2014.
  103. Sandoo A, Veldhuijzen van Zanten JJCS, Metsios GS, Carroll D, Kitas GD. The Endothelium and Its Role in Regulating Vascular Tone. *Open Cardiovasc Med J*. 2010;
  104. Durgan DJ, Crossland RF, Bryan RM. The rat cerebral vasculature exhibits time-of-day-dependent oscillations in circadian clock genes and vascular function that are attenuated following obstructive sleep apnea. *J Cereb Blood Flow Metab*. 2017;37(8):2806–19.
  105. Zhang SL, Yue Z, Arnold DM, Artiushin G, Sehgal A. A Circadian Clock in the Blood-Brain Barrier Regulates Xenobiotic Efflux. *Cell*. 2018;173(1):130-139.e10.
  106. Gachon F, Fonjallaz P, Damiola F, Gos P, Kodama T, Zakany J, Duboule D, Petit B, Tafti M, Schibler U. The loss of circadian PAR bZip transcription factors results in epilepsy. *Genes Dev*. 2004;18(12):1397–412.
  107. Gachon F, Olela FF, Schaad O, Descombes P, Schibler U. The circadian PAR-domain basic leucine zipper transcription factors DBP, TEF, and HLF modulate basal and inducible xenobiotic detoxification. *Cell Metab*. 2006;4(1):25–36.
  108. Wang Q, Maillard M, Schibler U, Burnier M, Gachon F. Cardiac hypertrophy, low blood pressure, and low aldosterone levels in mice devoid of the three circadian PAR bZip transcription factors DBP, HLF, and TEF. *Am J Physiol Regul Integr Comp Physiol*. 2010;299(4):R1013-9.
  109. Vyazovskiy V V., Cirelli C, Pfister-Genskow M, Faraguna U, Tononi G. Molecular and electrophysiological evidence for net synaptic potentiation in wake and depression in sleep. *Nat Neurosci*. 2008;

110. Kondratova AA, Dubrovsky Y V., Antoch MP, Kondratov R V. Circadian clock proteins control adaptation to novel environment and memory formation. *Aging (Albany NY)*. 2010;
111. A. G, D.J. K. Circadian rhythm disturbances in depression. *Hum Psychopharmacol*. 2008;
112. Taylor WD, Aizenstein HJ, Alexopoulos GS. The vascular depression hypothesis: Mechanisms linking vascular disease with depression. *Molecular Psychiatry*. 2013.
113. Storch KF, Paz C, Signorovitch J, Raviola E, Pawlyk B, Li T, Weitz CJJ. Intrinsic Circadian Clock of the Mammalian Retina: Importance for Retinal Processing of Visual Information. *Cell*. 2007;
114. Bachmanov AA, Reed DR, Tordoff MG, Price RA, Beauchamp GK. Nutrient preference and diet-induced adiposity in C57BL/6ByJ and 129P3/J mice. *Physiol Behav*. 2001;
115. Weger BD, Gobet C, Yeung J, Martin E, Jimenez S, Betrisey B, Foata F, Berger B, Balvay A, Foussier A, Charpagne A, Boizet-Bonhoure B, Chou CJ, Naef F, Gachon F. The Mouse Microbiome Is Required for Sex-Specific Diurnal Rhythms of Gene Expression and Metabolism. *Cell Metab*. 2018;
116. Kass RE, Raftery AE. Bayes factors. *J Am Stat Assoc*. 1995;
117. Valles A, Boender AJ, Gijsbers S, Haast RA, Martens GJ, de Weerd P. Genomewide analysis of rat barrel cortex reveals time- and layer-specific mRNA expression changes related to experience-dependent plasticity. *J Neurosci*. 2011;31(16):6140–58.
118. Xie L, Kang H, Xu Q, Chen MJ, Liao Y, Thiyagarajan M, O'Donnell J, Christensen DJ, Nicholson C, Iliff JJ, Takano T, Deane R, Nedergaard M. Sleep drives metabolite clearance from the adult brain. *Science (80- )*. 2013;
119. Deo AK, Borson S, Link JM, Domino K, Eary JF, Ke B, Richards TL, Mankoff DA, Minoshima S, O'Sullivan F, Eyal S, Hsiao P, Maravilla K, Unadkat JD. Activity of P-Glycoprotein, a -Amyloid Transporter at the Blood-Brain Barrier, Is Compromised in Patients with Mild Alzheimer Disease. *J Nucl Med*. 2014;
120. Van Assema DME, Lubberink M, Bauer M, Van Der Flier WM, Schuit RC, Windhorst AD, Comans EFI, Hoetjes NJ, Tolboom N, Langer O, Müller M, Scheltens P, Lammertsma AA, Van Berckel BNM. Blood-brain barrier P-glycoprotein function in Alzheimer's disease. *Brain*. 2012;
121. Zhao Z, Nelson AR, Betsholtz C, Zlokovic B V. Establishment and Dysfunction of the Blood-Brain Barrier. *Cell*. 2015.
122. Mongrain V, Hernandez SA, Pradervand S, Dorsaz S, Curie T, Hagiwara G, Gip P, Heller HC, Franken P. Separating the contribution of glucocorticoids and wakefulness to the molecular and electrophysiological correlates of sleep homeostasis. *Sleep*. 2010;
123. Musiek ES, Xiong DD, Holtzman DM. Sleep, circadian rhythms, and the pathogenesis of Alzheimer disease. *Experimental & molecular medicine*. 2015.
124. Ownby RL, Crocco E, Acevedo A, John V, Loewenstein D. Depression and risk for

- Alzheimer disease: Systematic review, meta-analysis, and metaregression analysis. *Arch Gen Psychiatry*. 2006;
125. Longden TA, Dabertrand F, Koide M, Gonzales AL, Tykocki NR, Brayden JE, Hill-Eubanks D, Nelson MT. Capillary K<sup>+</sup>-sensing initiates retrograde hyperpolarization to increase local cerebral blood flow. *Nat Neurosci*. 2017;20(5):717–26.
  126. Allen NJ, Bennett ML, Foo LC, Wang GX, Chakraborty C, Smith SJ, Barres BA. Astrocyte glypicans 4 and 6 promote formation of excitatory synapses via GluA1 AMPA receptors. *Nature*. 2012;
  127. Scemes E, Giaume C. Astrocyte calcium waves: What they are and what they do. *GLIA*. 2006.
  128. Fernández-Klett F, Priller J. Diverse functions of pericytes in cerebral blood flow regulation and ischemia. *Journal of Cerebral Blood Flow and Metabolism*. 2015.
  129. Agulhon C, Boyt KM, Xie AX, Friocourt F, Roth BL, Mccarthy KD. Modulation of the autonomic nervous system and behaviour by acute glial cell Gq protein-coupled receptor activation in vivo. *J Physiol*. 2013;591(22):5599–609.
  130. Hayashi Y, Kuroda T, Kishimoto H, Wang C, Iwama A, Kimura K. Downregulation of rRNA transcription triggers cell differentiation. *PLoS One*. 2014;
  131. Xu X, Xiong X, Sun Y. The role of ribosomal proteins in the regulation of cell proliferation, tumorigenesis, and genomic integrity. *Science China Life Sciences*. 2016.
  132. Marcon BH, Holetz FB, Eastman G, Origa-Alves AC, Amorós MA, de Aguiar AM, Rebelatto CK, Brofman PRS, Sotelo-Silveira J, Dallagiovanna B. Downregulation of the protein synthesis machinery is a major regulatory event during early adipogenic differentiation of human adipose-derived stromal cells. *Stem Cell Res*. 2017;
  133. Xie AX, Petravicz J, McCarthy KD. Molecular approaches for manipulating astrocytic signaling in vivo. *Front Cell Neurosci*. 2015;9(April):144.
  134. Srinivasan R, Huang BS, Venugopal S, Johnston AD, Chai H, Zeng H, Golshani P, Khakh BS. Ca<sup>2+</sup> signaling in astrocytes from Ip3r2<sup>-/-</sup> mice in brain slices and during startle responses in vivo. *Nat Neurosci*. 2015;
  135. Arlk YB, Van Der Helm MW, Odijk M, Segerink LI, Passier R, Van Den Berg A, Van Der Meer AD. Barriers-on-chips: Measurement of barrier function of tissues in organs-on-chips. *Biomicrofluidics*. 2018;
  136. Mansour AA, Gonçalves JT, Bloyd CW, Li H, Fernandes S, Quang D, Johnston S, Parylak SL, Jin X, Gage FH. An in vivo model of functional and vascularized human brain organoids. *Nat Biotechnol*. 2018;
  137. Bull C, Freitas KCC, Zou S, Poland RS, Syed WA, Urban DJ, Minter SC, Shelton KL, Hauser KF, Negus SS, Knapp PE, Bowers MS. Rat nucleus accumbens core astrocytes modulate reward and the motivation to self-administer ethanol after abstinence. *Neuropsychopharmacology*. 2014;

138. Coste B, Mathur J, Schmidt M, Earley TJ, Ranade S, Petrus MJ, Dubin AE, Patapoutian A. Piezo1 and Piezo2 Are Essential Components of Distinct Mechanically Activated Cation Channels. *Science* (80- ). 2010;330(6000):55–60.
139. Wu J, Lewis AH, Grandl J. Touch, Tension, and Transduction – The Function and Regulation of Piezo Ion Channels. *Trends Biochem Sci.* 2016;xx:1–15.
140. Saotome K, Murthy SE, Kefauver JM, Whitwam T, Patapoutian A, Ward AB. Structure of the mechanically activated ion channel Piezo1. *Nature.* 2018;
141. Ranade SS, Qiu Z, Woo S-H, Hur SS, Murthy SE, Cahalan SM, Xu J, Mathur J, Bandell M, Coste B, Li Y-SJ, Chien S, Patapoutian A. Piezo1, a mechanically activated ion channel, is required for vascular development in mice. *Proc Natl Acad Sci U S A.* 2014;111(28):10347–52.
142. Nonomura K, Lukacs V, Sweet DT, Goddard LM, Kanie A, Whitwam T, Ranade SS, Fujimori T, Kahn ML, Patapoutian A. Mechanically activated ion channel PIEZO1 is required for lymphatic valve formation. *Proc Natl Acad Sci.* 2018;
143. Wang SP, Chennupati R, Kaur H, Iring A, Wettschureck N, Offermanns S. Endothelial cation channel PIEZO1 controls blood pressure by mediating flow-induced ATP release. *J Clin Invest.* 2016;126(12):4527–36.
144. Fruttiger M. Development of the retinal vasculature. *Angiogenesis.* 2007;10(2):77–88.